Modelling and Simulation of Die Casting Process on Aluminum Alloys

Nélson Duro

UMinho | 2024


**Universidade do Minho**

Escola de Engenharia

Nélson Moura Pereira Duro


# Modelling and Simulation of Die Casting Process on Aluminium Alloys

October 2024

**Universidade do Minho**

Escola de Engenharia

Nelson Moura Pereira Duro

# Modelling and Simulation of Die Casting Process in Aluminium Alloys

Master's Dissertation

Integrated Master's Degree in Mechanical Engineering

Specialization in Advanced Manufacturing

Work supervised by.

**Hélder Puga**

**Inês Varela Gomes**

October 2024

## State of integrity

I hereby declare having conducted this academic work with integrity. I confirm that I have not used plagiarism or any form of undue use of information or falsification of results along the process leading to its elaboration.

I further declare that I have fully acknowledged the Code of Ethical Conduct of the University of Minho.

# ACKNOWLEDGMENT

I would like to express my deepest gratitude to my family and friends for their unwavering support, patience, and encouragement throughout the duration of my studies and during the preparation of this dissertation.

I am profoundly thankful to my mentors, Prof. Hélder Puga and Prof. Inês Gomes, for their guidance, trust in my capabilities, and for challenging me to push beyond my limits. Your insightful advice and the knowledge you imparted were crucial to my success over the past year, and I am deeply grateful for your mentorship.

I extend my thanks to Eng. Igor Villalobos from the ESI Group for his support, providing vital information and recommendations on the most efficient ways to utilize QuikCast.

I would also like to thank Eng. Sérgio from Donelab for his help and expertise in design for manufacturing of the inserts. Your assistance was fundamental to the completion of this work.

Finally, I am grateful to everyone who, in one way or another, contributed to the realization of this dissertation. Your encouragement and support made this journey not only possible but truly meaningful.

This work was carried out within the framework of the "Agendas para a Inovação Empresarial" (Project n° 49, acronym "INOV.AM", with reference PRR/49/INOV.AM/EE, operation code 02/C05-i01.01/2022.PC644865234-00000004), supported by the RRP - Recovery and Resilience Plan and by the European Funds NextGeneration EU. http://www.recuperarportugal.gov.pt/

# ABSTRACT

In today's modern world, the need for increased production to meet demand is ever-present. However, due to time constraints, the primary focus is on boosting productivity and minimizing time-consuming tasks. By doing so, better solutions can be found, or the intrinsic costs of processes can be reduced.

The Die Casting technology is no exception to this requirments. The time the engineers spent in the development and validation of gating design remains one of the bottlenecks of the process. Therefore, a solution must be found in order to improve the modelling and simulation of the die casting process.

This dissertation explores the potential of using Python as a programming tool for the gating design in die casting manufacturing. The knowledge gained has been compiled into software named Highly Efficient Labor-saving Program  Die Casting. This software can accommodate various casting alloys, it emphasizes aluminum alloys.

The software was applied at two stages of gating design validation. First, it was used to generate the gating design, overflow, and venting system for a valve cover, along with the corresponding dimensional data for each section. Second, it was employed during the die casting process simulation to calculate the boundary conditions and initial conditions.

The validation of the gating designs focused on three key aspects: die cycle simulation to ensure a stable thermal gradient, analysis of potential defects (such as shrinkage porosity, air entrainment, and cold shuts), and an evaluation of the process dynamics (based on the minor and major losses of the molten metal). In the process dynamics analysis, two distinct phases were identified where the losses behaved differently.

**Keywords:** Programming aided design; High-pressure die casting process; Aluminum alloys; Finite differences method

# Resumo

No mundo moderno de hoje, a necessidade de aumentar a produção para satisfazer a procura é constante. No entanto, devido a restrições de tempo, o foco principal está em aumentar a produtividade e minimizar o tempo despendido tarefas demoradas. Desta forma, podem ser encontradas melhores soluções ou os custos intrínsecos dos processos podem ser reduzidos.

A tecnologia de fundição em alta pressão (*Die Casting*) não é exceção a estes requisitos. O tempo que os engenheiros gastam no desenvolvimento e validação do *design* do sistema de enchimento continua a ser um dos estrangulamentos do processo. Portanto, é necessário encontrar uma solução para melhorar a modelação e simulação do processo de fundição injetada.

Esta dissertação explora o potencial de utilizar Python como ferramenta de programação para o *design* do sistema de enchimento no processo de fundição injetada. O conhecimento adquirido foi compilado num *software* denominado *Highly Efficient Labor-saving Program Die Casting*. Embora este *software* engloba várias ligas de fundição, é dada ênfase às ligas de alumínio.

O *software* foi aplicado em duas fases da validação do *design* dos canais de enchimento. Primeiro, foi utilizado para gerar o *design* do sistema de enchimento, dos *overflows* e do sistema de ventilação de uma tampa de válvula, juntamente com os dados dimensionais correspondentes a cada secção. Em segundo, foi utilizado durante a simulação do processo de fundição injetada para o cálculo das condições de fronteira e condições iniciais.

A validação dos *designs* do sistema de enchimento concentrou-se em três aspetos principais: simulação do ciclo do molde para garantir um gradiente térmico estável, análise de possíveis defeitos (como rechupe, aprisionamento de ar e frentes frias), e uma avaliação da dinâmica do processo (com base nas perdas localizadas e distribuidas do metal fundido). Na análise da dinâmica do processo, foram identificadas duas fases distintas onde as perdas se comportaram de forma diferente.

**Keywords:** Modelação assistida por programas; Processo de fundição injetada; Ligas de alumínio; Método das diferenças finitas

# INDEX

# FIGURE INDEX

# TABLE INDEX

# LIST OF ACRONYMS

| | |
|---|---|
| CAD | Computer-Aided Design |
| CAM | Computer-Aided Manufacturing |
| CAE | Computer-Aided Engineering |
| DIN | German Institute of Standardization |
| FDM | Finite Difference Method |
| FEM | Finite Element Method |
| FVM | Finite Volume Method |
| H.E.L.P. | Highly Efficient Labor-Saving Program |
| HPDC | High Pressure Die Casting |
| IGES | Initial Graphics Exchange Specification |
| ISO | Internation Standard Organization |
| NADCA | North American Die Casting Association |
| STEP | Standard for the Exchange of Product model data |
| STL | Stereolithography |
| VBA | Virtual Basic for Applications |
| VCF | Volume Correction Factors |

# List of Symbols

| Symbol | Description | Units |
|---|---|---|
| $v_{plunger,1^{st}}$ | Plunger’s velocity in the first stage | [m/s] |
| $d_{pungler}$ | Plunger’s diameter | [mm] |
| $\%filling$ | Shot sleeve’s filling ratio | [%] |
| $L_{plunger,1^{st}}$ | Plunger’s displacement in the first stage | [mm] |
| $V_{part}$ | Part’s volume | [mm$^3$] |
| $V_{Overflows}$ | Overflow’s volume | [mm$^3$] |
| $A_{plunger}$ | Plunger’s area | [mm$^2$] |
| $v_{plunger,2^{nd}}$ | Plunger’s velocity in the second stage | [m/s] |
| $L_{plunger,2^{nd}}$ | Plunger’s displacement in the second stage | [mm] |
| $v_{ingate}$ | Velocity at ingate | [m/s] |
| $A_{eff,ing}$ | Effective ingate area | [mm$^2$] |
| $C_d$ | Loss coefficient | [%] |
| $t_{fill}$ | Filling time | [s] |
| $K_1$ | Constant based on die’s material | [s/mm] |
| $T_{part}$ | Avarage thickness | [mm] |
| $T_i$ | Injection temperature | [°C] |
| $T_f$ | Minimum flow temperature | [°C] |
| $T_d$ | Die’s temperature | [°C] |
| $S$ | Percentage of solidified metal at the ending of the filling | [%] |
| $Z$ | Solids units conversion factor | [°C/%] |
| $A_{ac,ing}$ | Actual ingate area | [mm$^2$] |
| $\theta_{ef}$ | Flow angle | [°] |
| $T_{ac,ing}$ | Actual ingate thickness | [mm] |
| $J$ | Constant for atomized flow | [-] |
| $\rho$ | Density | [kg/m$^3$] |

| | | |
|---|---|---|
| $r_{ing,run}$ | Ingate-runner ratio | [-] |
| $A_{vent}$ | Venting area | [mm²] |
| $K$ | Thermal conductivity | [W/mK] |
| $C_p$ | Specific heat | [J/kgK] |
| $t$ | Time | [s] |
| x, y, z | Cartesian coordinate system | [-] |
| u, v, w | Component x, y and z of the velocity vector | [m/s] |
| $p_x, p_y, p_z$ | Component x, y and z of the pressure vector | [Pa] |
| $\mu$ | Dynamic viscosity | [Pa s] |
| $\nabla, \nabla^2$ | Nabla operator, Laplace operator | [-] |
| $F_x, F_y, F_z$ | Component x, y and z of the External force vector | [Pa] |
| $m$ | Mass | [kg] |
| $Q_{in}, Q_{out}$ | Flow inward and outward | [kg/s] |
| $Q$ | Heat transfer | [W] |
| $T$ | Temperature | [°C] |
| $h$ | Heat transfer convection coeffcient | [W/m²K] |
| $A$ | Surface area | [m³] |
| $T_\infty$ | Temperature of the fluid out of the boundary layer | [°C] |
| $\sigma$ | Stefan-Boltzmann constant | [W/m²K⁴] |
| $\varepsilon$ | Emissivity | [-] |
| $F_g$ | Geometric factor | [-] |
| $T_1, T_2$ | Temperature of two different surfaces | [K] |
| $g$ | Gravity accelaration | [m²/s] |
| $\beta$ | Coefficient of volume expansion | [1/°C] |
| $L$ | Characteristic length | [m] |
| $Gr$ | Grashof number | [-] |
| $Pr$ | Prandtl number | [-] |
| $Ra$ | Rayleigh number | [-] |
| $Nu$ | Nusselt number | [-] |
| $F_{locking}$ | Locking force | [N] |
| $p_{3^{rd}}$ | Third stage pressure | [Pa] |

| | | |
|---|---|---|
| $\boldsymbol{A_{projected}}$ | Projected area | [mm²] |
| $\overline{\boldsymbol{p_{die}}}$ | Average pressure on the die surface | [Pa] |
| $\boldsymbol{F_{m_{locking}}}$ | Maximum locking force | [N] |
| $\boldsymbol{A_{contact}}$ | Contact area | [mm²] |
| $\boldsymbol{C}$ | Numerical identification of each cell's volume | [-] |

# Chapter 1 - INTRODUCTION

The modern tools for the development of new products englobes CAD (Computer-Aided Design), CAE (Computer-Aided Engineering), and CAM (Computer-Aided Manufacturing) softwares. In the CAD software, the virtual model is conceived. CAE software plays a crucial role in validating these designs through the analysis and post-processing of simulation results. The CAM branch is directioned for the manufacturing of the product, it will not be addressed in this thesis.

In the foundry industry, the usage of the CAD/CAE technological advances has been remarkable. The implementation of casting simulation has significantly reduced costs, time, labor, shopfloor trials and the number of prototypes to test. Furthermore, it is possible to optimise designs and processes without the creating the all the prototypes of each iteration step.

Therefore, the development of new methodology to improve the CAD/CAE environments in High-Pressure Die Casting (HPDC) and reduce gating design time is necessary. The proposed methodology is grounded in the existing guidelines outlined in the North American Die Casting Association (NADCA) manual. This will increase the productivity and the accuracy of the solution and a reduction in high qualified labour costs. Nevertheless, this new methodology will not entirely replace the expertise required for HPDC processes, particularly in gating design and casting simulation. Instead, it serves as tool to complement and enhance the knowledge and skills of industry professionals.

## 1.1. MOTIVATION

The beginning of the casting simulation starts in the CAD software in the gating design's and mold's development. Then the CAE environment for the casting simulation which validates the gating design and process. This type of CAE software are already widely used in the foundry industry which simulates numerically the filling and solification processes and locate possible defects [1, 2].

These two stage reduce the number of shop-floor trials, time and costs, increasing performance and productivity.

The old bottleneck of the development of molds in die casting process, which was trial and error with different molds, was turned into the usage of CAD/CAE softwares. Even though it was an improvement, these two stages still requires qualified manpower and time [3].

Thereby, one way to improve the efficiency of the process, time, cost and manpower is to improve the modelling and simulation of the die casting process. This improvement can be achived increasing the virtualization of this bottleneck. The digital virtualization of the modelling process is an underdeveloped branch with the following benefits:

I. Reduced gating design time: modelling the gating design is a time consuming task for a highly qualified manpower and increases productivity;
II. Reliable solution: the methodology is always the same unless the program is modified
III. Storage of data: if the generated design is not accordingly with the user's desire, the generated data is kept stored for a later modification;

The virtualization of the die casting simulation is already in development, with some softwares already possessing some sort of Macros which automates through programming the user's tasks.

## 1.2. AIM

This dissertation thesis aims to develop and use the power of the programming in the creation of a gating design in HPDC process in aluminum alloys and use it to generate a gating design for the valve cover.

This dissertations will explore essential topics for the virtualization of the gating design for HPDC using the North American Die Casting Association (NADCA) gating manual [4] and other manuals [5–7]. Part of the gating design formulation will be translated into Python code for the programmed modelling. Not only the formulation of the gating design will be explored but all the variables to its design and fluid's mechanics principles of its dynamic.

At last, the numeric simulation of the die cycling and casting process will be done using QuikCast from ESI Group to predict defects. Properties such as density, specific heat/entalphy, thermal conductivity and solidus and liquidus temperature will be determined for the aluminum alloy which are required to the simulation.This analysis will include the evaluation of the process's dynamics and the defects within the casting. A comparison between different gating designs will be made and compare it the final solution.

## 1.3. Structure of the dissertation

In the first chapter, the motivation and objective of the dissertation are presented, along with the context of the problem, which involves the modeling and simulation of the high-pressure die casting process for aluminum alloys.

In chapter 2, the high-pressure die casting process is discussed, as well as the process's variables and the NADCA methodology for developing gating systems for die casting.

In chapter 3, the interface of the software developed for the modeling of the gating system and overflows is introduced. This software was designed in Python and uses the Autodesk Inventor API for automated modeling. The software also allows data to be stored in an Excel sheet format, which is later used in the simulation of the casting process.

In the fourth chapter, the preprocessing for the validation of the gating system is detailed, using the QuikCast simulation software. The inserts contain the mold cavity and cooling channels, which will be manufactured via additive manufacturing. This chapter also addresses the thermophysical properties of materials relevant to the simulation of the $AlSi_9Cu_3$ alloy and 1.2709 steel.

The validation of the gating systems will consist of two simulations: thermal cycles and filling. The thermal cycle simulation aims to achieve a stable thermal gradient for the filling simulation. To reduce computation time, only a single solidification scenario will be considered in the thermal cycle simulation.

In the fifth chapter, three solutions will be evaluated: the final solution, solution A, and solution B. This evaluation will include the analysis of the presence of shrinkage (and the reasoning for its location), air porosity, and cold fronts (if the defect occurs).

The preprocessing presented in the fourth chapter refers exclusively to the final solution. The differences between the solutions will be described in the corresponding chapter, noting that these changes do not affect the performance of the gating system.

In chapter 6, the conclusions of the work are presented, along with proposals for future developments of the software.

## 1.4. Chapter references

[1] E. Flender and J. Sturm, *Thirty Years of Casting Process Simulation.* [Online]. Available: https://link.springer.com/article/10.1007/BF03355463 (accessed: Sep. 23 2024).

[2] H.-J. Kwon and H.-K. Kwon, "Computer aided engineering (CAE) simulation for the design optimization of gate system on high pressure die casting (HPDC) process," *Robotics and Computer-Integrated Manufacturing*, vol. 55, pp. 147–153, 2019, doi: 10.1016/j.rcim.2018.01.003.

[3] B. Ravi, "Casting Simulation and Optimisation: Benefits, Bottlenecks and Best Practices," *ReseachGate*, pp. 1–2, 2008. [Online]. Available: https://www.researchgate.net/publication/228975218

[4] NADCA, *NADCA Gating Manual*. Illinois, United States of America: NADCA.

[5] H. Bakemeyer, *Operating the die casting: Machine.* [Online]. Available: https://www.dykast.com/user/files/operating_the_die_cast_machine.pdf (accessed: Sep. 15 2024).

[6] UPMOLD, *Casting Technique*. Estados Unidos da América: UPMOLD. Accessed: Jan. 5 2024. [Online]. Available: http://www.upmold.com/

[7] NADCA, *NADCA Product Specification Standards for Die Casting: Aluminum, Aluminum-MMC, Copper, Magnesium, Zinc and ZA Alloys,* 9th ed. Illinois, United States of America: NADCA, 2015.

# Chapter 2 - DIE CASTING TECHNOLOGY

The casting manufacturing process allows for the production of parts with near-final geometries, also known as near net shape. Currently, the two predominant casting processes in the market are sand casting and permanent mold casting [1]. In permanent mold casting, the mould material is steel, and consequently, it cannot be destroyed to remove the part from its interior compared to sand casting [2, 3].

Permanent mold casting has three branches: (i) low pressure, (ii) gravity, and (iii) high pressure [4]. In low-pressure casting, the molten metal is directed into the mold cavity by the pressure exerted on it, typically ranging from 0.1 to 1 bar [5]. In gravity casting, the molten metal is poured into the mold cavity, and gravity forces the cavity to fill. High-pressure casting is characterized by the application of higher pressures (up to 1200 bar) [6, 7] by a piston to push the molten metal into the die cavity. Consequently, the molds and the clamping mechanism used in high-pressure casting must withstand higher pressure levels.

At the beginning of the high—pressure die casting process, it is sprayed die lubricant in the die surface and then the hydraulic system closes the mold. Meanwhile, the metal is heated up until it reaches the pouring temperature. Then, the metal poured into the shot sleeve (if it is a hot chamber machine the shot sleeve is inside the furnace) [8]. In the shot sleeve, the molten metal is pushed by a plunger at high pressure into the die cavity which possess the negative of the casting.

At last, the casting alloy solidifies under high pressure applied by the plunger [9]. The solidification process is controlled by the cooling fluid (for example water or oil) passes through the cooling channels [10]. Lately, the hydraulic press opens the mold and the casting (Fig 2.1) is removed from the die cavity.

The casting consists of the biscuit, runners, part and overflows. The biscuit dimensions are based on the shot sleeve diameter and typically have a thickness of 20 mm [11]. The runners' and overflows' cross sections are calculated based on the Bernoulli's equation [6]. These parts are cut-off in the postprocessing of the casting [12]. Although the Bernoulli's equation is used for determining the dimensions of the runners [13], these are verified in CAE software whose rulling equations are the Navier-Stokes's.

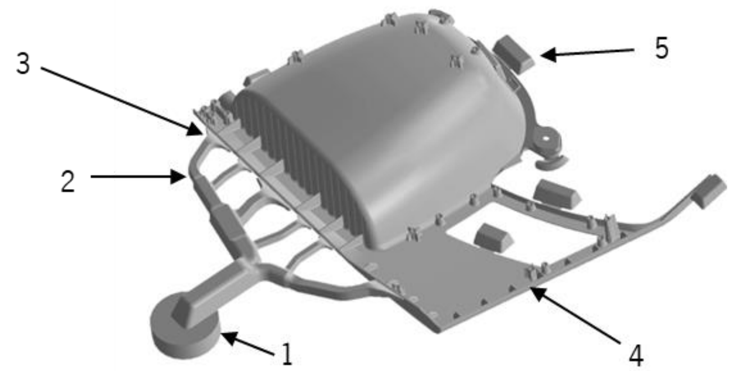


Fig 2.1 – Model constituted by the different elements. 1 – Biscuit; 2 – Runner; 3 – Ingate; 4 – Component; 5 – Overflow (adapted from [14]).

## 2.1. EQUIPMENT AND THEIR ELEMENTS

The equipment mentioned in this chapter are relevant in the virtualization of the gating design and in CAE software's boundary conditions. The equipment used in high pressure die casting which influence the gating design are [15]:

- Chamber
- Cooling system
- Venting system

The type of chamber influences the energy efficiency of the process, rulling the temperature drop of the molten metal. The type of chamber also constraint the type of casting alloy and the cycle time.

The cooling system modifies the solidification dynamic of the casting and is design to reduce the shrinkage porosity of the casting during solidification. Also it partially controls the cycle time by controlling the solidification time of the casting.

At last, the venting system removes the air in the die cavity, reducing the air porosity of the casting.

**Cold and Hot Chamber**

In the cold chamber, the molten metal is poured into the injection sleeve, manually or automatically [15], (Fig 2.2 (a)).In the hot chamber, the injection sleeve is immersed in the molten metal bath of the melting furnace [16] (Fig 2.2 (b)). From the injection sleeve (Fig 2.3) the metal is injection into the die cavity through the plunger rod.

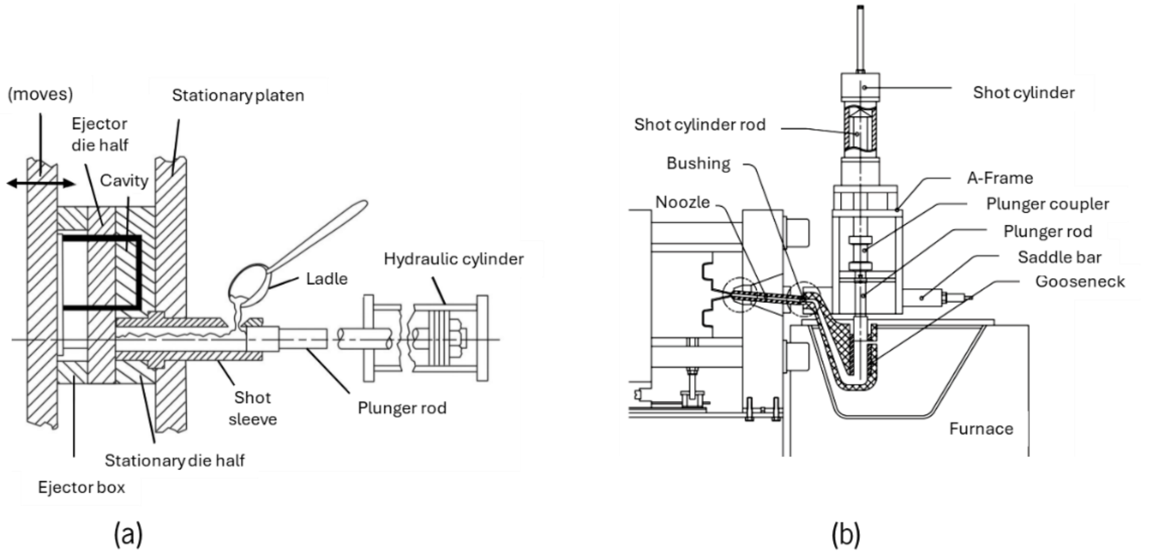


Fig 2.2 - Tipology of chamber and its components (adapted from [11, 17]). (a) - Cold chamber; (b) - Hot chamber;

The hot chamber's main disadvantages are the limitation in casting metal due to high melting point (as well as affinity of some casting materials) can provoke erosion and higher maintenance. In other hand, shorter cycle time, less damage to the die the casting alloy oxidate in a smaller rate than in the cold chamber [18]. The casting alloys used in hot chamber are Magnesium, Zinc (specifically Zamak alloys) [19, 20].

The cold chamber's main disadvantages are longer cycle time, higher wearing of the tools and higher air exposure of the molten. However, this tipology lowers costs in maintenance. The alloys used in cold chamber are aluminum and brass alloys [20].

This tipology affects the temperature drop of the molten metal. Transporting the molten metal from the furnace to the injection sleeve (Fig 2.3) causes an higher drop, therefore the required overheat is typically higher in the cold chamber than in the hot chamber.

Fig 2.3 - Injection sleeve (adapted from [21]).

**Cooling system**

A cooling system in a die casting mold is a network of channels to promote the heat transfer between the mold and the cooling fluid. The cooling system helps to control the temperature of the mold and the molten metal, which is important for producing high-quality parts and reducing cycle times [22].

The mould is pre-heated before the casting process begins with warm-up shots [23]. These warm-up shots are also used to reach a stable die temperature during the production phase [24, 25]. Pre-heating fluid can be used to heat it up.

The cooling rate of the system is dependent on geometric variables and non-geometric variables. The geometric variables of the cooling system such as channel's diameter, path and its length and the flow rate are decided during the gating design. The channels diameter is choosen based on the casting's thickness, path and its length based on the location of the hotspots and the flow rate. This variable is based on the fluid minor and major losses which is dependent on the cooling channels path, the simpler the higher the flow rate the pump can provide (Fig 2.4).

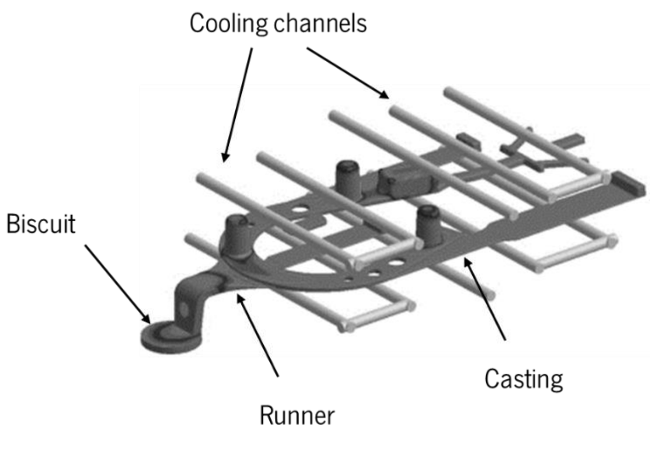


Fig 2.4 - Cooling channels and the designed path to cool down the casting (adapted from [26]).

The non-geometric variables are the thermophysical properties of the fluid. The type of fluids which are mostly used for cooling are mainly water and oil-based [26, 27].

**Venting system**

The venting system is responsible for the removal of air inside the cavity. The vaccum pump removes the air from the die cavity through the vents (Fig 2.5). This way, it is possible to reduce the air porosity present within the casting.

The vents' design is optimized for high major and minor losses of the molten metal to delay it which can be classified into two categories, air venting  and chill venting [28]. The main difference is that the profile of air vents are straight while the chill vents are in a zig-zag geometry [29] which maximize the cooling rate of the vent.

These vents have a small thickness and are connected to the die cavity through the overflows [30]. However, not all overflows possess connection with the venting system (Fig 2.6).

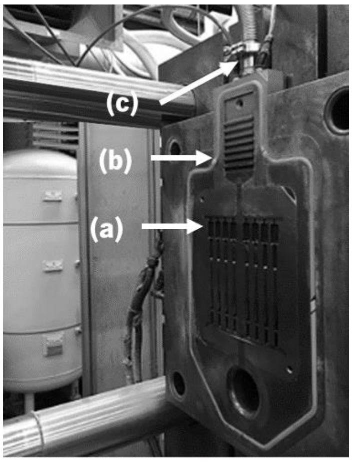


Fig 2.5–Air removal system in a mold to minimize air entrainment. (a) – overflows; (b) – chill vent; (c) vacuum system connection (adapted from [31]).

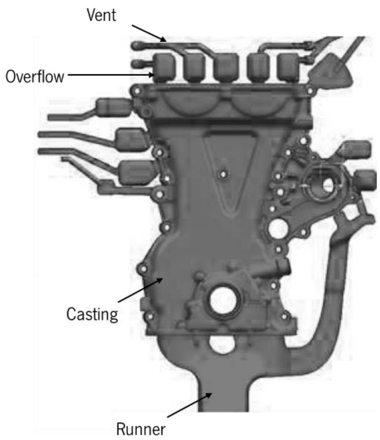


Fig 2.6 - Venting system (adapted from [32]).

## 2.2. MATERIALS OF THE PROCESS

The die casting process's materials are divided into two categories, the mold and casting materials.

The mold materials are used to produce each mold plate where the die cavity is located. The die cavity possess the negative of the casting, as well as the gating design's and venting system's. This cavity is frequently produced by machining or by additive manufacturing (as will be later detailed in chapter 4.2). The materials typically used is an alloy steel that requires high mechanical strength (both dynamic and static properties), as well as the ability to maintain its strength at elevated temperatures and resistance to fatigue.

The mechanical dynamic and static loads applied in the die cavity's surface reach its height in the second and third stage, respectively (shot dynamic will be detailed in chapter 02.3) [30]. In the second stage, the entrance of the casting alloy on the die cavity at high velocities originate wear its surface due to the its impact and viscous forces (proportional to the alloy's velocity). The thermal stress in the die plate also reach its height, since the heat transfer to the mold's cavity is the maximum (due to the fluid's velocity at a high temperature). In the third stage, the piston applies a pressure on the fluid. This phase lasts until the end of the solidification is static. This pressure does not provoke wearing in the die surface, but the die plate have to withstand the high intensification pressure.

For these applications, tool steel is used due to its thermal-mechanical properties. Some examples are the P-20 steel (ISO P steel), specified in ISO 4957 [33, 34], H-13 (which uses chromium, molybdenum and vanadium as alloying elements) [35], and H-21 (which uses tungsten as an alloying element), both classified under ISO H steel [36, 37].

The casting alloys are the materials that will originate the casting. This alloy will be heaten until its pouring temperature then injected into the die cavity. The requirement for this alloys are the good fluidity [38–40] and thermal inertia [41], which facilitate the injection and the reduction in shrinkage porosity [42], respectively. For this purpose, non-ferrous alloys such as Aluminium [43–47], Magnesium [48–50] and Zinc [51–54] alloys are used.

## 2.3. VARIABLES OF THE PROCESS

The process's variables involve aspects like shot dynamic, pressure levels, and cooling rate. These variables require a previous verification with the available technology before its operation such as injection pressure and clamping force and flow rate of the cooling fluid. These factors are critical to achive a sucessful casting. These variables can be easily modified by the operator

**Plunger's dynamic**

The plunger is responsible for the filling and the reduction of the shrinkage porosity during the intensification phase. Consequently, its dynamic changes throughout the casting process which can be divided into 3 stages [55].

The first stage is known as the prefilling stage. In this stage, the plunger moves slowly to push the casting alloy from the shot sleeve to near the ingate. This stage allows the removal of air and reduced mold erosion [56] in the die cavity. The velocity [11] and piston's displacement of this stage is defined using equation [2.1] and [2.2].

$$v_{plunger,1^{st}} = \sqrt{0.597}\sqrt{d_{pungler}\frac{(100\% - \%filling)}{100\%}} \quad [2.1]$$

$$L_{plunger,1^{st}} = \frac{V_{part} + V_{Overflows}}{A_{plunger}} \quad [2.2]$$

The second stage is the filling phase. This phase will fill the rest of the die cavity. In this stage, it is reached the maximum piston's velocity [57]. The velocity and piston's displacement is calculated based on the continuity equation [2.3] [58].

$$v_{plunger,2^{nd}} = v_{ingate}\frac{A_{eff,ing}}{C_d A_{plunger}} \quad [2.3]$$

$$L_{plunger,2nd} = L_{total} - L_{plunger,1^{st}} \quad [2.4]$$

In equation [2.3], $v_{plunger,2^{nd}}$ is the velocity of the second stage, $v_{ingate}$ the ingate velocity, $C_d$ is loss coefficient (typical values in Tab 2.1) and $A_{eff,ing}$ the effective ingate area (calculation methodology of this variable will be detailed in chapter 2.4) and $A_{plunger}$ are the ingate and plunger area, respectively. The loss coefficient, $C_d$ is required to determine the actual velocity of the piston to make up for the losses of the fluid's in the runner's.

Tab 2.1 – Typical loss coefficient for different alloys (adapted from [59]).

| **Alloy** | **Loss coefficient** [%] |
|---|---|
| Aluminum | 45 – 50 |
| Magnesium | 45 – 50 |
| Zinc | 55 – 65 |

Its injection dynamic is set accordingly with the machine's capacity. However, the operator must understand that it is impossible that a increase in flow rate will decrease the static pressure and vice versa. To a correct modification of this parameter, a P-$Q^2$ analysis must be performed to check its feasibility (Fig 2.7). The P-$Q^2$ analysis is done based on a fluid's mechanical perspective which will provide the operator to understand the operating pressure and flow rate [6].

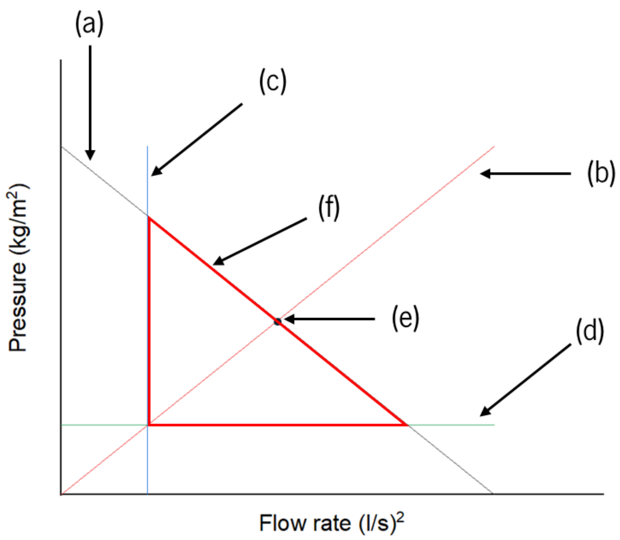


Fig 2.7 - Generic P-$Q^2$ graph and process constraints (adapted from [60]).

In Fig 2.7, (a) and (b) are the visual representations of the machine performance and system's minor and major losses, respectively. The limits (c) and (d) represent the minimum flow rate required to guarantee the maximum fill time and the minimum pressure to guarantee an atomized flow. The operating window and pressure and flow rate are (f) and (e), respectively. It is noticeble that the operating flow rate is typically higher than the required which guarantees the minimum fill time which is calculated.

Periodically, the machine has to be evaluated to update its curve. Meanwhile, the system's energy loss are based on the complexity of the casting.

The last stage is known as the intensification rate which last until the end of the solidification [61]. The high pressure during this stage reduces the appereance of shrinkage porosity and increase the quality of the casting produced. Normally, the piston's displacement of this phase is hard to measure its distance being considered in some CAE software as being a static phase (velocity near 0 m/s).

Depending on the casting alloy, the intensification pressure varies with the casting alloy (Tab 2.2). The required clamping force can be calculated using the Pascal's law [62] and should be compared with the campling force, equation [2.5].

Tab 2.2 – Intensification pressure based on the alloy (adapted from [30]).

| **Alloy** | **Pressure $[bar]$** |
|---|---|
| Aluminum | 400 – 1000 |
| Magnesium | N/A |
| Zinc | 100 – 400 |

$$F_{locking} = p_{piston,3^{rd}} A_{projected} \quad [2.5]$$

In equation [2.5], $F_{locking}$ is the required locking force, $p_{piston,3^{rd}}$ is the third stage intensification pressure and A the projected area of the component normal to the part line.

### Pouring and mold's temperature

The pouring temperature of an alloy is determined based on its liquidus temperature, and the casting alloy is typically overheated by 50°C. This overheating is necessary to compensate for the temperature drop that occurs during the casting process [63]. The extent of this temperature drop is influenced by several factors, including the:

- Type of chamber: cold chamber has an higher temperature drop than the hot chamber [64];
- Geometry of the runners: higher length of the runner results in an higher temperature drop. However, its geometric section outweights the runner's length during solidification;
- Shot velocity: a slower shot allows the casting alloy to lose more heat;
- Shot sleeve filling percentage: it can be a low filling ratio (20%-30%) [55] or high filling ratio (60%-80%) [56]. An higher filling ratio prevents an high temperature drop, due to the thermal inertia;

The die's temperature is also a parameter that influences the temperature drop, since heat transfer is proportional to the thermal gradient.

Initially, to maintain the desired thermal conditions, a cooling-heating system and warm-up shots are used to heat the mold and regulate its temperature [65]. Approximately 20 thermal cycles [66] are performed to establish a stable operating thermal gradient. Throughout these thermal cycles, the cooling-heating system also cools the die, playing a critical role in the solidification dynamics of the casting. It is desirable that mold's thermal inertia can hold enough energy to prevent re-heating the mold.

The parameters which influence the heat transfer is the temperature gradient, contact area, the type of flow and the thermophysical properties of the cooling fluid.

The initial mold temperature and pouring temperature are key variables required to calculate the filling time (detail in 2.4).

## 2.4. VIRTUALIZATION OF THE HIGH-PRESSURE DIE CASTING PROCESS

The gating design presented by NADCA [6] follows a methodology well defined which allows the user to adquire knowledge of the process and its effects on the gating design. The manual is divided into 9 different steps:

1- Casting quality requirements
2- Determine the flow pattern and location of the ingates and outgates
3- Segment volumes, Cavity fill time and flow rate
4- Process flow rate
5- Determine the ingate parameters
6- $PQ^2$ analysis
7- Design the fan and tangential runners
8- Design the overflows and vents
9- Simulation

The algorithm which will be presented is a simplified and compacted version of the actual algorithm. In this simplified version, step 1 and 2 are a prior task which will not be detailed, since those are mainly conceptual which can not be virtualized into the algorithm. The simplified algorithm is:

- Ingate area: englobes the 2nd, 3rd and 4th steps shown previously. The 6th step is performed if desired, which is only to validate the machines capacity (detailed in chapter 0);
- Runners definition: englobes the 7th step;
- Overflows and venting: englobes the 8th step;
- Simulation: detailed in chapter 4 and 5.

**Ingate Area**

Initially, it is done the conceptual division in segments of the component based on the number of ingates required by the component. Then, based on the segment's volume ($V_{segment}$) and the filling time ($t_{fill}$), it is possible to use the continuity equation to determine the ingate area (equation [2.3]). The equation to calculate the filling time of the part is shown in equation [2.6] [64].

$$t_{fill} = K_1 T_{part} \left( \frac{T_i - T_f + SZ}{T_f - T_d} \right) \quad [2.6]$$

In equation [2.6], $t_{fill}$ is the filling time of the component and overflows, $K_1$ constant based on die's material (related to the thermal conductivity), $S$ is percentage of solidified metal at the ending of the filling, $Z$ solids units conversion factor, $T_{part}$ avarage wall thickness and $T_f$, $T_i$ e $T_d$ as minimum flow temperature, injection temperature at the ingate and die's surface temperature, respectively.

For different alloys, the recommended ingate velocity is shown in Tab 2.3. The ingate velocity ($v_{ing}$) definition is based on the components. To calculate the effective ingate ($A_{eff,ing}$) area is based on continuity equation [2.3] [58].

$$A_{eff,ing} = \frac{V_{segment}}{t_{fill} v_{ing}} \quad [2.7]$$

Tab 2.3 – Ingate velocity for different alloys (adapted from [59]).

| **Alloy** | **Ingate velocity** $[m/s]$ |
|---|---|
| Aluminum | 18 – 40 |
| Magnesium | 25 – 50 |
| Zinc | 23 – 50 |

Due to fluid's inertia, the actual ingate area is bigger than the effective ingate area as it shown in Fig 2.8. The relation between the these two parameters is the flow angle which is presented in equation [2.3]. The flow angle ($\theta_{ef}$) is a parameter to verify in the postprocessing of the casting simulation.

$$A_{ac,ing} = \frac{A_{eff,ing}}{\cos \theta_{ef}} \quad [2.8]$$

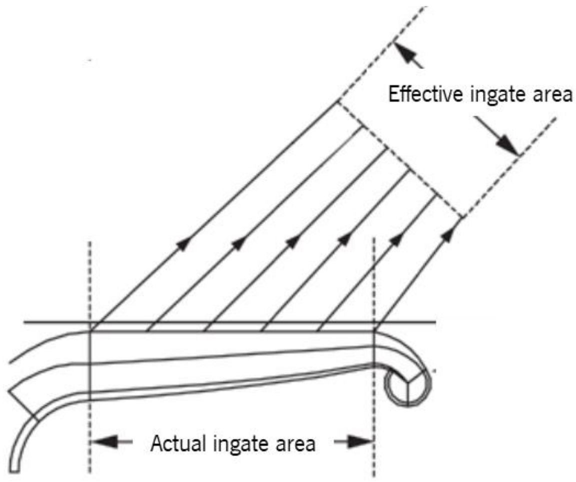


Fig 2.8 - Geometric representation of the effective and actual ingate area in a tangential runner.

The last parameter to a total definition of the ingate profile is the thickness. Normally, ingates vary from 0.75 mm to 2 mm based on ingate velocity. However, the usage of equation [2.9] is more precise.

$$v_{ing}^{1.707} T_{ac,ing} \rho = J \qquad [2.9]$$

In equation [2.9], $J$ is a constant based on the material for atomized flow, $v_{ing}$ is the ingate velocity (m/s), $T_{ac,ing}$ is the ingate thickness (mm) and $\rho$ is the density of the fluid (kg/m$^3$). The NADCA manual also provides some information for typcal thickness for ingate values for $J$ equal to 998000 [67].

In the end of the ingate definition step, the geometry of the ingate (trapezoid with 10° inward (Fig 2.9 (a))), ingate velocity and fill time are totally defined. The ingate dimensions will be required to the runner's definition. The ingate velocity will be required to the definition of the plunger's velocity (first and second stage). The fill time will be required to the definition of the transient boundary conditions in the CAE software.

**Runners definition**

The runners are divided into 3 categories: (i) curved sided fan, (ii) straight sided fan and (iii) tangential runner. The difference between these three is the way the the metal is distributed. IN both fans, the flow's direction in the fan during filling is colinear with the fan's length. In other hand, the tangential runner's flow's direction is perpendicular [6]. The selection of the runners is based on the part's geometry. The fans generate a strong centre fill. Tangential runner are more compact and can distribute the metal over a longer distance [30].

The difference between the fans is the width and thickness profile across the fan's length, but both profile section is the same (Fig 2.9 (a)). The thickness profile of a straight sided fan varies non-linearly with the length of the tangencial runner. In other hand, the curved sided fan has a linear thickness profile. This happens in both fans to avoid the creating of voids in the fans edges and guarantee that the whole fan is complely full during the filling stage.

The profile of the fans and tangential runner are presented in Fig 2.9. The equations to determine the parameters for the fans and tangential are presented in Tab 2.4 and Tab 2.5, respectively.

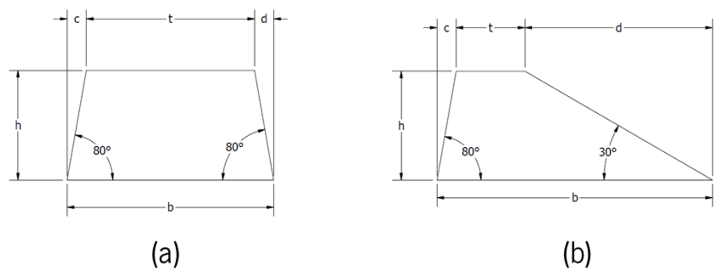


Fig 2.9 – Runners profiles. (a) - Fan; (b) - Tangencial runner with 30°C approach (adapted from [6]).

Tab 2.4 - Equation for fan's dimensions (adapted from [6]).

| Parameter | Equation |
|---|---|
| $\boldsymbol{h}$ | $\frac{\sqrt{A_{sec}}}{r_{asp}}$ |
| $\boldsymbol{c}$ and $\boldsymbol{d}$ | $h \cos 80°$ |
| $\boldsymbol{b}$ | $\frac{A_{sec}}{h} + 2h \cos 80°$ |

Tab 2.5 - Equation for tangencial runner's dimensions (adapted from [6]).

| Parameter | Equation |
|---|---|
| $\boldsymbol{h}$ | $\frac{\sqrt{A_{sec}}}{r_{asp}}$ |
| $\boldsymbol{d}$ | $h \cos 80°$ |
| $\boldsymbol{c}$ | $h \cos 30°$ |
| $\boldsymbol{b}$ | $\frac{A_{sec}}{h} + d + c$ |

The $r_{asp}$ is the aspect ratio, which is the ratio between the avarage width and the height (typically between 3:1 to 1:1). The higher the aspect ratio, the slower it solidifies, because the module of the section is maximized. The parameter $A_{sec}$ is the area of the cross section. The NADCA methodology presents a 9 cross section for the fans and a 5 cross sections calculation for the tangencial runner. The distance between these section is calculated based on the flow angle.

The calculation the $A_{sec}$ parameter is different for tangential runners and fans, Fig 2.10. The tangential runner's cross section's area increases linearly from the shock absorved to the main runner. Meanwhile, the fan cross section increases linearly from the ingate to the main runner. The main runner's area is based on the ingate area multiplied by the ratio ingate/runner, $r_{ing,run}$. The parameter $r_{ing,run}$ is the ingate/runner ratio, which increases the area of the runner to guarantee that the ingate is complely full before the beginning of the 2nd phase of the piston (injection), which varies with the casting alloy (Tab 2.6).

Tab 2.6 - Typical values of $r_{ing,run}$ (adapted from [6, 67]).

| **Alooy** | $r_{ing,run}[mm]$ |
|---|---|
| Aluminum | 1.1 – 1.5 |
| Magnesium | >1.1 |
| Zinc | 1.05 – 1.15 |

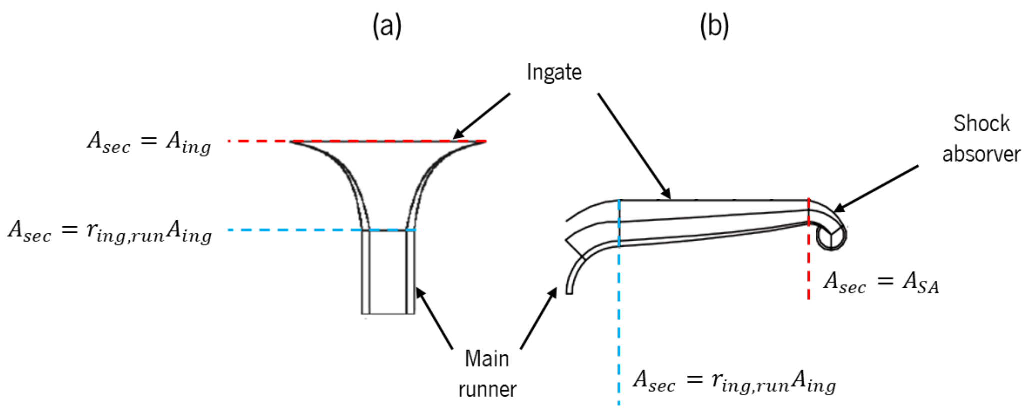


Fig 2.10 - Cross section of the curved sided fan (a) and tangencial runner (b) (adapted from [6]).

The main runner profile section is the same as the fan. In the main runner, it is important to notice that the section area have to remain constant throughout the runners.

## Overflows and venting

The overflows are typically found either in the last regions to be filled or in areas where air can be encircled away from other overflows originating high porosity region. Therefore, an early predition of a filling simulation is typically performed to predict the filling sequency of the casting.

The metal enters in the overflow through the outgate (the sum of all outgate areas represents half of the sum of all ingate areas), whose thicknessis presented in Tab 2.7. A large portion of overflow's volume is filled before the molten enters the vent region. The sum of all overflow's volume varies from 75% to 25% based on segment's volume, casting's thickness and required quality. The visual representation of an overflow is presented in Fig 2.11.

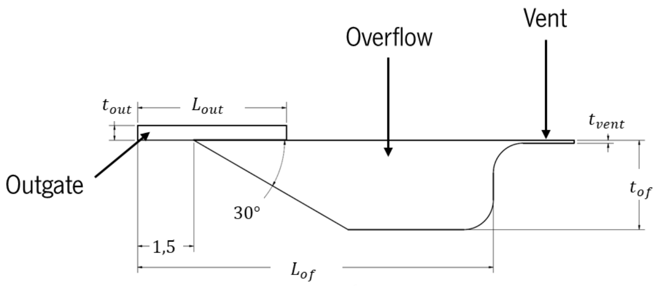


Fig 2.11 - Overflow overall dimensions (adapted from [68]).

Tab 2.7 - Outgate thickness (adapted from [59]).

| **Alloy** | $t_{out}$ $[mm]$ |
|---|---|
| Aluminum | 1< |
| Magnesium | 0.5< |
| Zinc | 0.5< |

The vents are extension of overflows to delay even further the molten metal, since these are region are the last to fill. Through the vents, the air is removed from the casting [68]. Therefore, vents must have high minor and major loss to delay the molten metal.

The vents area can be calculated based on the actual ingate area, [2.10]. Its thickness is typically 0.2 mm. Typically, the exit thickness is less half of the initial thickness.

$$A_{vent} = \frac{A_{ac,ing}}{4} \quad [2.10]$$

## 2.5. CHAPTER REFERENCES

[1] T. V. Sai, T. Vinod, and G. Sowmya, "A Critical Review on Casting Types and Defects," *IJSRSET*.

[2] H. S. Sodhi, "APPLICATION OF DIE CASTING: A REVIEW PAPER," *ReseachGate*, 2018. [Online]. Available: https://www.researchgate.net/publication/342349012_APPLICATION_OF_DIE_CASTING_A_REVIEW_PAPER

[3] M. S. Ramaprasad and M. N. Srinivas, "Permanent Molding of Cast Irons – Present Status and Scope," in *Science and Technology of Casting Processes*, M. Srinivasan, Ed.: InTech, 2012.

[4] M. Srinivasan, Ed., *Science and Technology of Casting Processes*: InTech, 2012.

[5] Rapiddirect, *Low Pressure Die Casting: A Simple Guide to Understand the Process.* [Online]. Available: https://www.rapiddirect.com/blog/low-pressure-die-casting/ (accessed: Sep. 19 2024.871Z).

[6] NADCA, *NADCA Gating Manual*. Illinois, United States of America: NADCA.

[7] Q. Hu, W. Guo, and H. Zhao, "Influence of wall thickness and intensification pressure on the microstructures and mechanical properties of AlSi7-SiC composites fabricated by the vacuum-assisted HPDC process," *Materials Science and Engineering: A*, vol. 819, no. 3, p. 141470, 2021, doi: 10.1016/j.msea.2021.141470.

[8] F. Bonollo, N. Gramegna, and G. Timelli, "High-Pressure Die-Casting: Contradictions and Challenges," *JOM*, vol. 67, no. 5, pp. 901–908, 2015, doi: 10.1007/s11837-015-1333-8.

[9] C. Bharambe, M. D. Jaybhaye, A. Dalmiya, C. Daund, and D. Shinde, "Analyzing casting defects in high-pressure die casting industrial case study," *Materials Today: Proceedings*, vol. 72, no. 4, pp. 1079–1083, 2023, doi: 10.1016/j.matpr.2022.09.166.

[10] G. M. Gonçalves, "Implementação de um Sistema de Controlo de Processo e Projeto de Coquilha numa Empresa de Fundição," Master's Degree Thesis, Escola de Engenharia, Universidade do Minho, Guimarães, 2014.

[11] H. Bakemeyer, *Operating the die casting: Machine.* [Online]. Available: https://www.dykast.com/user/files/operating_the_die_cast_machine.pdf (accessed: Sep. 15 2024).

[12] H. Liang and J. Qiao, "Analysis of Current Situation, Demand and Development Trend of Casting Grinding Technology," *MPDI*, 22 Sep., 2022. https://doi.org/10.3390/mi13101577

[13] G. Bar-Meir, *Fundamentals of Die Casting Design*. Illinois, United States of America, 2012. [Online]. Available: https://zenodo.org/records/8173341

[14] EKK Inc, *HPDC Gating Design.* [Online]. Available: http://www.ekkinc.com/consulting/gating-design/ (accessed: Mar. 22 2024.248Z).

[15] M. T. Murray and M. Murray, "High pressure die casting of aluminium and its alloys," in *Fundamentals of Aluminium Metallurgy*: Elsevier, 2011, pp. 217–261.

[16] Butler W. A., "Die Casting," *Encyclopedia of Materials: Science and Technology*, pp. 2147–2152.

[17] Mohamed Refaat Aboel-fotouh, Ahmed Shash, and Prof. Dr. Abd El-Halim El-Habak, "SEMI-AUTOMATED GATING SYSTEM DESIGN WITH OPTIMUM GATE AND OVERFLOW POSITIONS FOR HPDC," Philosophy degree, Unpublished, 2018. Accessed: Sep. 16 2024. [Online]. Available: https://www.researchgate.net/publication/330727487

[18] M. Okayasu, S. Yoshifuji, M. Mizuno, M. Hitomi, and H. Yamazaki, "Comparison of mechanical properties of die cast aluminium alloys: cold v . hot chamber die casting and high v . low speed filling die casting," *International Journal of Cast Metals Research*, vol. 22, no. 5, pp. 374–381, 2009, doi: 10.1179/174313309X380413.

[19] Oliveira, Steven Richerd Pires de, "High Pressure Die Casting of Zamak alloys," Master's Degree Thesis, Faculdade de Engenharia da Universidade do Porto, Universidade do Porto, Porto, 2018.

[20] Butler W. A., *Encyclopedia of Materials: Science and Technology: Die Casting (Permanent Mold)*. United States of America: Elsevier Science.

[21] Aços Ramada, *Camisas de Injeção.* [Online]. Available: https://www.ramada.pt/pt/aplicacoes/acos-ligas_/industria-automovel/moldes-de-fundicao/camisas-de-injecao.html (accessed: Mar. 22 2024.741Z).

[22] E. spa, *What is Cooling System in Die Casting Mold – What Affects the Cooling Rate of Die Casting.* [Online]. Available: https://www.diecasting-mould.com/news/what-is-cooling-system-in-die-casting-mold-what-affects-the-cooling-rate-of-die-casting (accessed: Sep. 16 2024.661Z).

[23] L. Maldonado, C. Shi, C. Sinclair, C. Vian, and J. Ostanek, "Rapid die preheating using a high-power infrared lamp array," *Elsevier*, 2022. [Online]. Available: https://pdf.sciencedirectassets.com/271641/1-s2.0-S1359431121X0018X/1-s2.0-S1359431121011455/main.pdf?X-Amz-Security-Token=IQoJb3JpZ2luX2VjEN7%2F%2F%2F%2F%2F%2F%2F%2F%2FwEaCXVzLWVhc3QtMSJIMEYCIQDLkbSXapp8qnu5hnNymbTWX6AkeRNyr40IsIgyIzknbwIhAIIaXhdPfxFT7gKbDuJdBMCiQ95XRODMGnddHArT304WKrMFCBcQBRoMMDU5MDAzNTQ2ODY1Igy16ImY19ezUpK6OfQqkAUJTprKeL2u2TCOYEfd8No5LuDn8KtnS7HEjQK%2F0%2B2DN%2BJJy6cXjhM36BYdIUDduflxO1RCi62XmPehua5tFIXssf2%2B9J5eQ8%2Frq2paSh4bIZCt9mKS93x70mDVeLmpwE8fgRcSq9O8f%2BLfEKD69isDeOaADbEwEgsdEYRHQ97h0CkOVRFaJ3OZiC5IooBK8xGQK3aW7fHPmXD60B4UGbfxRWd1aXnz%2BNqdJduZJf6FRa9Ia0gPgt91YFr38gjnsEZL8JpHOHsyfX8IsQZ%2FW%2B3Z18P4NkQY2OvD2527SX8BU

jX11E5MO71fWqdte1e434GWActjeWudLP6wxHZAcFOYvPvExc0XZrc7no%2B0nNxjT6xd4TafCnBHz
xb7UaYg8FFmkzHNWxN%2B6NqKBpR5KpGiyfV1O748VCx5t%2FIqWpc9aZm%2FwYTMtmSmhxbN
%2B3Q%2Fjo1D2PzQm4JIvLNCPk%2FRs%2F02GzRVjAsPXyDUc7y81iFASFcxkxGRmuICdgsU5hInp
Drq9xNM7tBAntrypI8%2F3I9BJTga6Z9aHM1IABMQD%2BT8m8v024f3RzIy%2Foo2H37hJISxIaTivO
UvxeaAMu07CP1v1PkXXDE02U5Efp597nXWNuK%2Bxj6DsXDu5PhyfjjwIxxI6krQxgnyByHyiyvEx0Lc
3H9hJN3cYnvgefyHbI4E8id%2FgjR6HV8bVDn%2BCUFdxpv%2BUhsh%2FAcEcN1CQPygRdJas9Ipd
Kn2N0wCecFZfR6eGI%2BqOUfRVYMtivoYnYUJhVvu7jn%2FcrICch6GSHJfPFqumopRq4eDZ%2FSQ
W9sQgduxHjI2C5Ffwy3886XD7Q6nsLgIp0teQPKR0Ee1gqIzBI9NX1F0UTqGPKcS%2FVI7SIe5sTDX
8qC3BjqwAf%2B%2BI2v%2F3tV1HJpKbQo%2FmWTI0ohrXRIL8ijxB048hRH8EZONhrXIgt4Yt17Nrkd
hj5isMhLG4MeZr7pU%2FIGQcQNWKC5CymCiwjktmDPfi%2FtFDCrWJizCi3DMQIZz0wMpI%2Fn1gxZ
Iqe8rDO4STbGuZmjRMONkm%2BRJK3IVvevGzifrGADmtdXgeYhQ5FYZ2HzUGwTUuS7uIU5jhMhIho
v9PvIPVOTIAx0RRCUdwzdD%2B52s&X-Amz-Algorithm=AWS4-HMAC-SHA256&X-Amz-Date=
20240916T151557Z&X-Amz-SignedHeaders=host&X-Amz-Expires=300&X-Amz-Credential=
ASIAQ3PHCVTYQC2DT7EW%2F20240916%2Fus-east-1%2Fs3%2Faws4_request&X-Amz-
Signature=d363799883566bdbf99146c1ac4b6e991f8b1af624d2b9845a6b2cdb3585c6a8&
hash=b2ca3136ca4096a270169a82c36c8c9bd376d8f2288e5e05438a2f043fb7ee42&host=
68042c943591013ac2b2430a89b270f6af2c76d8dfd086a07176afe7c76c2c61&pii=
S1359431121011455&tid=spdf-67ff3871-2bfb-425f-bf73-db8010f004b5&sid=
0d38888225c940461429a8d308fdc73cddd4gxrqb&type=client&tsoh=
d3d3LnNjaWVuY2VkaXJlY3QuY29t&ua=1e105a035355055556&rr=8c41d09b19fe692a&cc=pt

[24] A. Long, D. Thornhill, C. Armstrong, and D. Watson, "The Impact of Die Start-Up Procedure for High Pressure Die Casting," *SAE Int. J. Mater. Manf.*, vol. 6, no. 3, pp. 416–426, 2013, doi: 10.4271/2013-01-0829.

[25] A. Long, D. Thornhill, C. Armstrong, and D. Watson, "Predicting die life from die temperature for high pressure dies casting aluminium alloy," *Applied Thermal Engineering*, vol. 44, pp. 100–107, 2012, doi: 10.1016/j.applthermaleng.2012.03.045.

[26] P. Callegaro, *Comparative analysis of temperature control systems for high pressure die casting dies: Numerical methods for the thermal analysis of the HPDC process are needed to shorten the cost, the design and production time and the samples to involve in finding acceptable operating conditions.* [Online]. Available: https://www.enginsoft.com/expertise/comparative-analysis-of-temperature-control-systems-for-high-pressure-die-casting-dies.html (accessed: Sep. 16 2024.864Z).

[27] Foundry - Lexicon, *Mold Pre-heating*. [Online]. Available: https://www.giessereilexikon.com/en/foundry-lexicon/Encyclopedia/show/mold-pre-heating-4798/?cHash=e2c59dd4f61aed8272f325420b0d1bee (accessed: Sep. 16 2024.192Z).

[28] Piyanut Meethum and Chakrit Suvanjumrat, "Evaluate of Chill Vent Performance for High Pressure Die-Casting Production and Simulation of Motorcycle Fuel Caps," *MATEC Web Conf.*, vol. 95, p. 7025, 2017, doi: 10.1051/matecconf/20179507025.

[29] D. Minamide, K. Yano, M. Sano, and T. Aoki, "Automatic Design of Overflow System for Preventing Gas Defects by Considering the Direction of Molten Metal Flow," *Computer-Aided Design*, vol. 163, p. 103586, 2023, doi: 10.1016/j.cad.2023.103586.

[30] UPMOLD, *Casting Technique*. Estados Unidos da América: UPMOLD. Accessed: Jan. 5 2024. [Online]. Available: http://www.upmold.com/

[31] P. Szalva and I. N. Orbulov, "The effect of vacuum degree on the porosity and mechanical properties of die cast AlSi 9 Cu 3 (Fe) alloy," *Resolution and Discovery*, vol. 3, no. 2, pp. 33–38, 2018, doi: 10.1556/2051.2018.00061.

[32] Q. Han, C. Vian, and D. Siu, "Casting Quality Comparison: Verical vs HorizontalHPDC," *ReseachGate*, 2017. [Online]. Available: https://www.researchgate.net/publication/366696493_Casting_Quality_Comparison_Vertical_vs_Horizontal_HPDC

[33] *Tool steels*, 4957:2000, Slovenski Standard; International Standard Organization, Slovakia. [Online]. Available: https://standards.iteh.ai/catalog/standards/sist/e3a193ff-daea-42ba-872a-dc409ccee5c6/sist-en-iso-4957-2018

[34] Otai Special Steel, *P20 Steel Plate | 1.2311 | 3Cr2Mo | Plastic Mold Tool Steel.* [Online]. Available: https://www.astmsteel.com/product/p20-steel-plate-1-2311-3cr2mo-mold-tool-steel/ (accessed: Mar. 22 2024.423Z).

[35] Otai Special Steel, *H21 Tool Steel | 3Cr2W8V | SKD5 | X30WCrV9-3 | 1.2581 | 2730 Tungsten steel - Special steel china supplier-OTAI Special Steel.* [Online]. Available: https://www.otaisteel.com/products/hot-work-tool-steel/h21/ (accessed: Mar. 22 2024.466Z).

[36] Virat, *H13 steel | DIN 2344 | 1.2344 steel | H13 Die Steel Supplier | AISI H13.* [Online]. Available: https://www.viratsteels.com/h13.html (accessed: Jul. 1 2024.661Z).

[37] T. Xometry, "H13 Tool Steel: Uses, Composition, Properties," *Xometry*, 09 Sep., 2023. https://www.xometry.com/resources/materials/h13-tool-steel/ (accessed: Mar. 22 2024.938Z).

[38] Multiview, *Silicon: Increasing the Properties of Aluminum and Copper Alloys.* [Online]. Available: https://www.belmontmetals.com/silicon-increasing-the-properties-of-aluminum-and-copper-alloys/ (accessed: Sep. 5 2024.184Z).

[39] H. R. Thresh, *The viscosity of pure liquid zinc. Determined by oscillating a cylindrical vessel: Physical Metallurgy Division*. Ottawa, Canada: Department of mines and techincal surveys, 1964.

[40] A. T. Dinsdale and P. N. Quested, "The viscosity of aluminium and its alloys—A review of data and models," *Journal of Materials Science*, pp. 7221–7228.

[41] B. Callegari, T. N. Lima, and R. S. Coelho, "The Influence of Alloying Elements on the Microstructure and Properties of Al-Si-Based Casting Alloys: A Review," *Metals*, vol. 13, no. 7, p. 1174, 2023, doi: 10.3390/met13071174.

[42] H. Mehdi, "Effect of Silicon content on the Mechanical Properties of Aluminum Alloy," 2015. [Online]. Available: https://www.researchgate.net/publication/282704257_Effect_of_Silicon_content_on_the_Mechanical_Properties_of_Aluminum_Alloy

[43] MatWeb, *Aluminum A360.0-F Die Casting Alloy.* [Online]. Available: https://www.matweb.com/search/datasheet.aspx?MatGUID=87a0d0817ebd44008a967cbf3e9cd378 (accessed: Feb. 5 2024.705Z).

[44] MatWeb, *Aluminum A390.0-T6, Permanent Mold Cast.* [Online]. Available: https://www.matweb.com/search/datasheet.aspx?MatGUID=2bb0732f70724d9787d277fec128cc29 (accessed: Feb. 5 2024.905Z).

[45] MatWeb, *Aluminum A380.0-F Die Casting Alloy.* [Online]. Available: https://www.matweb.com/search/DataSheet.aspx?MatGUID=5f92a8f7d6ad416c8ce9398cae14a363 (accessed: Feb. 5 2024.553Z).

[46] MatWeb, *Aluminum 384.0-F Die Casting Alloy.* [Online]. Available: https://www.matweb.com/search/datasheet.aspx?MatGUID=392ac894c0d642c0947f8d6b975d55de (accessed: Feb. 5 2024.206Z).

[47] MatWeb, *Aluminum A356.0-T6, Sand Cast.* [Online]. Available: https://www.matweb.com/search/datasheet.aspx?MatGUID=d524d6bf305c4ce99414cabd1c7ed070 (accessed: Feb. 5 2024.071Z).

[48] MatWeb, *Magnesium AM60B-F, Die Cast.* [Online]. Available: https://www.matweb.com/search/datasheet.aspx?matguid=f311ea86cd814ff8b7a70efb42eb9f41 (accessed: Feb. 5 2024.793Z).

[49] MatWeb, *Magnesium AZ91D-F, Cast.* [Online]. Available: https://www.matweb.com/search/datasheet.aspx?matguid=07baafbb9c364fb18fd413bceced867f (accessed: Feb. 5 2024.378Z).

[50] MatWeb, *Magnesium AM50A-F, Die Cast.* [Online]. Available: https://www.matweb.com/search/DataSheet.aspx?MatGUID=a39cbb3aee8944259f0146ec21cbbfcf (accessed: Feb. 5 2024.057Z).

[51] MatWeb, *Zinc ZA-27 (Zn-27Al-2Cu-0.015Mg), Sand Cast.* [Online]. Available: https://www.matweb.com/search/datasheet.aspx?matguid=5c017f3a462c44fa8a5eb71b2e304d96 (accessed: Feb. 5 2024.562Z).

[52] MatWeb, *Zinc AG40A (Zinc Alloy 3; Zn-4Al-0.4Mg; Zamak 3), Cast.* [Online]. Available: https://www.matweb.com/search/DataSheet.aspx?MatGUID=bb106cf30fba409d9a18bfb7e0a2bc79 (accessed: Feb. 5 2024.058Z).

[53] MatWeb, *Zinc Alloy 7; AG40B; Zn-4Al-0.015Mg; Zamak7.* [Online]. Available: https://www.matweb.com/search/datasheet.aspx?matguid=94693e4ab7a54246965309d0c0af803f (accessed: Feb. 5 2024.697Z).

[54] Dynacast, *Zamak 5 Properties | Zinc Alloy 5 | Dynacast.* [Online]. Available: https://www.dynacast.com/en/knowledge-center/material-information/zinc-casting-metals/zamak-5 (accessed: Feb. 5 2024.171Z).

[55] Become a master of CAD Design, *What is injection phase of HPDC Die Casting | Die Casting.* [Online]. Available: https://www.youtube.com/watch?app=desktop&v=SG3xR9d7IPM (accessed: Sep. 5 2024.122Z).

[56] R. b., T. Nallusamy, and M. B. Bhaskar, "injection Parameter Setting in High-Pressure Die Casting," *Journal of Polymers & Composites*, 2024. [Online]. Available: https://www.researchgate.net/publication/379955232

[57] W. YU, Z. YUAN, Z. GUO, and S. XIONG, "Characterization of A390 aluminum alloy produced at different slow shot speeds using vacuum assisted high pressure die casting," *Transactions of Nonferrous Metals Society of China*, vol. 27, no. 12, pp. 2529–2538, 2017, doi: 10.1016/S1003-6326(17)60281-4.

[58] J. G. Fairman, *Experiment on Fluids.* [Online]. Available: https://www.grc.nasa.gov/www/k-12/WindTunnel/Activities/exper_on_fluids.html (accessed: Apr. 15 2024.220Z).

[59] NADCA, *NADCA Gating Manual.* Illinois, United States of America: NADCA.

[60] A. Ruggles, "P-Q Squared Analysis," *FLOW-3D*, 27 Oct., 2015. https://www.flow3d.com/p-q-squared-analysis/ (accessed: Sep. 9 2024.093Z).

[61] Genick Bar-Meir, "Intensification Pressure in Die Casting," 2023, doi: 10.5281/ZENODO.7925440.

[62] Wikipedia, *Pascal's law.* [Online]. Available: https://en.wikipedia.org/w/index.php?title=Pascal's_law&oldid=1211459295 (accessed: Mar. 23 2024).

[63] V. Deev *et al.,* "Effect of Melt Overheating on Structure and Mechanical Properties of Al-Mg-Si Cast Alloy," *Metals*, vol. 11, no. 9, p. 1353, 2021, doi: 10.3390/met11091353.

[64] NADCA, *NADCA Product Specification Standards for Die Casting: Aluminum, Aluminum-MMC, Copper, Magnesium, Zinc and ZA Alloys,* 9th ed. Illinois, United States of America: NADCA, 2015.

[65] M. Petric, P. Mrvar, and L. Lavtar, "Optimization of cooling-heating system in HPDC tools," *ResearchGate*, 2016. [Online]. Available: https://www.researchgate.net/publication/309647490

[66] K. Dou, E. Lordan, Y. J. Zhang, A. Jacot, and Z. Y. Fan, "A complete computer aided engineering (CAE) modelling and optimization of high pressure die casting (HPDC) process," *Journal of Manufacturing Processes*, vol. 60, pp. 435–446, 2020, doi: 10.1016/j.jmapro.2020.10.062.

[67] V. Kumar and J. Madan, "A system for computer-aided gating design for multi-cavity die-casting dies," *Proceedings of the Institution of Mechanical Engineers, Part B: Journal of Engineering Manufacture*, vol. 231, no. 11, pp. 1983–1999, 2017, doi: 10.1177/0954405415614727.

[68] J. Majerník, M. Podařil, and D. Gojdan, "Influence of Overflow Connecting Channel Cross-Section Design on Selected Parameters of High Pressure Die Casting," *Archives of Foundry Engineering*, pp. 75–80, 2020, doi: 10.24425/afe.2021.136101.

# Chapter 3 - HIGHLY EFFICIENT LABOUR SAVING PROGRAM GATING DESIGN

The title of this dissertation is referent to the 3D modelling of the die casting process. For this purpose, it was choosen a CAD software (Autodesk Inventor [1]) which macro programming was open to the public and a programming language (Python) which could communicate with to conceive a software capable of modelling the gating design. Later on, the developed software was baptised as H.E.L.P. Gating Design an acronym for Highly Efficient Labor-saving Program Gating Design.

The methodology used in this software was the NADCA methodology (described in chapter 2.4) which gave the programmer possibility to translate the entirety of the high pressure die casting process information in a form of a programming language, since it was well structured and continuous. Initially, H.E.L.P. Gating Design database was based exclusively on NADCA information. However, it was given the capacity to the software to adapt and allow the user to add information to keep up with the current challenges.

In Fig 3.1 is shown the logical sequence of calculations. Due to its loyal algorithm to the NADCA gating design, each step shown is directly related to the calculations step of NADCA manual.

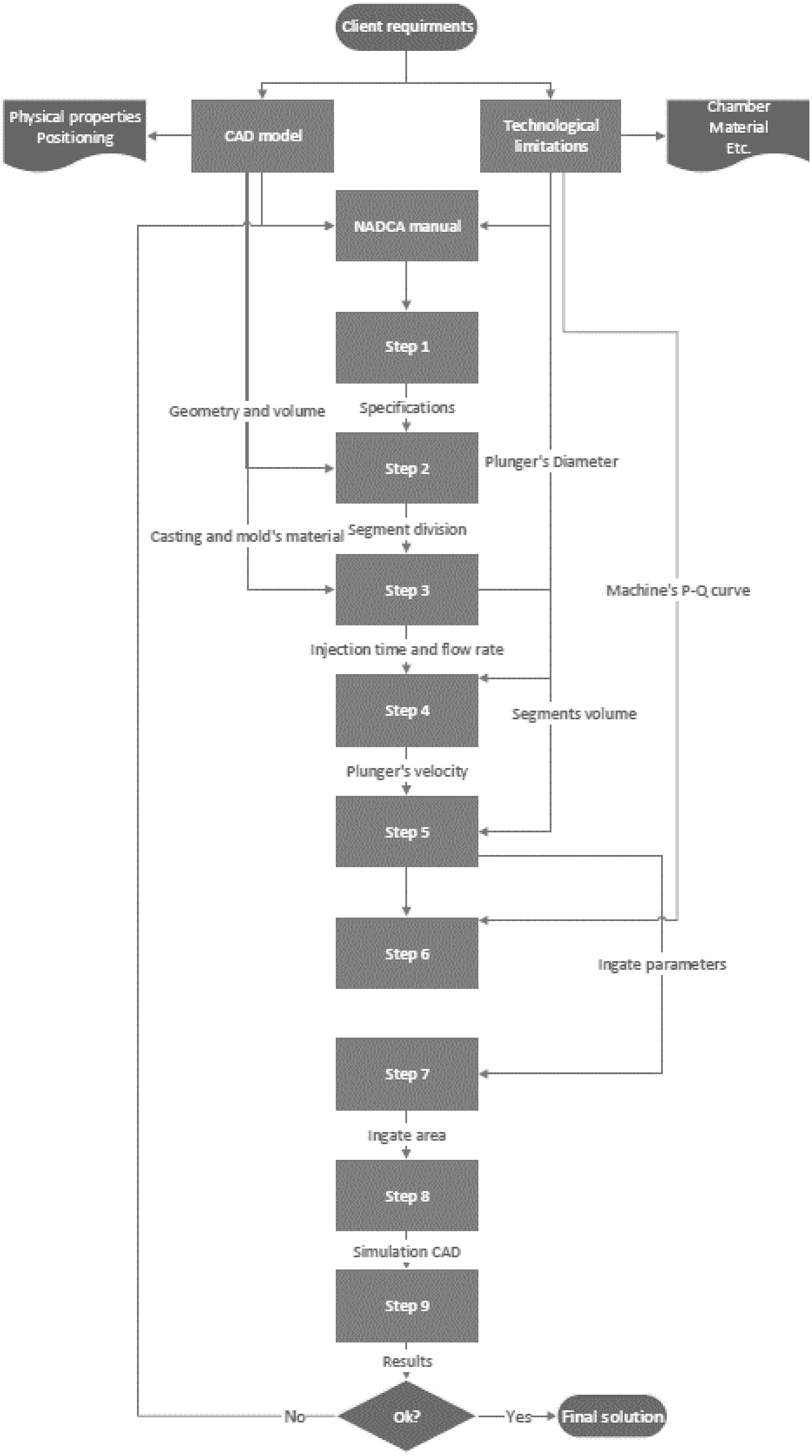


Fig 3.1 – The NADCA methodology was utilized in the development of H.E.L.P. Die Casting.

A previous study of the path to be taken in order to match the proposed challange was made and the following reasons defined the programming language and the CAD software:

- Python is indeed a widely used programming language, as it is a high-level language that is easy to learn and has an excellent interface with any type of database/data storage software, including Excel. Another reason for using Python is the possibility of the software also interfacing with CAD software [2].
- The program is only available for Autodesk Inventor. To make it compatible with SolidWorks, it would be necessary to "translate" the language to Virtual Basic for Applications (VBA). For Autodesk Fusion 360, only a slight change in keywords is needed since the core modeling program is similar to that of Autodesk Inventor, as both software are developed by the same company..
- Another near-solution for programmed modeling is to have the model fully parameterized linked to an Excel spreadsheet, then an overwrite of these parameters would be made. However, this is not a viable solution. According to the content studied in the NADCA's "Gating Design" manual, there are various models for gating—Curved Sided Fan, Straight Sided Fan, and Tangential Runner. Considering the different scenarios, the number of files to be parameterized could exceed 48 different scenarios (excluding the various parameter values). This would make it impractical to have software with 48 associated CAD files to calculate a single situation—the one requested by the user—with at least 41 parameters to be filled out in every CAD file.

## 3.1. SYSTEM REQUIREMENTS

The development of H.E.L.P. Die Casting was conceived for a one-user only, which in this scenario is it's author, the software ergonomics was not the main concern during its development. So a organization model was simplified which can be divided into 3 main folders, Fig 3.2. In the folders "Excels", "Figures" and "Parts" are stored the databases in Excel file (".xlsx"), figures used in the software to help the user to fill the gating parameters and 3D model of gating design and overflow, respectively. The Python files, which are responsible for the software itself, are presented in Tab 3.1.

A new folder, QuikCast Macro, was being developed in the free time of this dissertation which main goal was to allow the user to save time. In this macro folder, a new macro was conceived to help the user at defining the boundary conditions in Visual-Cast. This macro stablished all the boundary conditions after defining the surfaces where they would be attributed.

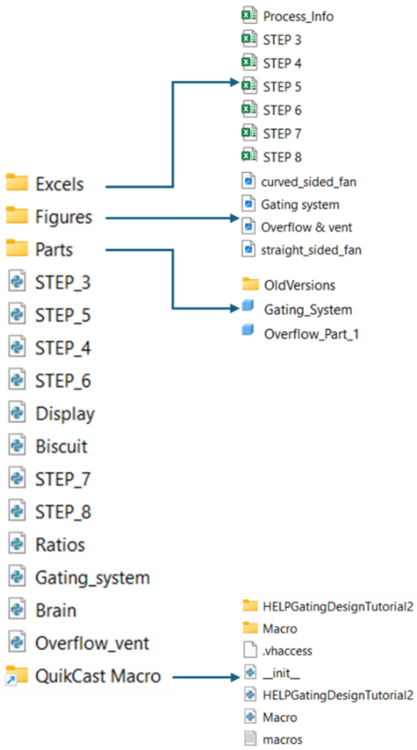


Fig 3.2 - Organization of H.E.L.P. Gating Design.

Tab 3.1 – Function of each Python file.

| **Python file** | **Function** |
|---|---|
| **Biscuit** | Generates the 3D model of the biscuit |
| **Brain** | Initializing file and is the bridge for every file |
| **Display** | Interface HELP Gating Design – user |
| **Gating System** | Generates the 3D model of the gating design |
| **Overflow_vent** | Generates the 3D model of the overflow |
| **Ratios** | Provides ratios for a proportional of the gating system |
| **STEP_X** | Calculates every step's variables based on input |

As a consequence of unecessary user-friendliness, there are some pre-requirements are needed in order to run the program which can be allocated in two main groups:

- Files location: The software is designed to write information to an external database (Excel, in this case) stored in the same folder as the executable. In addition to the database, other folders, such as 'Figures' and 'Parts,' used by the software require their file locations to be specified;

- Python libraries: the Python libraries is a requirement only to the user who runs the Python files instead of an executable or an installable. In such cases, Python libraries are annexed to the program increasing the file size.

**Files location**

The file directory could be a variable which the user could define. However due to its time-consuming activity of searching for its location and one user-only, another approach was choosen. It was defined a fixed folder was defined to facilitate the file's search (Fig 3.3). If the program was converted into an installable, this problem would be supressed, since during the installation it is defined a permanent file directory.

In Fig 3.3, the variable "rootDir" could be changed based on the user's file location. In this case, the file to find is in the excel folder (Fig 3.2). If this variable is empty (notation is: "") the program would have to search for the desired file in the entire computer storage, increasing the time consumption (aout 30 seconds everytime it was required to open a new file).

```
def Encontrar_Excel(Ficheiro):
    fileToSearch = Ficheiro
    rootDir = r"C:\Users\nelso\OneDrive - Universidade do Minho\Programa\Excels"
    for (
        relPath,
        dirs,
        files,
    ) in os.walk(rootDir):
        if fileToSearch in files:
            fullpath = os.path.join(rootDir, relPath, fileToSearch)
    return fullpath
```

Fig 3.3 – Block code which searches for each file in a fixed folder.

**Python libraries**

As mentioned previously, Python libraries required a previous installation if the user intends to run the program from a Python file. In Tab 3.2 is presented all libraries required to create the software. It is worth mentioning that libraries such as "numpy" and "math" were not mentioned, since they were pre-installed when downloading Python.

The "tkinter" library [3] allows programmers to design a functional GUI that enhances the HELP Gating Design user interface, making it more user-friendly. Without this interface, users would need to input all parameters through a command terminal.

The "openpyxl" library [4] is responsible for reading and writing Excel files. It handles data input provided by the user and is utilized during the modeling phase. While entering data into the filling system, the Excel files must remain closed, as the program needs to save the data and close Excel during execution. However, during the modeling phase, users can access the Excel files.

The "OS" library [5], short for "operating system," is included with the Python installation. Its presence should be confirmed, as it facilitates communication between Python and the computer. This library is used to locate files that the software needs to read or write, such as Excel sheets or images for the GUI. Similarly, the "win32com.client" library [6] is derived from the computer's operating system and allows Python to access all applications installed on the computer.

To run the software without having to open any Python file, those files can be compiled and then executed just like a generic application with “Auto Py-to-Exe” library [7].

Tab 3.2 – Required libraries.

| Library | Function |
|---|---|
| **tkinter** | Interface Python – User |
| **openpyxl** | Interface Python – Excel |
| **os** | Interface Python – System 32 |
| **win32com.client** | Interface Python – Inventor |
| **Auto Py-to-Exe** | Create an executable file of the program |

## 3.2. INTERFACE USER - SOFTWARE

In the design of the Guided User Interface (GUI), the programmer ensured that the information required from the user was organized in a way that minimized the number of windows the user would need to fill out. The arrangement of the information was carefully considered to reduce the number of steps needed for user input. For instance, the software needs to be informed about the two points that define the machine's curve (required for step 6) (Fig 3.4, parameter (g)) before it receives information about the volume of the part (required for step 3) (Fig. 4.5, parameter (a)).

In the initial GUI (Fig 3.4), the user first specifies the type of chamber, based on the material to be used (parameters (a) and (b)), the mold material (parameter (c)), the average thickness of the thinnest walls (parameter (d)), the number of parts in each mold (parameter (e)), and the piston diameter (parameter (f)). The machine’s parameters (parameter (g)) units for pressure and flow rate are MPa and l/s, respectively.

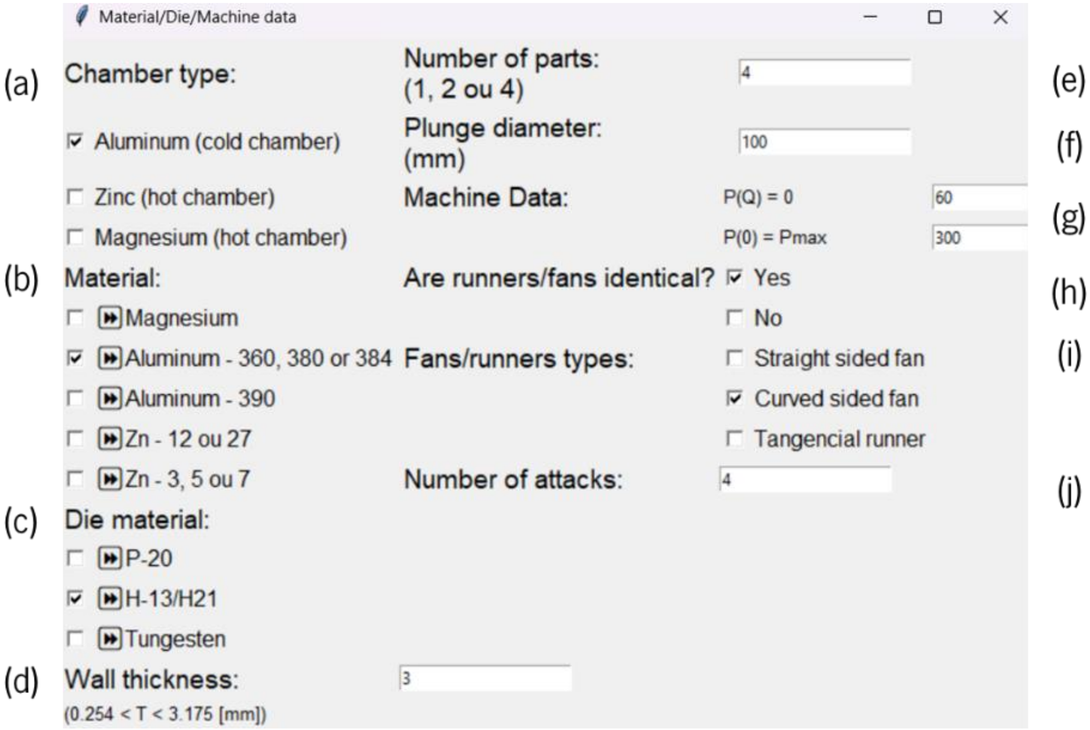


Fig 3.4 - First GUI layout which the user will fill.

The last three parameters, (h), (i), and (j), are related to the type/number of gates that will be applied to the part. If the parts are identical and have identical gates, parameter (h) should be set to "Yes." This will reduce the amount of data that needs to be introduced, as the software will automatically apply the same parameters to all the gates.

Depending on the type and number of gates, it may be necessary to input variables that are not common to all approaches, such as the orientation of the gates (parameters (d), (e) and (f) in Fig 3.5) when there is more than one attack. If there is more than one attack, the H.E.L.P. Gating Design provides functionality to calculate the gate layout, ensuring there are no geometric incompatibilities between the parts. To perform this calculation, additional information about the mold plate alignment and the part is required (Fig 3.7).

However, certain variables must be defined regardless of the approach, such as volume, entry velocity, and the runner-to-ingate ratio (parameters (a), (b), and (g) in Fig 3.6).

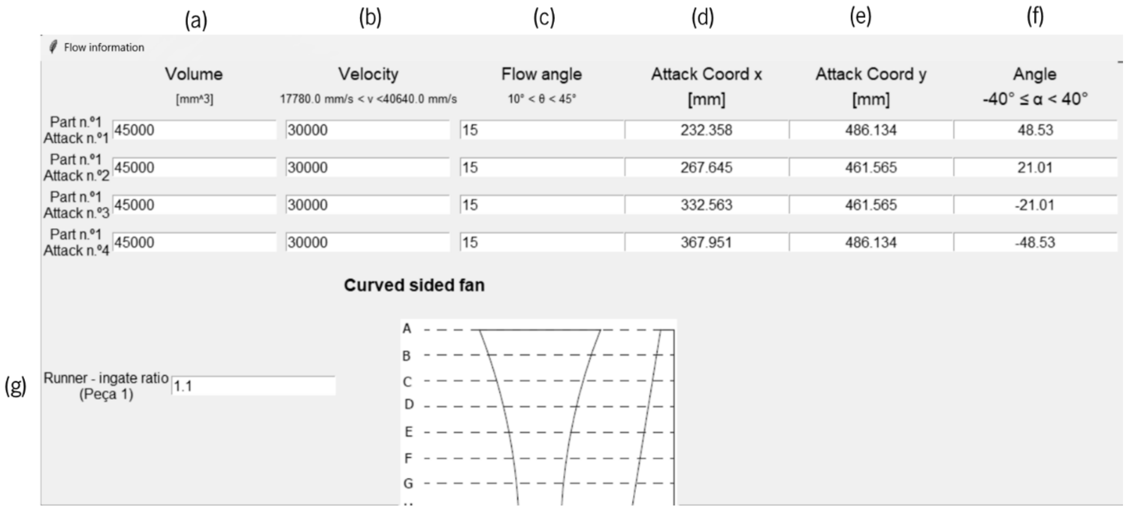


Fig 3.5 - Second GUI layout which the user will fill for a scenario of 4 attacks to 4 equal parts using a curved sided fan.

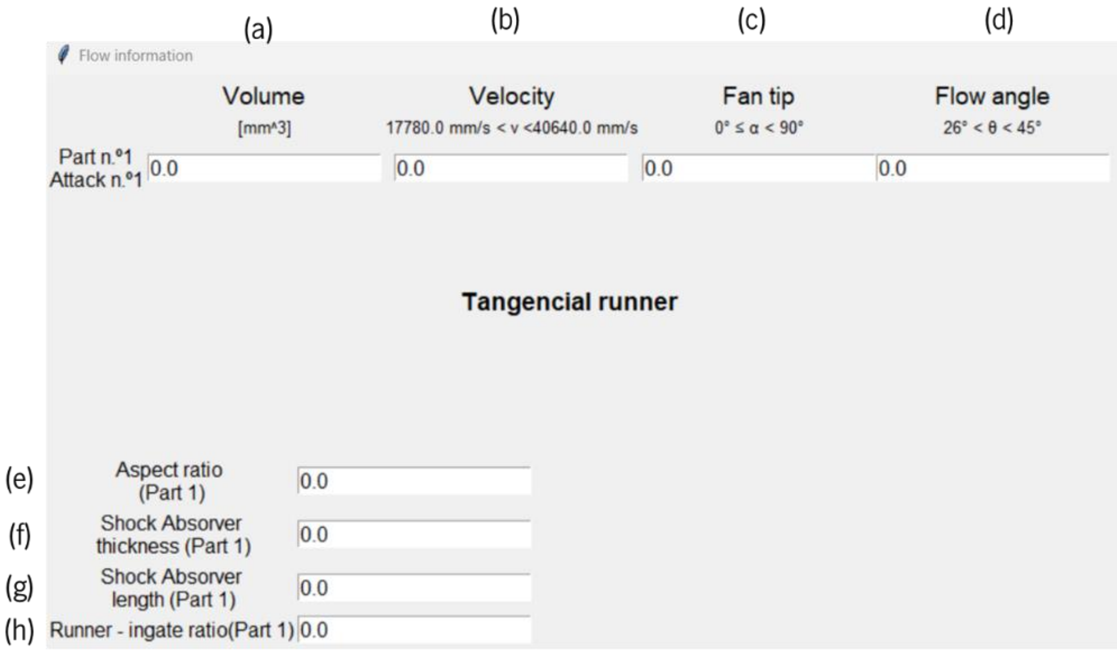


Fig 3.6 - Second GUI layout which the user will fill for a scenario of 1 attack to 4 equal parts using a tangential runner.

In the third GUI (Fig 3.7), the alignment of the mold and the part is defined (parameters (a) and (b)), along with the information required to set up the air removal system and the final casting quality (parameter (c)). The combine overflow volume is based on the parts volume, following NADCA methodology. Defining its length and number of overflows, the implicit variable is the width of the overflow.

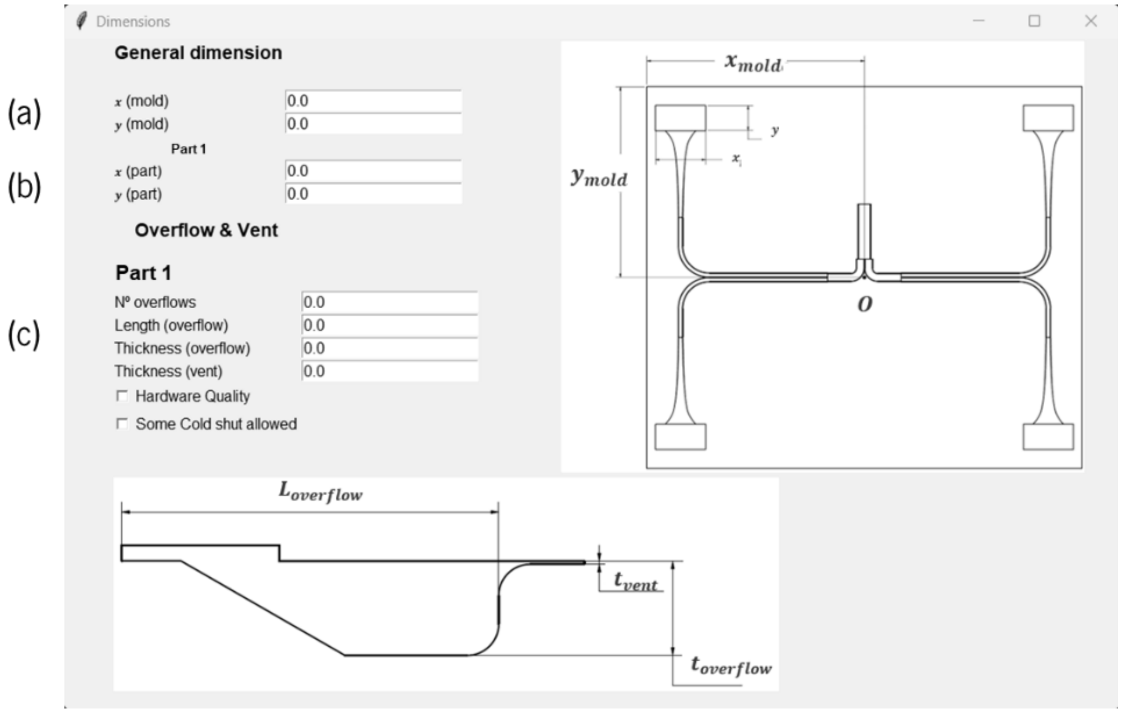


Fig 3.7 - Third GUI which the user might fill.

## 3.3. WORKFLOW

The recommended workflow using this software passes through three main phases, as it is presented in Fig 3.8.

The first step, initial decisions, is based in understanding the components geometry and prepare it to the casting process, such as dividing the component in segments and the attacks' location, applying drafts and fillets, definition of parting line, etc. As auxiliay tool, a solidification simulation may be performed to determine the exact location of the hotspots to the definition of the cooling system. This simulations is a mere approximation of the real casting conditions.

The second phase, the gating design phase, is the where the H.E.L.P. Die Casting software is applied to reduce time consumption of the user. The process's data is stored in databases which will be used lately in the die casting simulation.

The gating design phase is the most complex phase, since it evolves the manipulation of CAD files with excel which both work as data storage and database (Fig 3.2). To distinguish the worksheets that serve as database from those which are data storage, the designation format is "Table X, Page X". This format was based on what page and which table the data was in the NADCA Manual.

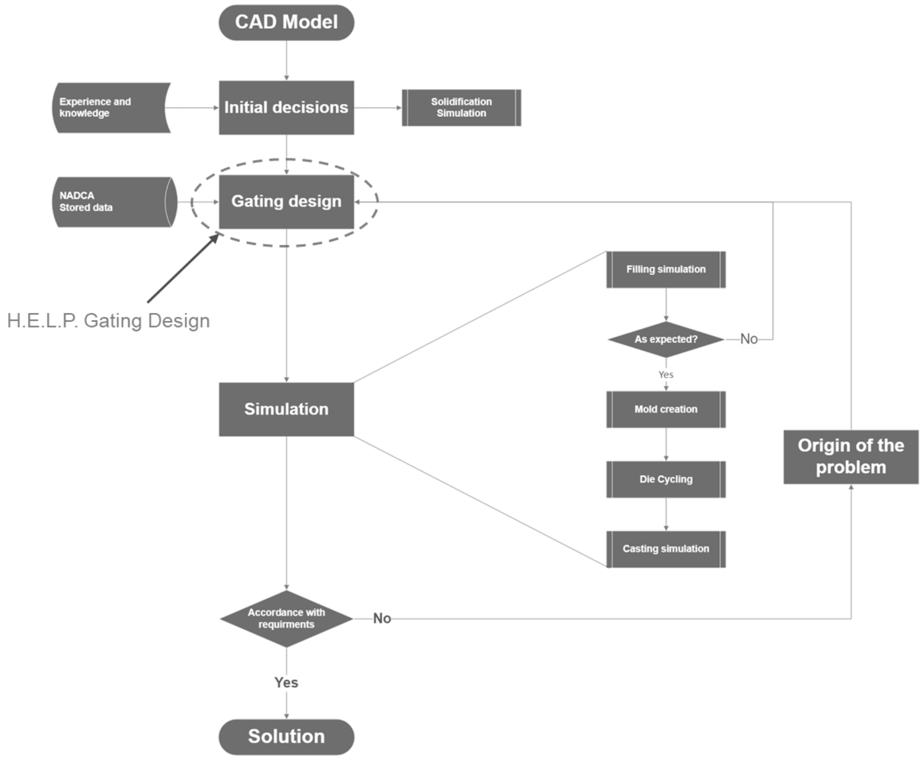


Fig 3.8 – Workflow of gating design and the positioning in the iterative process H.E.L.P. Gating design software.

In a detail view, in this phase is generated two CAD files, the Gating Design and the overflows, and stored information of the process introduced by the user and postprocessed by the H.E.L.P. Gating Design. The file "STEP_3"'s function is to provide information of constant values to the calculation of the injection time, as well as the flow rate for different segments. This information is presented in different worksheets if the part presents more than one segment. The file "STEP_4"'s function is to determine an approximation of ingate dynamic pressure and plunge speed. This information can be lately compared and corrected with the $PQ^2$ analyis in "STEP_6" file, to determine the actual shot velocity (this step can be replaced based on CAE postprocessing). The file "STEP_7" and "STEP_8" are related to the attacks section dimensions and overflows, respectively. These last 2 files are exclusively to data storage.

As a result of a programmed CAD modelling, some details as well as the assembly require to be done manually. These details include adding fillets, removing emboss, correcting the ingate section as it is presented in Fig 3.9 as well as the assembly. This is the easiest part of the gating design where the user takes a few minutes to make small changes and the assembly (assembly of the following components: gating design and overflow and part)depending on the user experience to the software.

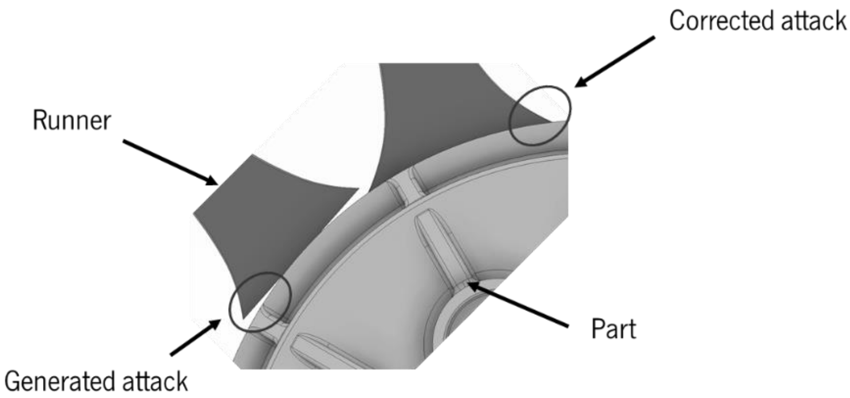


Fig 3.9 - Attack correction in a round surface.

The simulation process can be divided in three simulations to save computation time. The first simulation is to verify the filling pattern and sequency to guarantee that the overflows are located in key regions where the air can be encircled and trapped within the casting. This simulation only deals with the filling simulation module, considerating that the fluid's temperature remain constant throughout the filling simulation (ending when the die cavity is full).

If the first simulation's results are satisfactory, the second simulation shall be done before the casting simulation, the die cycling simulation. This simulation only deals with the solification of the casting, which provides the casting simulation a more accurate die's thermal field.  The third simulation consists in using the die's therm field from the die cycling simulation as initial conditions for the mould for the die casting simulation.

## 3.4. CHAPTER REFERENCES

[1] Autodesk, *Inventor*. Autodesk, 2023. [Online]. Available: https://www.autodesk.com/products/inventor/overview?term=1-YEAR&tab=subscription

[2] B. Ekins, *Inventor API Object Model*. California, United States of America: Autodesk. Accessed: Feb. 5 2024. [Online]. Available: https://www.autodesk.pt/

[3] A. D. Moore, *Python GUI Programming with Tkinter: Develop responsive and powerful GUI applications with Tkinter*. Birmingham: Packt Publishing, 2018. [Online]. Available: https://search.ebscohost.com/login.aspx?direct=true&scope=site&db=nlebk&db=nlabk&AN=1813737

[4] C. Clark and E. Gazoni, *openpyxl - A Python library to read/write Excel 2010 xlsx/xlsm files — openpyxl 3.1.2 documentation.* [Online]. Available: https://openpyxl.readthedocs.io/en/stable/ (accessed: Feb. 5 2024.421Z).

[5] Python documentation, *OS: Miscellaneous operating system interfaces.* [Online]. Available: https://docs.python.org/3/library/os.html (accessed: Aug. 19 2024.878Z).

[6] Python Package Index, *pywin32.* [Online]. Available: https://pypi.org/project/pywin32/ (accessed: Aug. 19 2024.402Z).

[7] B. Vollenbregt, *auto-py-to-exe 2.42.0.* [Online]. Available: https://pypi.org/project/auto-py-to-exe/ (accessed: Feb. 5 2024.428Z).

# Chapter 4 - CASTING SIMULATION

In the past years, Computer Aided Engineering (CAE) provided manufacturers with the best cost-effective operations. CAE eliminated the need to build multiple prototype to verify the concept before large scale production [1, 2].

The casting processes was one of the most benefitted manufacturing sector, since the gating design is an iterative process. The application of CAE allowed reducing shrinkage scrap, optimazing the gating system and predict thermal fatigue life and costs. These softwares can predict possible defects such as shrinkage and air porosity and its location, process variables, etc.. Since this predition is based on a mathematical model, there are some differences between the mathematical model and the physical model which may result in errors. In order to minimize the errors CAE engineers need to define the problem accurately.

Even though with this sort of technological advances in the casting simulation, simulation results and prior knowledge and experience complement each other and can not be seen as rivals in finding the best solution the in the best time possible (Fig 4.1). The first step of the iterative process is the result of the prior knowledge. Meanwhile, simulation results impact in finding with accuracy a better solution.

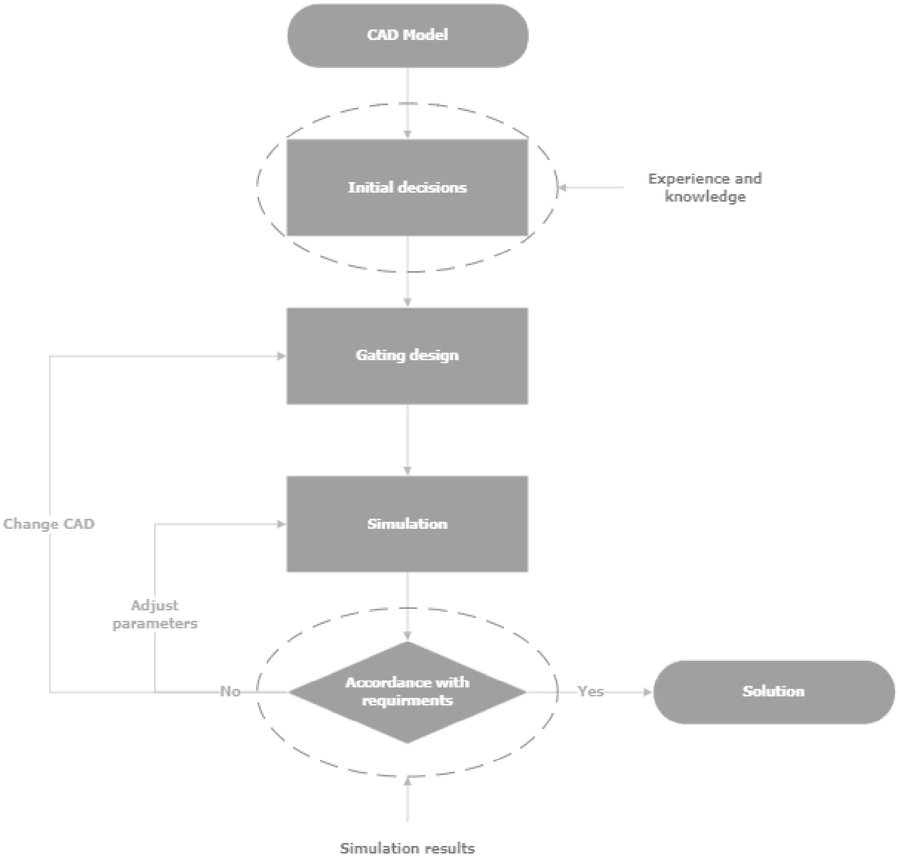


Fig 4.1 - Flowchart to generate a gating design (adapted from [2]).

## 4.1. CASTING AND MOLD MATERIALS

In die casting process, the using materials are seperated in two groups, the casting material and mold materials. The casting material is used to produce the casting, these have to heaten up in order to surpass its liquidus temperature. Meanwhile, the mold materials are used to produce the mold.

The application of these materials is very distinguished, consequently the requirements of each other are very different. For example, casting materials for high-pressure applications require fluidity and themal inertia. In other hand, the mold materials require wear resistance and excellent mechanical properties at high temperatures as well as thermal inertia and conductivity.

Even though thermal inertia is a characteristic present in both alloys, this property avoids an early solidification for the casting alloy. Meanwhile this property and the thermal conductivity reduces mold's heat losses avoiding the needing of re-heating the mold [3].

The mold materials used were H13 and tool steel 18Ni300. The steel H13 is used in mold's frame which manufacturing technology was machining. This alloy is typically used in High Pressure Die Casting and Low Pressure Die casting for its thermo-mechanical properties. The steel

18Ni300 is used in the additive manufacturing of inserts of the die cavity which would originate the component.

The mold's materials impact the thermal field and cooling during the solidification process. Since these materials do not reach its solidus temperature, the flow properties of these alloys do not required the definition of its viscousity. The thermal properties to be defined are the density, specific heat and thermal conductivity.

### Steel H13

The steel H13 is presented in the german standards (DIN 2344). It is a high alloyed tool steel as it is possible to verify in Tab 4.1 known for its wearing resistance and good mechanical properties in high temperature conditions [4].

Tab 4.1 - Chemical composition of steel H13 [5].

| **Element** | **C** | **Cr** | **Mn** | **Mo** | **Si** | **V** |
|---|---|---|---|---|---|---|
| **wt (%)** | 0.45 | 5.13 | 0.35 | 1.43 | 1.00 | 1.00 |

In Fig 4.2 (a) and (b), it is shown the properties' thermal behaviour with data from QuikCast libraries of thermal conductivity ($K$) and thermal inertia (product of the multiplication of density ($\rho$) by specific heat ($C_p$)).

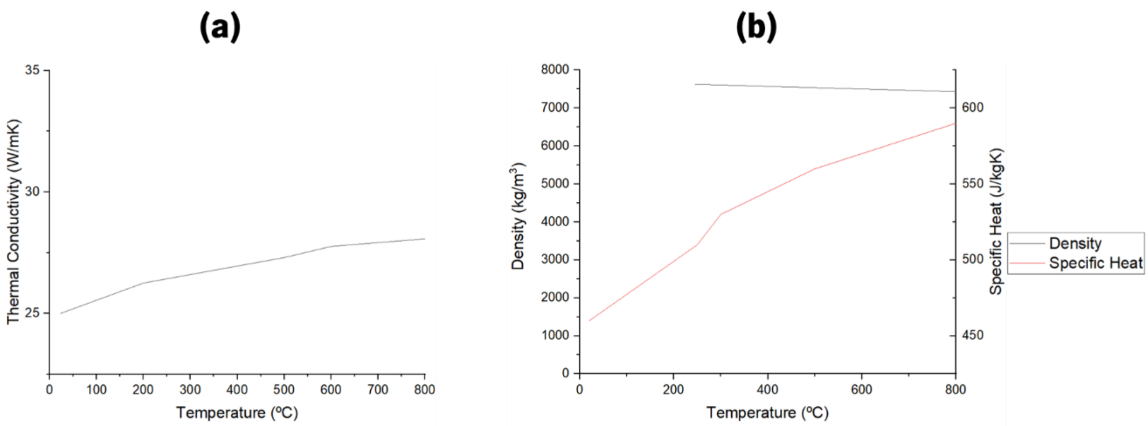


Fig 4.2 - Thermal behaviour of H13 (adapted from [5]). (a) – Temperature effect on thermal conductivity; (b) – Temperature effect on density and specific heat.

**Steel 18Ni300**

Steel 18Ni300 designation by european standards is 1.2709 [6, 7]. It is known for its good mechanical properties and usage in additive manufacturing (some companies provide it in powder form). Its chemical composition is shown in Tab 4.2 [8]. Its thermal conductivity and thermal inertia properties are shown in Fig 4.3 (a) and (b), respectively.

Tab 4.2- Chemical composition of steel 18Ni300 (adapted from [5]).

| Element | C | Co | Cr | Mn | Mo | Ni | Si | Ti | V |
|---|---|---|---|---|---|---|---|---|---|
| wt (%) | 0.03 | 10.00 | 0.25 | 0.15 | 5.20 | 19.00 | 0.10 | 1.20 | 1.00 |

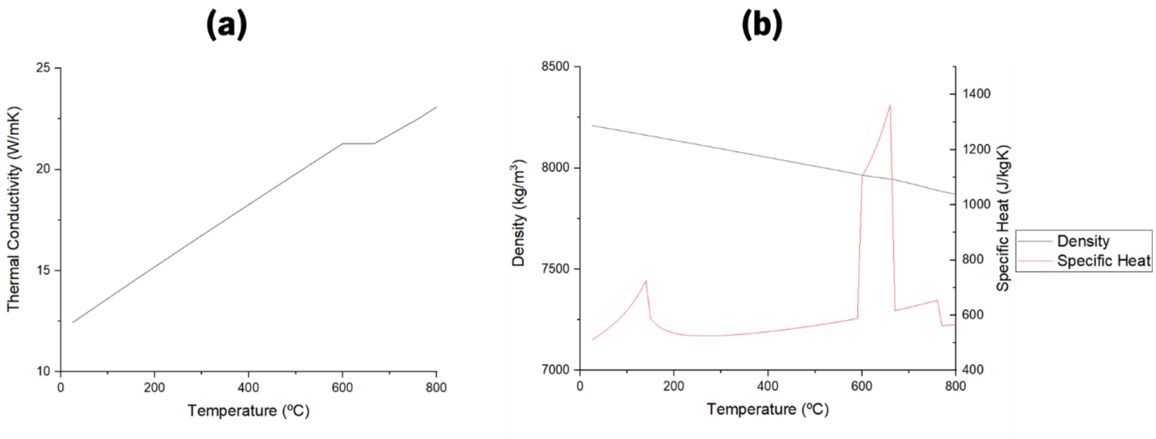


Fig 4.3 - Thermal behaviour of 18Ni300 (adapted from [5]). (a) – Temperature effect on thermal conductivity; (b) – Temperature effect on density and specific heat.

**Alloy $AlSi_9Cu_3(Fe)$**

The casting material is the aluminium based alloy ISO $AlSi_9Cu_3(Fe)$ which is also referenced in english standards as EN AC-46000 or in german standards as 3.2163 [9]. In such standards, the chemical composition range is presented in Tab 4.3 [10]. This alloy is widely used in high-pressure die casting for its fluidity and its thermal inertia as a consequence of having a percentage of sillicon in its constitution allows provides an higher thermal inertia.

Tab 4.3 - Chemical composition allowed by international standards (adapted from [11]).

| Element | Si | Cu | Fe | Zn | Mn | Mg |
|---|---|---|---|---|---|---|
| wt (%) | 8 .00– 11.00 | 2.00 – 4.00 | <1.30 | <1.20 | <0.55 | 0.05 – 0.55 |

Even though approximations are made in CAE environment to describe the process mathematically, it is possible to determine with an high accuracy the thermal properties of the aluminium reducing the simulation error. The alloy's chemical composition in use to determine its properties is shown in Tab 4.4 [11, 12].

Tab 4.4 - Chemical composition of the casting alloy (adapted from [11]).

| **Element** | **Si** | **Cu** | **Fe** | **Zn** | **Mn** | **Mg** |
|---|---|---|---|---|---|---|
| **wt (%)** | 9.15 | 2.25 | 0.66 | 0.47 | 0.26 | 0.18 |

The CAE definition of this alloy can not only englobe the thermal properties of such as thermal conductivitym, density and enthalpy (Fig 4.4 (a) and (b)), but also the fluid properties of casting alloy above liquidus temperature, such as dynamic viscosity (Fig 4.4 (c)). An additional property, solid fraction, requires to be defined in order to indicate the transition within the alloys' bi-phase domain [13, 14]. Based on chemical composition it is possible to determine the alloys properties [5].

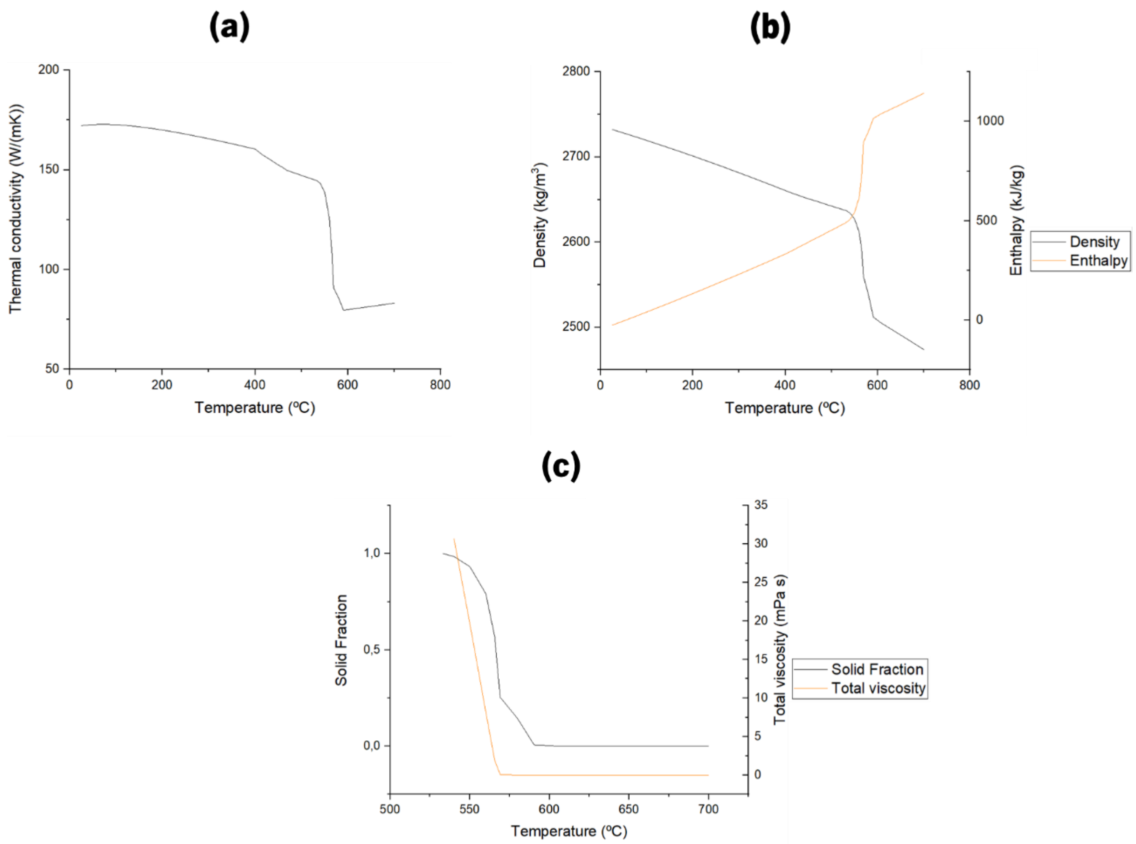


Fig 4.4 - Thermal behaviour of $AlSi_9Cu_3$(Fe) (adapted from [5]). (a) – Temperature effect on thermal conductivity; (b) – Temperature effect on density and specific heat; (c) – Temperature effect on solid fraction and total viscosity.

In contrary to the mold material, the enthalpy was defined instead of the specific heat due to the fact that a during solidification there is more than one phase. Therefore, it would be necessary to define one extra variable, latent heat ($\Delta H$), which would represent the the energy loss due to phase transformation.

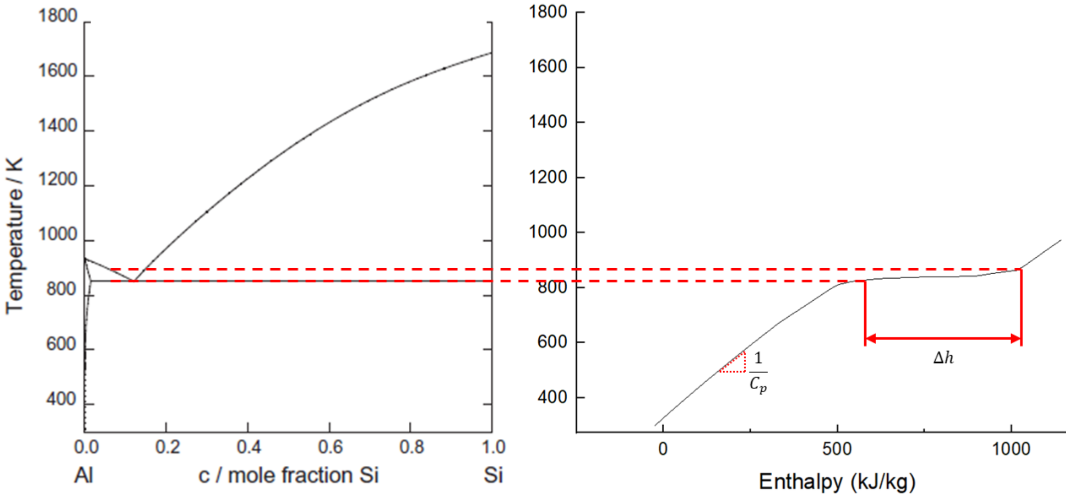


Fig 4.5 – Visual representation of the inverse of specific heat and latent heat (adapted from [5]).

## 4.2. CAD Model

The study case part belongs to a valve cover is shown in Fig 4.6. The respective model was received in STEP AP242 which corrections and mold were made in Autodesk Inventor.

Fig 4.6 - Component's model of the study case part.

The CAD model was edited (exit angles, fillets, etc) in accordance with NADCA products specifications standards [15]. Then, the part's properties relevant to the its gating design is shown in Tab 4.5. Mass and volume properties are required to determine flow rate and dimensioning gating design, component's size is required to determine the size of mold plates and project area required to verify the locking force.

Tab 4.5 – Relevant properties to the gating design.

| Property | Value |
|---|---|
| **Mass** | 134 g |
| **Volume** | $49.5\times10^3$ $mm^3$ |
| **Dimensions (X, Y, Z)** | 39×125×95 mm |
| **Projected area** | 4753 $mm^2$ |

Before using H.E.L.P. Die Casting to the gating design, an initial idealization of segments based on part's hotspots. In case of a small and uniformal component the unique present segment is the entire component. However, as it is presented in Fig 4.6, it is possible to identified that there are critical regions which the solidification time gradient would be higher than others.

Fig 4.7 - Identification of the hotspots.

### Filling time and Ingate velocity

The algorithm shown in chapter Chapter 3 - 3.3 is applied to this scenario in to calculate the filling time using equation [4.1] of the entire die cavity which results in the component. In this equation, $K$, $T_{part}$, $S$, $Z$, $T_i$, $T_d$ and $T_f$ values were 0.0346 s/mm, 2 mm, 0.2°C/%, 4.6%, 710°C, 577°C and 300°C respectively. Therefore, filling time ($t_{fill}$) was 0.0361 seconds. It is to note that die temperature value $T_d$ was based on initial temperature of the mold before the first cycle.

$$t_{fill} = K_1 T_{part} \left( \frac{T_i - T_f + SZ}{T_f - T_d} \right) \qquad [4.1]$$

NADCA gating design manual did not possess any information about the alloy, therefore there had to be determined. The $T_i$, $T_d$ and $T_f$ values are the pouring, die and minimum flow temperatures. $T_f$ and $T_i$ values attributed were 577°C (liquidus temperature) and 690°C. However prior simulations results indicated that the pouring temperature had to be increase to 710°C to avoid an early solidification. The die temperature was based on NADCA information with small adjustments based on simulation results.

$K_1$ was a constant based on the mold's material (steel H13), $T_{part}$ avarage thickness of the narrowest regions, the variable $S$ was based on surface finishing and variable $Z$ value was based on the alloy volume change property which was 4.6%.

As mentioned in chapter 2.4, for aluminium alloys the ingate velocity is within 18 to 40 m/s. The gating design was dimensioned to a ingate velocity ($v_{ing}$) of 20 m/s. This value was choosen in order to reduce mold's wearing and fatigue. Furthermore, it would reduce heat loss during the injection phase since higher velocities results in an higher convective heat transfer coefficient.

**Ingates and Runners section**

Each ingate would directionate the flow to both segments previously defined as it is shown in (Fig 4.8). It was defined an non-uniformal attack's distribution through part's length in Y direction, since it was oriented to the most critical regions which are more susceptible to shrinkage.

The attacks section are a crucial part of the design. Not only it is responsible for the fluid's orientation but it is also responsible for the compaction phase during solidification. If the attacks solidify before the most massive region of the part, shrinkage porosity is expected. This occurs because the piston cannot push the material in the runner into the part.

However, an attack section too robust may not distribute the molten metal through the part but it will concentrate it in one place and may increase the difficulty of cutting it off in the post process operation. Therefore, the used attack thickness ($T_{attack}$) was 1.8 mm.

Fig 4.8 Attacks to each segment and its non-uniformal division through the parts length in Y axis and its critical regions.

Analyzing the attacks position, it was idealized that the flow orientation angle was 35°, this value will be later verified and analyzed. Furthermore, it is possible to determine attacks width, equation [4.2].

$$w_{eff,ing} = \frac{V_{part}}{T_{ac,ing} v_{ac,ing} t_{fill} \cos\theta_{ef}} \quad [4.2]$$

The equation [4.2] is the continuity equation written in order to the attack width ($w_{eff,ing}$), 23 mm, with the correction factor for flow orientation, $\cos\theta_{ef}$.

The ingate area actual is normally 1.1 times bigger than the theoric value and the tangential runner section's area is typically 1.2 to 1.5 times bigger than the ingate area actual. This happens in order to make sure the entire section is completely full and avoid backflow [16]. The tangential runner/ingate choosen was 1.5 in order to delay the solification. This value was found the best during the iterative process in trade off for some process efficiency.

To delay the solidification even further, the selected aspect ratio for tangential runners was 1:1. Meanwhile, the main runner aspect ratio was 2:1, since it would take too long for the main runner to solidify, resulting in an time increase in cycle time.

The runners for both parts and main runners profile sections are shown in Tab 4.6 and Tab 4.7, which variables visual representation are shown in Fig 4.9. As both segments were idealized as having the same volume, both attack's section would be the same and the tangential runner's would be equal, therefore the software only generated the result for only one attack. The modelling process only has to read the data twice, instead of rewritting it.

Tab 4.6 - Generated data using H.E.L.P Die Casting for tangential runners.

| Section | Distance [mm] | Area [mm²] | Thickness [mm] | b [mm] | t [mm] | c [mm] | d [mm] |
|---|---|---|---|---|---|---|---|
| **A_1_Attack_1** | 0.00 | 4.00 | 2.00 | 2.54 | 1.46 | 0.54 | 0.54 |
| **B_1_Attack_1** | 16.82 | 28.42 | 5.33 | 6.27 | 4.39 | 0.94 | 0.94 |
| **C_1_Attack_1** | 33.63 | 52.85 | 7.27 | 8.55 | 5.99 | 1.28 | 1.28 |
| **D_1_Attack_1** | 50.45 | 77.27 | 8.79 | 10.34 | 7.24 | 1.55 | 1.55 |
| **E_1_Attack_1** | 67.27 | 101.70 | 10.08 | 11.86 | 8.31 | 1.78 | 1.78 |
| **F_1_Attack_1** | 84.08 | 126.12 | 11.23 | 13.21 | 9.25 | 1.98 | 1.98 |
| **A_2_Attack_1** | 0.00 | 4.00 | 2.00 | 2.54 | 1.46 | 0.54 | 0.54 |
| **B_2_Attack_1** | 16.82 | 28.42 | 5.33 | 6.27 | 4.39 | 0.94 | 0.94 |
| **C_2_Attack_1** | 33.63 | 52.85 | 7.27 | 8.55 | 5.99 | 1.28 | 1.28 |
| **D_2_Attack_1** | 50.45 | 77.27 | 8.79 | 10.34 | 7.24 | 1.55 | 1.55 |
| **E_2_Attack_1** | 67.27 | 101.70 | 10.08 | 11.86 | 8.31 | 1.78 | 1.78 |
| **F_2_Attack_1** | 84.08 | 126.12 | 11.23 | 13.21 | 9.25 | 1.98 | 1.98 |

Tab 4.7 - Generated data using H.E.L.P Die Casting for main runners.

| Feeding | Area [mm²] | Thickness [mm] | b [mm] | t [mm] | c [mm] | d [mm] |
|---|---|---|---|---|---|---|
| **1** | 126.12 | 11.23 | 13.21 | 9.25 | 1.98 | 1.98 |
| **2** | 126.12 | 11.23 | 13.21 | 9.25 | 1.98 | 1.98 |
| **12** | 252.24 | 11.23 | 24.44 | 20.48 | 1.98 | 1.98 |

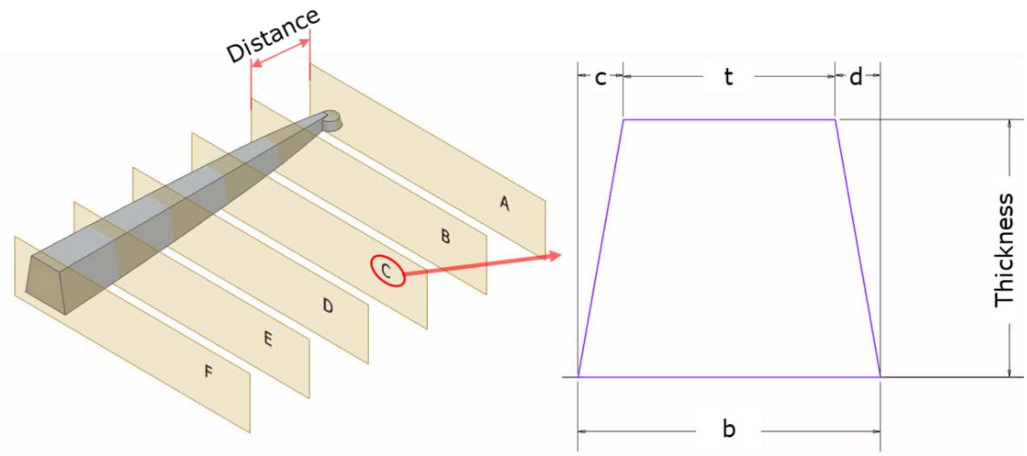


Fig 4.9 - Design parameters of the tangential runner.

The codename "Section" shown in Tab 4.6 for the last line (which name is "F_2_Attack_1"), means sections F (Fig 4.9) of the second part which attack number is 1. While the the codename “Feeding” in Tab 4.7 represents the part number of each tangential runner, i.e., “Feeding” 1 means the data in the following lines is referent to the tangential runner which is responsible for feeding the first part. While “Feeding” 12 is reffered to the runner (main runner in this case) which is responsible to feed the first and the second tangential runners.

**Overflows**

The determination of the right number of overflows is an iterative process. The initial step would be based on the flow pattern previous prediction followed by an only flow simulation is required to find out what are the last filling regions. The main reason for a only flow simulation is to have an higher accuracy in the casting process, since the negative pressure caused by the venting system influence the flow pattern.

Overflow’s overall dimensions was based on part’s size, casting material and avarage thickness. The NADCA manual recommended an total overflow volume equal to 25% of the part’s volume and an outgate and vent thicknes of 0.6 and 0.5 mm, respectively. In order to reduce insert’s size insert’s volume  without compromising the number of overflows and its volume, it was considerated that aspect ratio of overflow would be approximated to 1:3 and it would be a square, nominal dimensions in Fig 4.10. Lately, draft would be added as well as extractor pins to facilitate overflows extraction from the die cavity.

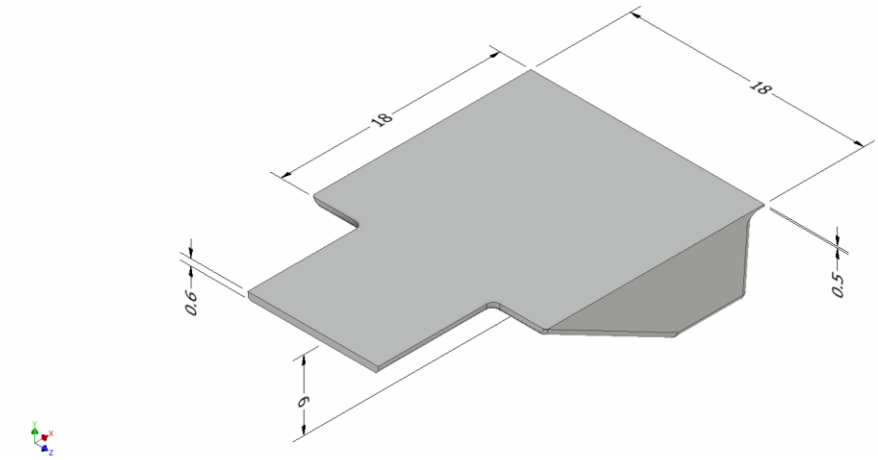

Fig 4.10 - Overflows nominal dimensions (dimensions in milimeters).

It was predictable, the air entrappement in critical region 1 would be unavoidable.While regions behind the holes (shadow areas) in each corner of the part was predictable as well as the overflow in position shown in Fig 4.11.

Fig 4.11 - Overflow location in the part (dimensions in milimeters).

**Gating design assembly**

As a result of the previous iterative process, a gating design was made (Fig 4.12). Due to the fact that the component is not symmetric, the first attack of one part is directed to the critical region 1 (Fig 4.7 (a)) while the other part was attacked in critical region 2. Therefore is expected different result in both parts and defects have to be analized and checked for both parts.

Fig 4.12 - Gating design made using H.E.L.P. Die Casting.

Nowadays, the conformed channels (CC) technology is widely used to injection molding using polymers. This technology still in development to die casting applications [17], which part of this dissertation’s project was included in.

The CC technology consists in using additive manufacturing (AM) to the production of mold’s inserts (Fig 4.13) [18]. In these inserts, the negative of the casting geometry will be allocated. To reduce the construction time using AM, only the die cavity that originates the part is produced using this technology (Fig 4.14 (b)), die cavity which originates the runners are manufactured using the traditional way (subtractive manufacturing) (Fig 4.14 (a)). During the production stage, an additional finishing machining phase is made to guarantee geometric tolerance.

Fig 4.13 - Mold's inserts assembled in the mold plate.

The main advantages of using CC is to increase the local cooling rate by permiting the designer to adapt (as it is shown in Fig 4.16), keeping casting's quality without trading it off for accuracy and allowing the replacement of high wearing regions (die cavity which originates the component), without the need of making a new mold [19].

Fig 4.14 - Mold's filling cavity. (a) - filling cavity to be produce by machining; (b) - filling cavity to be produce by AM and machining.

The mould's and inserts' dimensions are shown in Fig 4.15. Initially, the mold dimensions were based on giving a minimum offset of 100 mm from the inserts to in all directions to guarantee the mould's stiffness. The decision taken to define insert's dimensions was different from the one taken previously. The insert would have at least an offset of 15 mm from the die cavity which would originate the component. This value was chosen in order to reduce AM-producing time and spent material without compromising mechanical resistance [20].

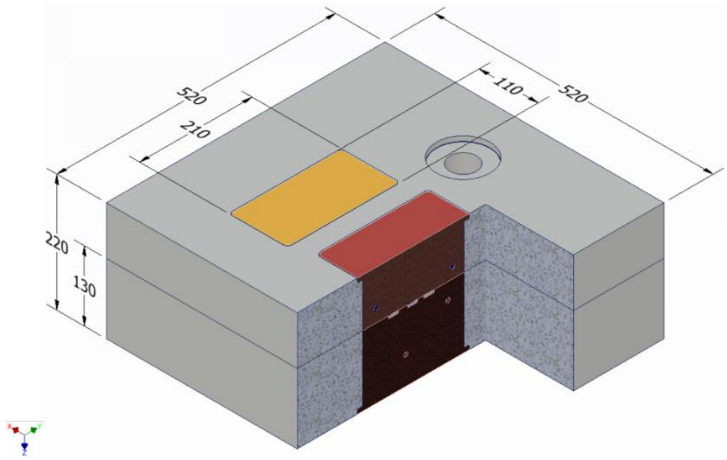


Fig 4.15 - General mold's and insert's dimensions (dimensions in milimeters).

This new method of producing cooling channels also affect the die's thermal field, due to the fact that there is not a domain continuity in the mold (die plates and inserts). This happens since it is impossible to have a perfect contact between the die and the inserts as result of surfaces' roughness which originates a contact resistance. This contact resistance is based on surfaces's roughness, interstitial fluid and contacts pair materials. Based on this knowledge, a contact resistance of 6971 $W/m^2K$ [21] was defined.

Cooling channels configuration is shown Fig 4.16. It was possible to notice that in the critical region 1, it would require an intensive cooling to cool down the hotspot. During the iterative process, it was necessary to add the cooling system on the opposite side of the casting.

Fig 4.16 - Cooling channels positioning relatively to the part.

Based on the avarage thickness of the casting (defined in chapter 1) it was possible to set channel's diameter as 8 mm. The distance between the cavity's surface and the distance from the cooling channel was 2 time the diameter and the cooling channels pitch (distance between parallel cooling channels) as well as the distance to extractor pins (positioning in Fig 4.17) was 1.5 times the diameter [18, 20].

Fig 4.17 - Positioning of extractor pins.

## 4.3. NUMERICAL MODEL

After the conception of the CAD model, it is needed to verify the gating design and overflows. This verification is made in computer aided engeneering software for the casting process.

The choosen software is Quikcast [22] of ESI Group. This software uses a different formulation (finite differences method), when compared to other softwares like Procast [23] (finite elements) or Flow-3D (finite volumes) [24]. The main difference between these types of discretization is the computational time and the accuracy of the results.

In these softwares, it is possible to simulate virtually the high pressure die casting process to predict possible to verify part's sanity and the process without having a cost to produce a mold.

The casting process can be described as a transient computacional fluid dynamics problem. Therefore the most important equation which will describe the fluid's behaviour are the Navier-Stokes equations (equation [4.3] to [4.5]) [25, 26] and the continuity equation (equation [4.7] and [4.8]) considering time dependent variables. It is important to note that these equations are only appliable to an incompressible and newtonian fluid in which the domain is isothermal.

$$\rho\left(\frac{\partial u}{\partial t}+\frac{du^2}{dx}+\frac{duv}{dy}+\frac{duw}{dz}\right)= -\nabla p_x+\mu\nabla^2 u+F_x \qquad [4.3]$$

$$\rho\left(\frac{\partial v}{\partial t}+\frac{duv}{dx}+\frac{dv^2}{dy}+\frac{dvw}{dz}\right)= -\nabla p_y+\mu\nabla^2 v+F_y \qquad [4.4]$$

$$\rho\left(\frac{\partial w}{\partial t}+\frac{duw}{dx}+\frac{dvw}{dy}+\frac{dw^2}{dz}\right)= -\nabla p_z+\mu\nabla^2 w+F_z \qquad [4.5]$$

Navier-Stokes equations can be described as Newton's second law [27] applied to fluids dynamics field to a discretized system. In the first member, it is represented the inertial forces originated by the a spatial and temporal velocity gradient. In case of a stationary study, which is not the case, the temporal inertial force is 0. The second inertial force results of a velocity gradient due to a spatial gradient of velocities [28]. The second member describes all forces applied on the fluid. The pressure gradient component considerates different pressures might be applying on fluid, such as vaccum pressure originated by the venting system. The tangential forces are originated by viscosity considerating the fluid as newtonian. Furthermore, it is considerated external forces which can be applied on the fluid such as hydrostatic and static.

Other equation which was used for the calculating the fluid pressure was the Poisson's pressure equation, equation [4.6] [29].

$$\nabla^2 p=\rho\nabla(\vec{u}\cdot\nabla)\vec{u} \qquad [4.6]$$

The continuity equation shown in equation [4.8] [25, 30] is the differential form of the transient equation [4.7] which can be applied to the mathematical system in order to guarantee the mass conservation.

$$\frac{dm}{dt}+\rho Q_{in}=\rho Q_{out} \qquad [4.7]$$

$$\frac{d\rho}{dt}+\rho\cdot\nabla u=0 \qquad [4.8]$$

In equation [4.7], $m$ is represents the mass, $Q_{in}$ the flow rate inward and $Q_{out}$ the flow rate outward.

Whenever there is any sort of thermal gradient, heat transfer is envolved. As well as the flow model, casting process is a transient heat transfer problem. However this numeric model occurs during the entire process and not all forms of are present or have the same weight in heat transfer during the injection cycle.

During the injection phase, convection weight in heat transfer from the casting alloy to mold is much higher than the other two forms, due to fluid's high velocity, equation [4.10]. During the solidification phase conduction is the highest form of heat transfer within the part, equation [4.9] [31], excluding the fact that there also is convection in the cooling channels.

When the component is removed when its surface temperature reaches 250°C/300°C, the main for of heat transfer within solid is conduction and the main form of heat tranfer to the environment is radiation, equation [4.11] [31]. Even though convection is present when the casting is removed from filling cavity, radiation weight is higher, since temperature' units in radiation formula are in Kelvin and are power four.

$$k\left(\frac{\partial^2 T}{\partial x^2}+\frac{\partial^2 T}{\partial y^2}+\frac{\partial^2 T}{\partial z^2}\right)=\rho c_p \frac{\partial T}{\partial t} \qquad [4.9]$$

$$Q = hA(T - T_\infty) \qquad [4.10]$$

$$Q = \sigma A\, \varepsilon F_g (T_1^4 - T_2^4) \qquad [4.11]$$

The equations from to are simple to applied during the solidification stage and casting's interface with the mold. Whenever there is any form of heat transfer within the fluid applied to its dynamic, it is needed to use a more complex equation [32, 33].

$$\rho c_p \frac{\partial T}{\partial t}+\rho c_p\left(\frac{duT}{dx}+\frac{dvT}{dy}+\frac{dwT}{dz}\right)=Q+k\left(\frac{\partial^2 T}{\partial x^2}+\frac{\partial^2 T}{\partial y^2}+\frac{\partial^2 T}{\partial z^2}\right) \qquad [4.12]$$

## 4.4. Domain discretization for CAE

The solve the physical system, QuikCast requires the definition of two types of meshes, a 2D mesh and a 3D mesh. The 2D mesh' main function is to delimiter the physical volume by discretizing every surface of system's component such as shot sleeve, shot sleeve and casting. Meanwhile, 3D mesh's main function is to discretize the domain described by the 2D mesh and solve the equation's shown in chapter 4.2, momentum and energy equations, using Finite Differences Method (FDM).

QuikCast software has several limitations when it comes to modelling. Therefore, a CAD model file format conversion will be required to import the geometry to Visual Mesh.

This CAD file format conversion will result in information loss between the CAD model and the importing file. This information loss depends on the the file format chosen for conversion, one of the most used formats is Standard for the Exchange of Product model data (STEP). However, the current industrial version of STEP, AP214, doesn't convert certain features, new developments are being made to reduce CAD information loss [34].

The file formats available for the student's version of QuikCast are stereolithography [35] (STL) and Initial Graphics Exchange Specification (IGES) [36]. The first format converts the exporting geometry to mesh, the surfaces are discretized by triangular facets no modifiable in Visual Mesh. Although, there won't be needed any sort of user's geometric or mesh correction, because the importing software will repair it automatically.

In the other hand, the IGES format converts the CAD model to a surface geometry with components's relations information losses. Consequently, a poor choice of geometric tolerance importing the IGES file, may result in some tangential surfaces penetrate each other. Therefore a geometric correction will be needed to make sure the assembly model is within software's tolerance.

STL file format doesn't permit the user to modify the imported mesh. This will result in a either very coarse mesh due to the existance of long edges (external mold's edges) which won't describe casting's geometry accurately or very fine mesh wich will increase the computation time.

Consequently, it was file format IGES, so it was possible to generate/edit the 2D mesh manually. As mentioned before, geometric and mesh corrections were required.

The geometric corrections consisted in correcting/eliminating surfaces that would be either overlapped or intersected by other surfaces or poorly defined edges. These correction were mostly made in the CAD software Autodesk Inventor, since it was originated by a previous faulty CAD model.

**2D Mesh**

As a consequence of an execellent methodology of gating design, it was possible to create a CAD model for gating design without any geometric problem, consequently any geometric correction were not done.

The tipology of the elements choose was triangular and its topology was first order. In case a second order element was used, it was possible to use curved elements. The usage of curved elements improve the geometry definition (Fig 4.18), since it allows to described curved surfaces by having 3 extra nodes in each element when compared to non curved elements, Fig 4.18 (b). For flat surfaces, which correspond to largest surfaces, using higher order elements does not bring any geometric advantage.

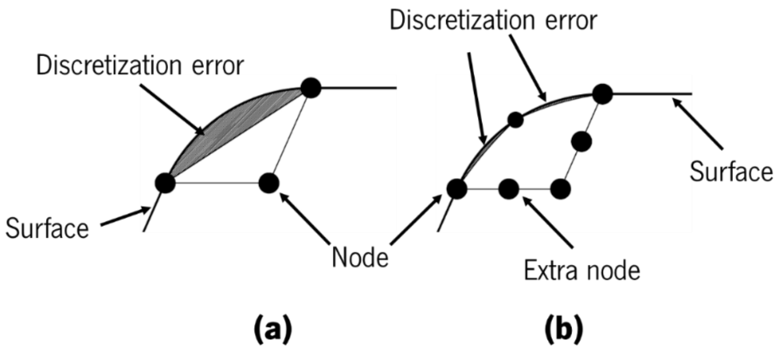


Fig 4.18 - Discretization error for different element topology. (a) - first order element; (b) - second order element.

Even though a higher element order increases geometric accuracy, it was prefered to used a finer mesh than an higher order, due to computacional time during mesh generation and simulation.

To reduce the computacional time even further, it was defined that different edges would have different element size in order to reduce the number of elements as it is shown in Fig 4.19.

The largest surfaces with straight edges or with low geometric relevance for the numeric model were assign with a element size of 20 mm. These regions were the outer surface of the mold and the shot sleeve (Fig 4.19 (a)).

The casting metal inside shot sleeve, runner, outside of the inserts and the cooling channels where assign with a element size of 4 mm (Fig 4.19 (b)). This size was choose based on cooling channels diameter and runner's dimensions such as width and height.

For narrow regions of shot sleeve and ingates and component it was choosen a 1.25 mm element size (Fig 4.19 (c)). Element size was choosen based on components narrowest region which thickness was 1.25 mm.

The mesh corrections consisted in a localized remesh to eliminate low quality elements, which characteristics for such consideration is shown Tab 4.8, and surface's normal's orientation.

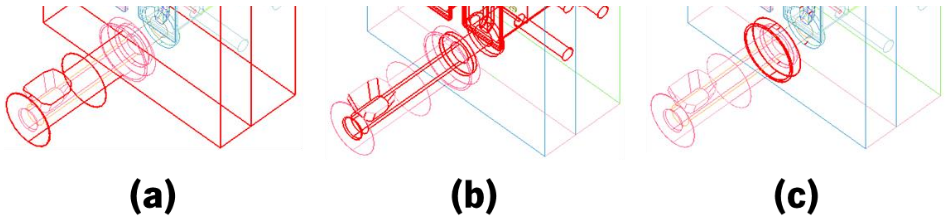


Fig 4.19 – Assembly edges with different element size. (a) – edges with 20 mm size; (b) – edge with 4 mm size; (c) – edge with 1.25 mm size.

Tab 4.8- Low quality element's consideration.

| | |
|---|---|
| **Minimum side length** | 0.001 mm |
| **Minimum triangular height** | 0.001 mm |
| **Maximum aspect ratio** | 5 |
| **Minimum triangular internal angle** | 5° |

A face normal's orientation and nodes connectivity are directily related. To determine a normal's orientation, it is possible to use rotational operator of two tangent vectors in point P of a surface, equation [4.13]. The result of this mathematical concept is the direction vector pointing towards volume's outside. The visual representation of mathematical relation is shown in Fig 4.20.

$$N = \vec{T} \times \vec{B} = \begin{vmatrix} i & j & k \\ T_x & T_y & T_z \\ B_x & B_y & B_z \end{vmatrix} \quad [4.13]$$

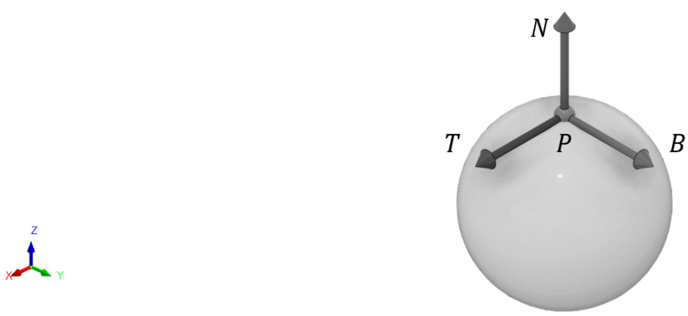


Fig 4.20 - Visual representation of a surface's normal and the two tangent vector which intersect it at point P (adapted from [37]).

The order in which the vectors appear, $T$ and then $B$, is determined by the nodes' connectivity. In Fig 4.21 (a) is shown the result of the counterclockwise connectivity, which result in a positive orientation and is described by equation [4.13]. In the other hand, a connectivity clockwise (Fig 4.21 (b)) results in a negative orientation, which rotational's vectorial order is shown in equation [4.14] [37].

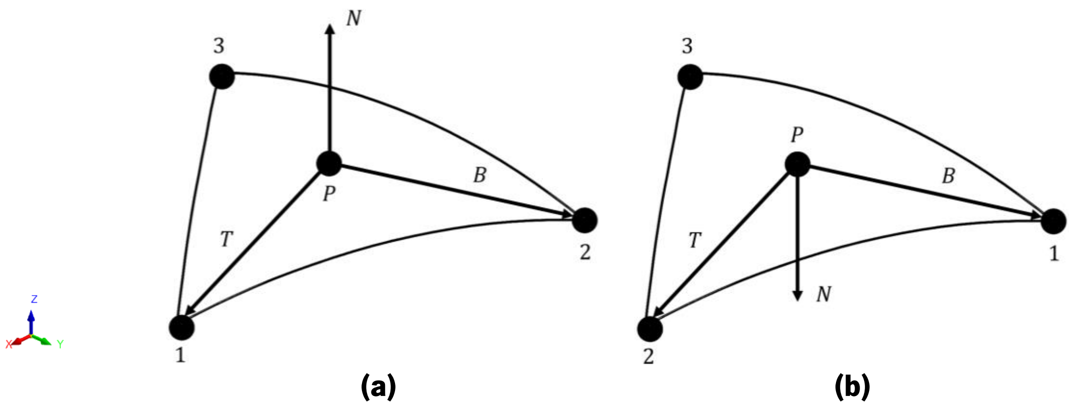


Fig 4.21 - Nodes connectivity and its influence in normal's orientation. (a) node connectivity is counterclockwise so normal's orientation is positive; (b) node connectivity is clockwise so normal's orientation is negative.

$$N = \vec{B} \times \vec{T} = \begin{vmatrix} i & j & k \\ B_x & B_y & B_z \\ T_x & T_y & T_z \end{vmatrix} \qquad [4.14]$$

In commercial software such as QuikCast, the user can only change normal's orientation and consequently node connectivity is changed.

Due to the component's geometric complexity, QuikCast by default considers considers surfaces normal's direction as inwards which appears in component and mold's insert, Fig 4.22 and Fig 4.23.

In some softwares which use Finite Element Method (FEM)  to solve mathematical equations, not checking normals orientation will originate in negative volumes.

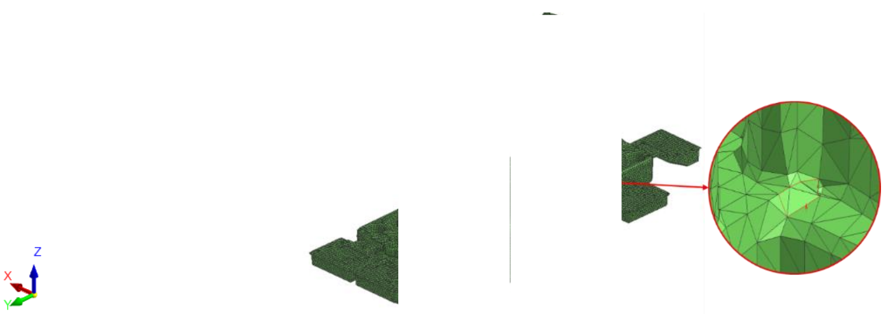

Fig 4.22 – Component's elements with normal's orientation in the wrong direction.

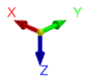

Fig 4.23- Mold's insert's elements with normal's orientation in the wrong direction

**3D Mesh**

All CAD's domain were defined using a triangular mesh (2D mesh). However, the internal domain's discretization will require a definition of a nodal network [38] (Fig 4.24) which englobes all present domains. In this mesh, Navier-Stokes and energy equations will be solved using FDM.

Therefore, it will be needed to use a cell size equal or smaller than the thinniest region of the assembly, in order to describe it's geometry. The recommended size is equal to of the thinnest region (ingate region), since it is able to describe the narrow region geometrically and with a good accuracy without increasing the computacional time [39]. The reason it is possible to describe a geometry with only one cell is related to the fact that Navier-Stokes equation has a second order term (viscous forces), therefore it takes at least 3 points to determine its solution for the narrowest region.

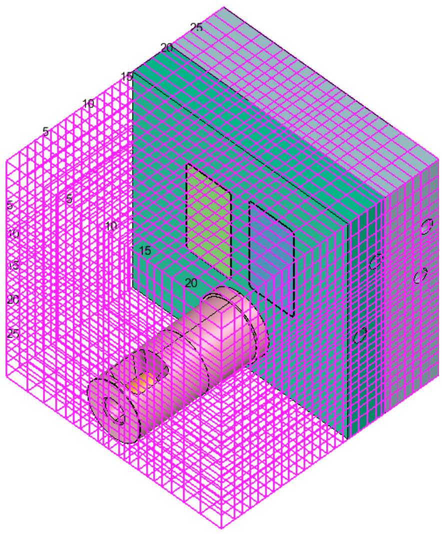

Fig 4.24 – Staggered grid generated by QuikCast mesh solver.

Furthermore, it is possible to define an non-uniformal grid to better fit to the casting volumes, since these volumes require a fine mesh.

In case a cell generated by the 3D is intercepted by component's 2D mesh, volume corrections factors (VCF) will be added to the formulation. These VCF vary between 1 and 0 which indicate the fraction of casting metal which cell will be fulfilled [40]. As it is possible to verify in Fig 4.25 (a), mold's surface intercept some cells, which will have its factor respective factor to calculate each cell's properties (such as area, volume, density), Fig 4.25 (b).

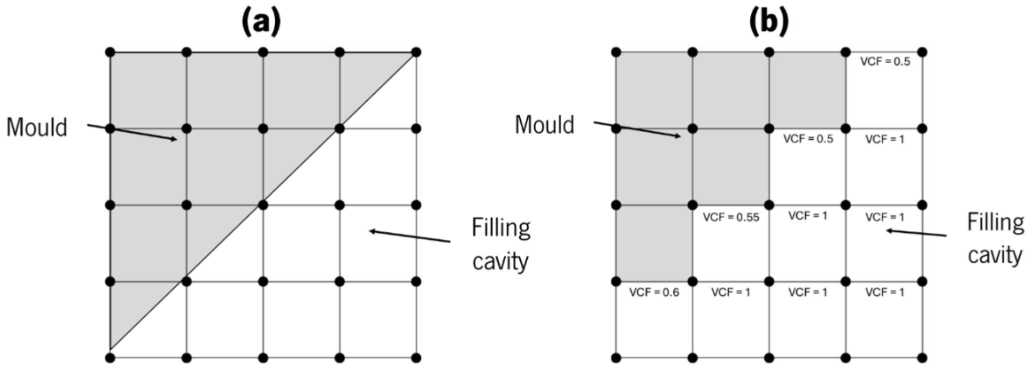


Fig 4.25 – Influence of volume correction factors. (a) – real geometry without VCF; (b) – repesctive volume correction factors as well as its discretized geometry (adapted from [22]).

Consequenly, using a coarse 2D mesh will not impact volume's properties as much as a coarse 3D mesh. A rectangular flat surface can be described perfectly by two 2D elements, however regarding surface's tilt, two 3D elements to discretize such geometry would result in enormous error when calculating its properties.

For the generation of a nodal network which could fit the presented problem, it was defined the mesh would be non uniformal with properties shown in Tab 4.9 which generated 3180375 cells. The presented mesh definition is used to all simulations later.

Tab 4.9 – 3D mesh properties used for the simulations its definition.

| Property | Value |
|---|---|
| **Minimum size** | 1 mm |
| **Avarage size** | 1.8 mm |
| **Maximum size** | 36 mm |
| **Maximum growth rate** | 1.4 |

The generated mesh is in accordance with the discretization method of finite differences method (FDM). This discretization method approximates derivatives with finite differences for both spatial and temporal domains [41]. This descretization method convert non-linear partial different equations such as Navier-Stokes and energy equation as shown in chapter 4.3, respectively into a linear system of equations which can be solved iteratively [42, 43]. In order to have accurate results, it requires a small element size either to delineate the component's commplexity and to compensate for the low accuracy discretization method when compared to Finite Volume Method (FVM) [44].

The system's discretization schematics is shown in Fig 4.26, where the determination of the central node property is based on neighbouring nodes. To determine the first and second derivative in the respective orientation, equations [4.15] and [4.16] are used, respectively [45].

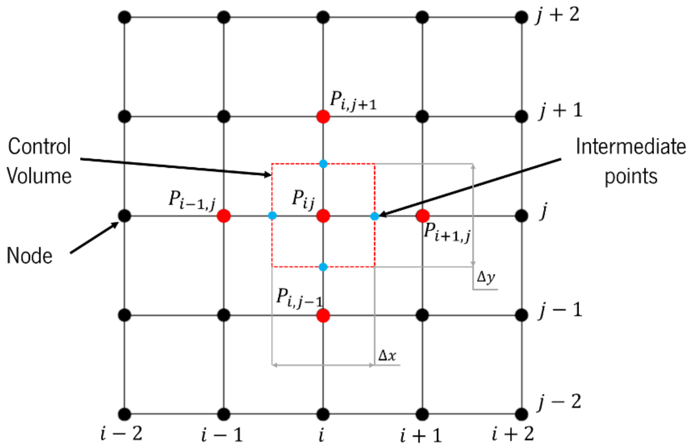


Fig 4.26 – 2D staggered grid for the simulation problem with the respective connectivity of each node (adapted from [31]).

$$\left.\frac{dP}{dy}\right|_{+} = \frac{P_{i,j+1} - P_{i,j}}{\Delta y} \tag{4.15}$$

$$\frac{d^2P}{dy^2} = \frac{\left.\frac{dP}{dy}\right|_{+} - \left.\frac{dP}{dy}\right|_{-}}{\Delta y} = \frac{P_{i,j+1} - 2P_{i,j} + P_{i,j-1}}{\Delta y^2} \tag{4.16}$$

**Thermal model**

The casting process is a transient heat transfer problem, therefore in heat conduction equation it will be needed to add a transient term. Discretizing heat transfer equation into a finite differences problem within the same volume, as it is presented in Fig 4.26, it is possible to get equation [4.18] [46, 47].

$$\phi = \Delta y \Delta x \frac{\rho c_p\left(T_{i,j}^{n} - T_{i,j}^{n-1}\right)}{\Delta t} \tag{4.17}$$

$$\frac{k}{\Delta x}\left(T_{i-1,j}^{n} - 2T_{i,j}^{n} + T_{i+1,j}^{n}\right) + \frac{k}{\Delta y}\left(T_{i,j-1}^{n} - 2T_{i,j}^{n} + T_{i,j+1}^{n}\right) = \phi \tag{4.18}$$

In equation [4.17] and [4.18], $i$ and $j$ is the node position in the staggered grid and $n$ is the number of the time-step.

If it's the case of node is in a surface, as it is presented in Fig 4.27, the convective term has to be introduced in order to describe heat transfer through the surface, equation [4.19]. In case of an interface mold/casting metal during the injection phase, the convective term, $h$, is calculated automatically. During solification, user has to define it.

$$\frac{\Delta y}{h}\left(T_{i,j}-T_{\infty}\right)+\frac{2k}{\Delta x}\left(T_{i+1,j}^{n}-T_{i,j}^{n}\right)+\frac{k}{\Delta y}\left(T_{i,j-1}^{n}-2T_{i,j}^{n}+T_{i,j+1}^{n}\right)=\phi \qquad [4.19]$$

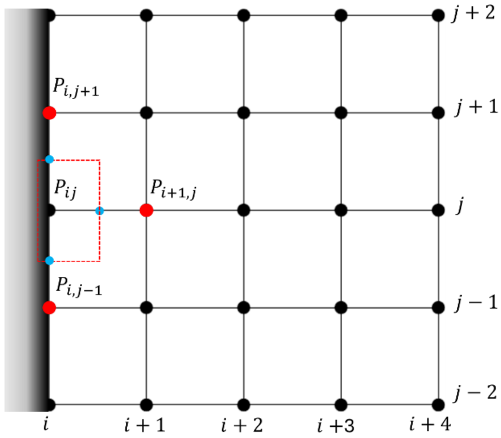


Fig 4.27 - Case of a node in a surface (adapted from [42]).

The equations [4.17], [4.18] and [4.19], are valid to solids, this means that are only appliable for the heat transfer within the mold domain and casting domain during solidification. During the injection phase, energy equation within the fluid domain is incorporated with Navier-Stokes equations, since most of the heat transfer occurs due to convection and not conduction.

**Flow model**

The flow model is only useful for during the injection phase where the main computational challenge is the solving Navier-Stokes equations. During this phase heat transfer is also present, however only the Navier-Stokes equations will be presented, since energy conservation equation is similar to the one shown in thermal model.

The need of the usage of staggered grid is appear when it is required to discretize Navier-Stokes equation. The pressure term is calculated in the node, while the local velocities are calculated in the intermidiate points ($\vec{u}^{n}$). Lately, it is calculated in the nodes ($\vec{U}^{n}$) the avarage local velocities [28].

$$\frac{\vec{U}^{n+1}-\vec{U}^{n}}{\Delta t}+\left(\vec{U}^{n}\cdot\nabla\right)\vec{U}^{n}=\mu\nabla^{2}\vec{U}^{n}+\nabla p+\rho g \qquad [4.20]$$

**Explicit and Implicit methods**

Both models presented before have different methods to solve the transient term, which can be explicit and implicit [48].

The difference between these two methods is that the explicit method uses a variable value in $(n)^{th}$ time-step to calculate it's value in timestep $(n+1)^{th}$. Meanwhile the implicit method solves the differencial in order to find the value when the transient term of the previous timestep, $(n)^{th}$, equals the weight of system's variables of the same instant, $(n+1)^{th}$.

For a dynamic problems, the method used is the explicit one, where the velocity in the timestep $(n+1)^{th}$ is determined adding the value of the velocity in instant $(n)^{th}$ to its time variation, equation [4.21].

$$\vec{U}^{n+1} = \vec{U}^{n} + \left(-\left(\vec{U}^{n} \cdot \nabla\right)\vec{U}^{n} + \mu\nabla^{2}\vec{U}^{n}\right)\Delta t + \rho\nabla\vec{U}^{n} \quad [4.21]$$

In equation [4.20], the term $\rho\nabla\vec{U}^{n}$ is the pressure gradient in Navier-Stokes equation. As it is possible to verify, $\vec{U}^{n+1}$ is calculated entirely based on the previous step ($\vec{U}^{n}$). For the Heat transfer problem during filling, QuikCast also uses the explicit method.

In other hand, for the solificiation process, QuikCast uses implicit method. In this method, equations [4.17] and [4.18] are used to determine the temperature in timestep $(n)^{th}$. This method is used, since it has a smaller error and computation time is the same, since the matrix for the linear problem remains constant.

Both methods can be attributed to a factor in which represents the $(n+1)^{th}$ timestep's weight in solution, equation [4.22] to [4.24]. To an explicit method, $f$ is 0. For the implicit method, the factor $f$ is different from 0, with two exceptions. These exceptions are for $f$ equals to 0.5 which represents Crank-Nicolson's method and $f$ equals to 1 which represents a total implicit method [49].

$$\frac{k}{\Delta x}\left(T_{i-1,j}^{n} - 2T_{i,j}^{n} + T_{i+1,j}^{n}\right) + \frac{k}{\Delta y}\left(T_{i,j-1}^{n} - 2T_{i,j}^{n} + T_{i,j+1}^{n}\right) = \phi^{n} \quad [4.22]$$

$$\frac{k}{\Delta x}\left(T_{i-1,j}^{n-1} - 2T_{i,j}^{n-1} + T_{i+1,j}^{n-1}\right) + \frac{k}{\Delta y}\left(T_{i,j-1}^{n-1} - 2T_{i,j}^{n-1} + T_{i,j+1}^{n-1}\right) = \phi^{n-1} \quad [4.23]$$

$$(1-f)\phi^{n-1} + f\phi^{n} = \Delta y \Delta x \frac{\rho c_p\left(T_{i,j}^{n} - T_{i,j}^{n-1}\right)}{\Delta t} \quad [4.24]$$

Crank-Nicolson's method has an even lower error to small timesteps than implicit method [42], however its computation is higher than the implicit method, since the calculation of each temperature requires the temperature of two timesteps of neighbour nodes, $(n)^{th}$ and $(n+1)^{th}$, while implicit only requires one.

## 4.5. High Pressure Die Casting Simulation Conditions

The simulation of the high pressure die casting process needs 2 types of simulation. The first one is the cycling simulation and the second one the actual high pressure die casting simulation.

A die cycling simulation is required to simulate the impact of previous cycles in the numeric model. The number of cycles it required validate the process was 20 cycles [50]. After 20 Cycles it was considerated that the thermal variation across the mold would remain the same spatially and temporally when compared to the same instant of the previous cycle.

In this cycles will be only considerated the thermal module to reduce computational time without trading it off for accuracy. Using the flow module to simulate the effect of the casting alloy thermal gradient would increase massively the computing time. The cycling simulation would increase from 90 minutes to 16 hours and 47 minutes, an 2675% increase, without considering possible interruptions. The mesh used for both simulations was presented in Tab 4.9.

After the cycling simulation, it was possible to simulate a real injection with the flow model and solidification to verify the solution.

### 4.5.1. Die Cycling simulation

The non consideration of previous cycles not only does not describe the casting process after each shot accuratly, but it also influence negatively the prediction of defects. Since it does not consider that the mould's thermal field is affected by the thermal cycles. Consequently, increasing the apperence of shrinkage porosity defect in the casting postprocessing.

The casting simulation requires the definition of the initial conditions and boundary conditions which QuikCast's designation is volume manager and process conditions, respectively.

The definition of the thermal cycle of the process requires the definition of the transient thermal conditions. To define such conditions, it's needed to define it's value, starting and ending time (Fig 4.28). These process conditions are adjust according to the available technology such as die spray machines.

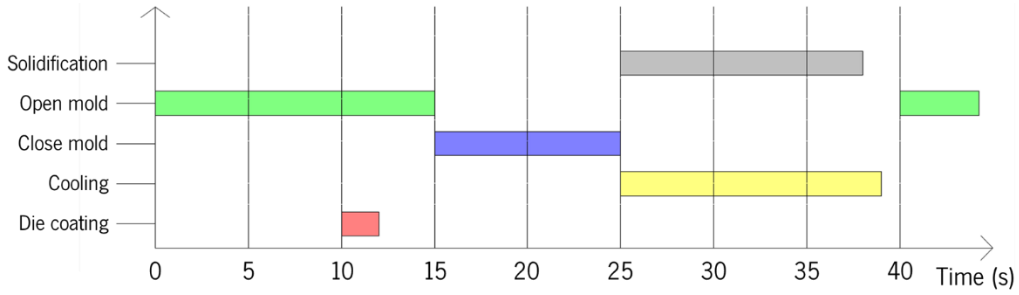


Fig 4.28 - Thermal scheme of the process.

The solidification mentioned in Fig 4.28 is referent to the injection and solification of the casting alloy. As flow module is disable for the cycling, only the solidification stage is mentioned in the die cycling simulation.

The open mold condition defines the moul's condition when it is open after the casting is removed. Therefore, the external temperatures for both forms of heat transfer (radiation and convection) were defined as 25°C. The emissivity was considerated 0.9 [31] for steel-steel surfaces (between mold plates) and 0.35 to aluminium-steel surfaces (between mold plates and casting). The convection heat transfer coefficient ($h$) was calculated based on natural convection [51]. The approximation of its value was based on Grashof, Prandlt, Rayleigh and Nusselt number adimensional numbers [31], equations [4.25] to [4.28], respectively.

$$Gr = \frac{L^3 \rho^2 g \beta \Delta T}{\mu^2} \quad [4.25]$$

$$Pr = \frac{\mu C_p}{k} \quad [4.26]$$

$$Ra = Gr Pr \quad [4.27]$$

$$Nu = \frac{hL}{k} = \left( 0.825 + \frac{0.387 Ra^{\frac{1}{6}}}{\left[1 + \left(\frac{0.492}{\mathrm{Pr}}\right)^{\frac{9}{16}}\right]^{\frac{8}{27}}} \right)^2 \quad [4.28]$$

To calculate the $h$,Casting simulation, initially it is calculated the Grashof number and Prandlt, then the Rayleigh's. Lately, it can be calculated Nusselt number to calculate the convection coefficient, which value is 5.3 $\frac{W}{m^2 K}$.

The close mold condition defines the condition when the mold is closed before the injection. In this condition, it was only considerated a heat transfer between the air inside the mold and the mold surface. Relatively to the open mold condition, it was only considerated an equal convection heat transfer coefficient and it was not considerated any ratiation, since both surfaces have the same temperature.

The cooling system starts at the beginnig of the injection and would last one second after the end of the solidification period. It was considerated that the cooling oil would have an avarage temperature of 160°C and a convection heat transfer of 8595 $\frac{W}{m^2K}$[22]. This convection heat transfer coefficient is based on Nusselt number using Colburn Formula, equation [4.29].

$$Nu = 0.023Re^{0.8}Pr^{0.33} \quad [4.29]$$

The cooling system is based on a new technology (conformed cooling channels) which main goal is to optimize heat transfer from the casting to the cooling fluid. Therefore, a better numerical model would be required in order to predict accurately the local heat transfer coefficient and the effect of the fuild's temperature increase along the channel instead of an analitical approximation of constant temperature.

The application of a die coating keeps the die cooled increasing mold's lifespan [52, 53], lubricated to facilitate the casting's removal [54], enhance surface quality and dimensional accuracy [55]. These types of die coating are a moisture with the a stripping agent and a cooling agent. The cooling agent can be water, oil or air. The stripping agent responsible for the lubrication of the die cavity can be graphite, $TiO_2$, $Al_2O_3$ and $Fe_2O_3$, etc [56]. The die coating used is a water-based moisture which stripping agent is graphite.

The film size of a the die coating is typically between 0.1 to 0.3 mm [40] with thermal porperties shown in Tab 4.10.

Tab 4.10 - Thermal properties required by QuikCast to define die coating interface (adapted from [22]).

| Property | Value [unit] |
|---|---|
| **Thermal conductivity** | 1.05 [W/mK] |
| **Aderence resistance** | $10^{-5}$ [W/m$^2$K] |

The systems initial conditions are shown in Fig 4.29. It is only relevant to define for the first cycle, initial conditions for the other cycles are based on thermal fields of the previous cycle.

The inserts were defined as a mold with a filling volume of 100% with tool steel 1.2709 at 300°C. The material of the shot sleeve and mold plates was H13.

The casting alloy volume which would originate the runners, parts and overflows had a filling volume of 100% at 710 °C, while the volume casting alloy in the shot sleeve volume had a 0% filling. Even though the casting alloy volume in the shot sleeve was 0%, it was required to define it for casting simulation.

If the third stage effect is used during solidification only simulation, QuikCast considers that the shot sleeve's volume is full, even though it was defined as 0% full. This happens, because applying pressure only makes sense if there is any metal. To overcome this difficulty, an extra boundary condition is applied to impose that there is not any liquid. This boundary condition was to impose that casting alloy in shot sleeve to be at 300°C (at same temperature than the mold's), to minimize error. It was choosen the usage of the third stage effect since it is the best way do describe solidification.

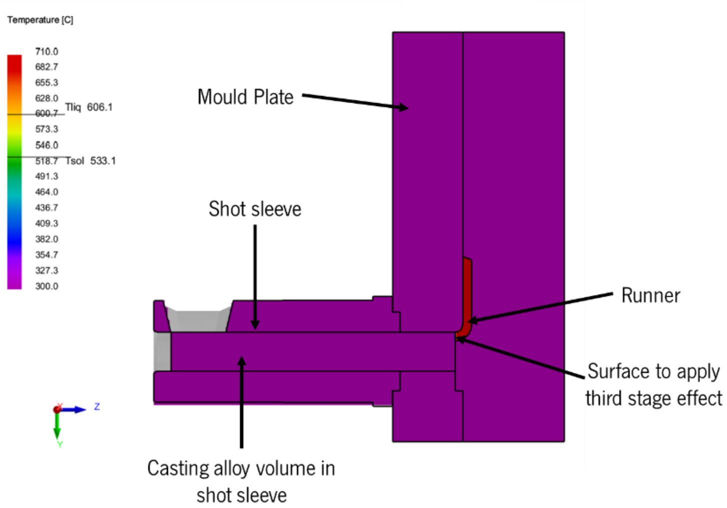


Fig 4.29 - Initial conditions to the die cycling simulation.

After the cycling simulation, the resulting thermal field will be used as a start temperature of the mold. It is also possible to analise temperature during different times of the cycle to guarantee the mold's local temperature does not reach critical temperatures.

From the Fig 4.30 to Fig 4.33, are presented the thermal's field of the last cycle in different instants. The chosen instants were at 0, 12, 15 and 25 seconds. The instant 0 second's thermal field is the same as the last instant from the previous cycle. The instant 7 second's thermal field is referred to the moment after applying the die spray, which main source of thermal energy loss was the cooling agent. The instant 25 represents the mold's temperature before the next injection.

In initial instant of the last cycle, mold's thermal field is presented in Fig 4.30. It is possible to notice very low temperatures which are surface of the cooling channels.

In instant 12 seconds, Fig 4.31, die cavity's surface is lowest during the process and its temperature gradient is the highest. This happens due to the cooling agent of the die spray during die coating, since a relatively high heat transfer is happening in the die cavity, its surface temperature is abruptally reduced. Once the the die coating process is finished and it is given enough time, die cavity's surface temperature increases due to thermal conductivity of the thermal energy in present in the mold.

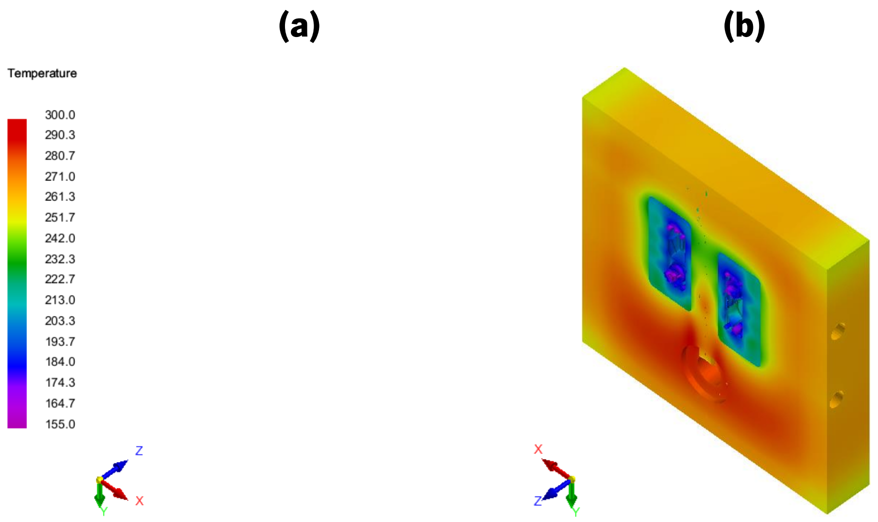


Fig 4.30 – Mold's Thermal field in instant 0 seconds. (a) - Fix mold plate; (b) - Mobile mold plate.

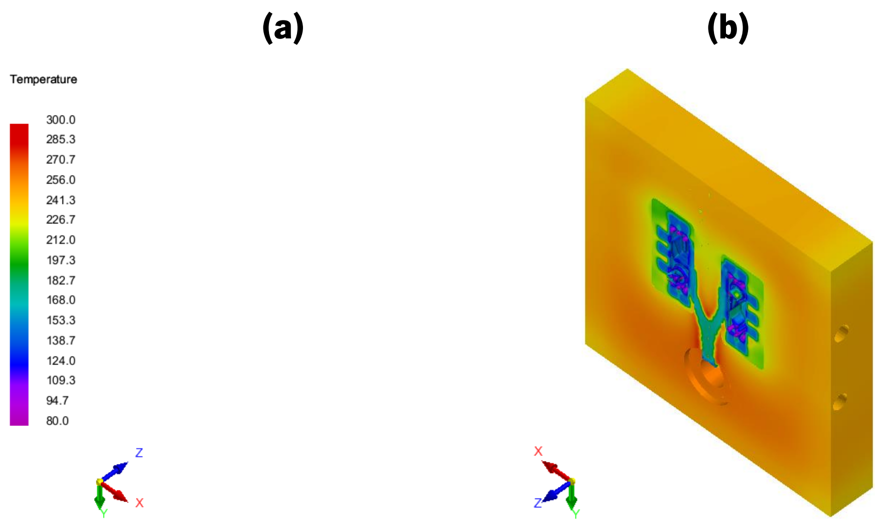


Fig 4.31 – Mold's Thermal field in instant 12 seconds. (a) - Fix mold plate; (b) - Mobile mold plate.

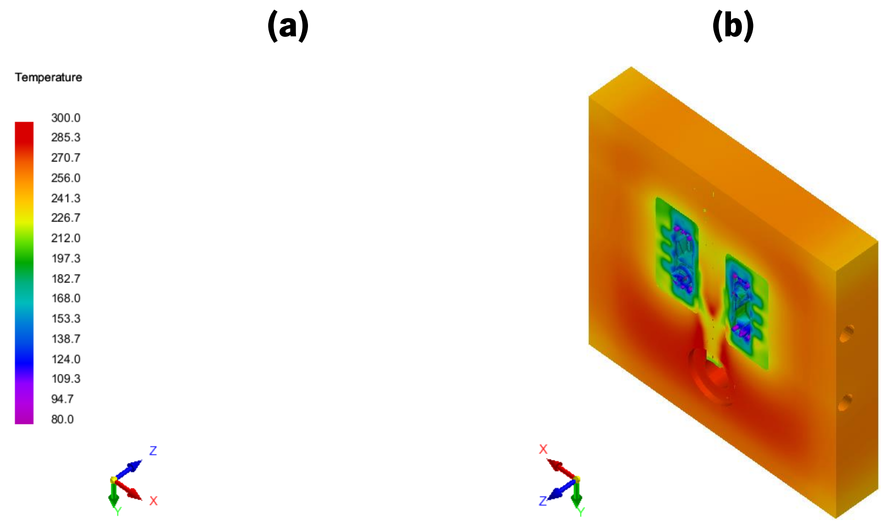


Fig 4.32 – Mold's Thermal field in instant 15 seconds. (a) - Fix mold plate; (b) - Mobile mold plate.

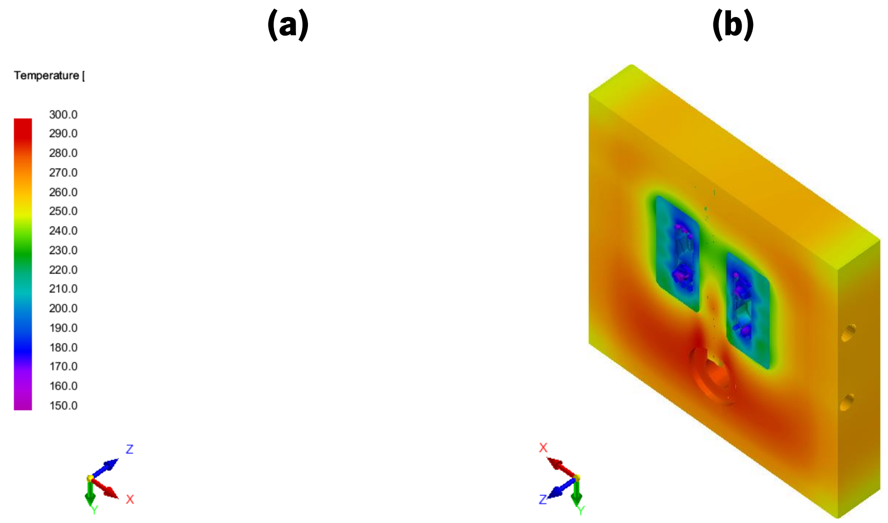


Fig 4.33 – Mold's Thermal field in instant 25 seconds. (a) - Fix mold plate; (b) - Mobile mold plate.

### 4.5.2. CASTING SIMULATION

The injection simulation requires the definition of the physical system with flow conditions in order to evaluate the process's dynamic. Therefore, the initial conditions of volumes and boundary conditions will vary of those defined in chapter 4.5. However last cycle's mold's thermal field will be used in the injection simulation, thermal field shown in Fig 4.33.

At the initial instant of the casting process, it was stipulated that both the shot sleeve and the filling cavity pertained exclusively to the "Alloy" volume, meaning these volumes would only contain the molten material, alluminum alloy $AlSi_9Cu_3$. The pouring temperature of the "Alloy" was 710°C. The shot sleeve was filled to a capacity of 29% full, whereas the filling cavity remained unoccupied, 0% capacity, Fig 4.34. Commonly, the shot sleeve is filled to a capacity of 60%-80% full [57] for high filling ratio, due to geometric constraints of the existing shot sleeve, it was choosen the low filling ratio (20%-30%).

In QuikCast software, there are two types of ways to define mathematically the injection process. The first way to define it is to apply transient inlet and "Third stage effect". Inlet boundary condition is necessary to define the first and the second piston's advancing phase, filling of shot sleeve cavity and filling cavity respectively. Lately, it would require the user to set a "Third stage effect" boundary condition to describe the compaction phase (third piston's advancing phase) in the same surface of the inlet condition (Fig 4.35 (a)).

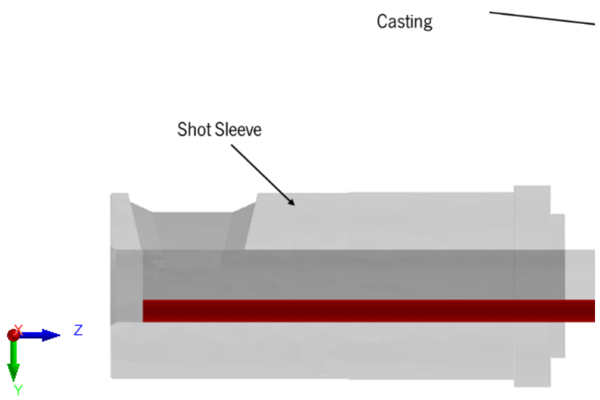


Fig 4.34 – Initial state of volume's capacity. Shot sleeve's fill ratio is 29%.

The second way is to consider shot sleeve casting material as part of the the physical system and then define the piston's surface as it is presented in Fig 4.35 (b). The third stage is defined the same as in the first method. This method is more precise (considers velocity profiles within shot sleeve domain and heat losses) and intuitive but more time consuming than the first method.

The piston's advancing stages are devided in 3 stages, which possess very distinguished function and kinematics. The first advancing stage is characterized by a low velocity. This stage lasts until the casting alloy reaches the ingate piston's position until 295 mm (Fig 4.37 (a)). It allows the vaccuum machine to remove the maximum quantity of air from the die cavity reducing the porosity caused by entrapped air inside filling cavity. Low speed during first stage allows the removal of air, however it increases the metal's temperature losses. Therefore, the definition of this parameter regards casting temperature, mold's temperature and air entrainment variables.

The definition of this stage kinematics was initially based on the literature and NADCA gating manual [56] and then small adjustments were taken based on previous results in order to avoid an early solidification. At the end of the iterative process, it was concluded that the ideal working velocity was an initial speed of 0.4 m/s that would be increased linearly to 0.6 m/s and the NADCA formulation.

The linear increase was chosen in order to reduce air entrainment in the casting metal as it is shown in Fig 4.36, where (a) has a linear increase in velocity and (b) does not.

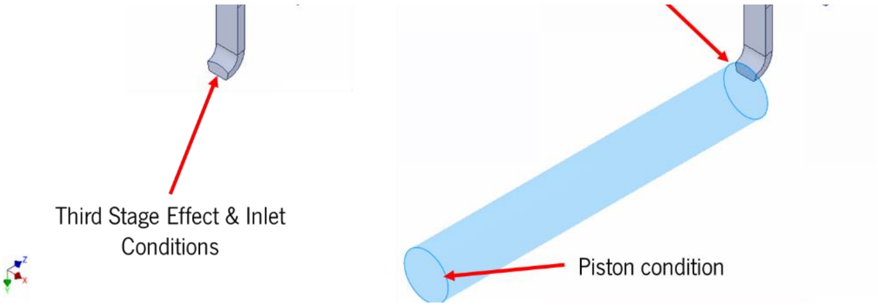


Fig 4.35 Surfaces of application of boundary conditions by two methods. (a) - first method: it is considerated a method of definition of injections condition of Inlet and third stage effect and Inlet. (b) – second method: it is considerated a method of definition of injection condition of third stage effect and piston.

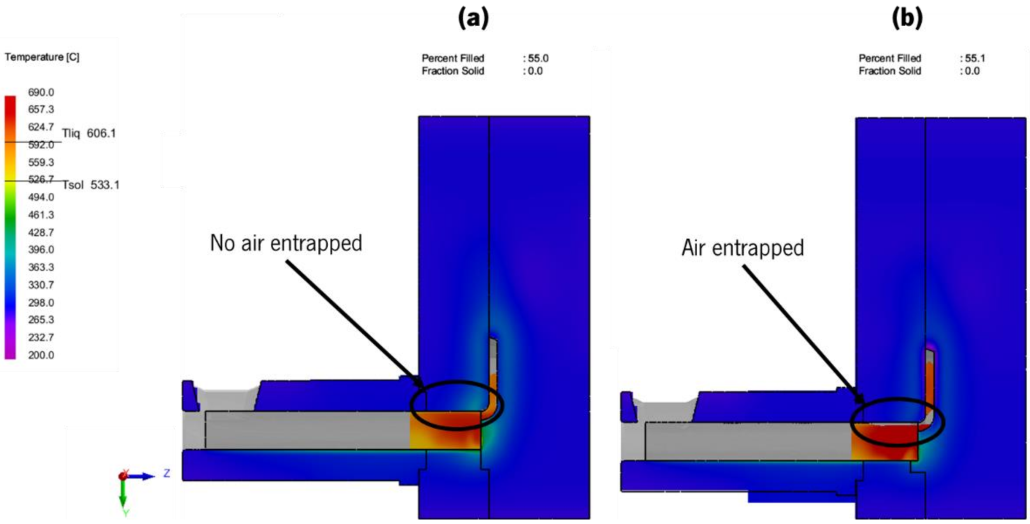


Fig 4.36 - Influence of velocity increase in air entrainment in shot sleeve. (a) - Situation of no air entrainment. (b) - Situation of air entrainment.

The second advancing stage lasts until all the filling cavity is full, which can be expressed using the equation [4.30], piston's position between 295 mm to 345 mm (Fig 4.37).

$$t_{2^{nd}} = \frac{V_{overflows} + V_{part}}{\sum_{i=1}^{n} Q_i} \quad [4.30]$$

In the equation [4.30], $V_{gating}$ is the volume of the gating system, $V_{overflows}$ is the volume of the overflows, $n$ is the number of segments defined during the gating design, $Q_i$ is the flow rate of each segment and $t_{fill}$ value calculated using equation [4.1], which value is 0.0424 seconds (higher than the previous calculated, since it considers the overflows).

However, due to this energy losses, will be important to apply Bernoulli's equation and continuity equation [58, 59] in order to determine the real piston's pressure and velocity, equation [4.31], which $C_d$ is the remaining kinetic energy of the fluid [16] (value of 0.45).

$$p_{piston} = \frac{\rho v_{ingate}^2}{2C_d} \quad [4.31]$$

$$v_{piston}A_{piston} = v_{ingate}A_{ingate} \quad [4.32]$$

This stage is characterized by an higher piston's velocity (1.75 m/s), the highest during the casting process (Fig 4.37). The second advancing stage's maximum velocity is limited by the machine's injection force, since the pressure applied by the piston has to be higher than the dynamic pressure required considering the inertial and viscous forces.

The last stage is characterized by a low velocity and displacement and high pressure (Fig 4.37), which main goal is to push the remain casting metal to the cavity and reduce shrinkage porosity [57]. The maximum pressure is defined based on machine's capacity and characteristics given by the manufacturer which value is 930 bar. Generally, this stage ends when 100% of the casting solidifies [40].

Using Pascal's Law [60], equation [4.33], it is possible to calculate the required locking force, 1837 kN. Furthermore, it is possible to determine the avarage contact pressure between plate mold, equation [4.34].

$$F_{locking} = p_{3^{rd}}A_{projected} \quad [4.33]$$

$$\overline{p_{die}} = \frac{F_{m_{locking}} - F_{locking}}{A_{contact}} \quad [4.34]$$

The contact pressure (100 bar) between die plates influence the thermal contact resistance for heat transfer, due to the fact that the casting is not symmetric and temperature's distribution in the dies are not equal.

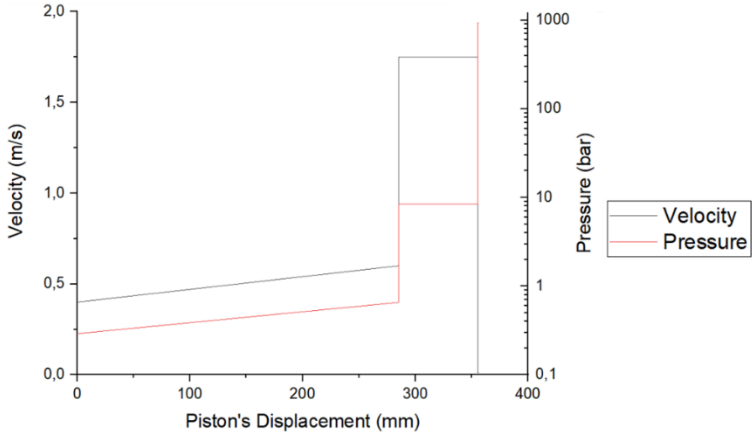


Fig 4.37– Theoric evolution of velocity and pressure with piston's position.

Piston's kinematics during the three injections phases are summed up in Tab 4.11. These values are merely theoric, since it does not consider the inertial effect of the fluid during the piston's advance. Therefore, these values have to be evaluated with numeric and experimental data.

Tab 4.11 - Piston's kinematics in each cycle.

| Phase | Displacement (mm) | time (s) | velocity (m/s) | pressure (bar) |
|---|---|---|---|---|
| **Phase 1** | 295 | 0.589 | 0.400-0.600 | 0.045-0.102 |
| **Phase 2** | 345 | 0.631 | 1.75 | 9.67 |
| **Phase 3** | Solid, 100% | | | 930 |

**Venting**

The removal of air inside filling cavity is made through the usage of the venting system as mentioned in chapter 2.1. The filling cavity minimum vacuum pressure is limited by the vacuum pump, mold's and vaccum connection's air-thighness. The air removal condition is only active after the vaccum position is reached and ends when the injection cycle is over, Fig 4.38. An early activation of the vaccum system may result in a less effective process [61].

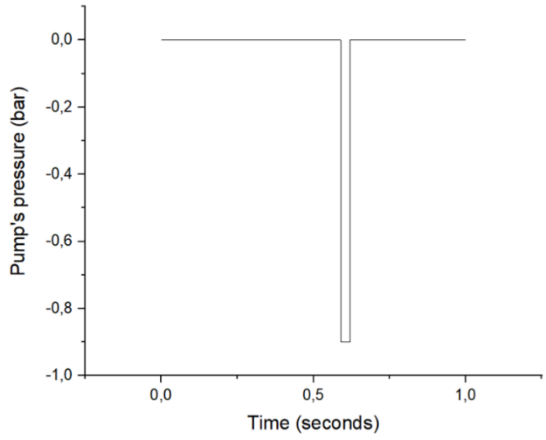


Fig 4.38 - Transient venting pressure.

## 4.6. Chapter References


[1] Hewlett Packaard Entreprise and AMD, "Enhance engineering productivity through CAE innovation solution brief,"

[2] M. J. Marques, *CAE Techniques for Casting Optimization.* [Online]. Available: https:// www.esi-group.com/sites/default/files/resource/publication/1284/finegi-ans.pdf (accessed: Jul. 2 2024).

[3] T. Nandi, "Application of Simulation Softwares for Analysing the Solidification Pattern of Aluminium Alloy (LM6) Casting," *SJET*, vol. 4, no. 7, pp. 312–324, 2016, doi: 10.21276/sjet.2016.4.7.4.

[4] Regloplas, *The basics and benefits of temperature control for die casting.* [Online]. Available: https://www.regloplas.com/en/technologies/mould-temperature-control/the-basics-and-benefits-of-temperature-control-for-die-casting (accessed: Jul. 3 2024.780Z).

[5] Sente Software Lda., *JMatPro*: software.informer, 2015. Accessed: Feb. 5 2024. [Online]. Available: https://jmatpro.software.informer.com/download/

[6] CONCEPTLASER, *Maraging steel 1.2709*. Brochure. Accessed: Mar. 19 2024. [Online]. Available: https://outlook.office.com/mail/id/ AAQkADEyNmVmNTFhLWU5YzMtNGVhMC1hNjYxLTlmNWY3YzI4YTk2MQAQANj4ZaiQmEZz vAytZc4BaVM%3D/sxs/ AAMkADEyNmVmNTFhLWU5YzMtNGVhMC1hNjYxLTlmNWY3YzI4YTk2MQBGAAAAAACP8Utt AoosQLFmRUt5nqUEBwDKciLTekemQrkRnNPMcy6ZAAAAAAEMAADKciLTekemQrkRnNPMc y6ZAAQ9Fii0AAABEgAQAM7dBEBb1ktJmaG9gCbvz00%3D

[7] mecdata, "MARAGING STEEL | 3D METAL - ADDITIVE MANUFACTURING," *3D Metal S.r.L.*, 09 Jun., 2021. https://3dmetal.it/additive-manufactoring/en/materials/maraging-steel/ (accessed: Jul. 1 2024.671Z).

[8] EU - EOS Store, *EOS ToolSteel 1.2709.* [Online]. Available: https://store.eos.info/products/ eos-toolsteel-12709 (accessed: Jul. 1 2024.216Z).

[9] RAFFMETAL, *EN 46000 AlSi9Cu3(Fe).* [Online]. Available: https://www.raffmetal.com/ scarica_file.asp?c=/dati/SearchAlloy/ENG/&f=EN%2046000%20AlSi9Cu3(Fe).pdf (accessed: Jul. 15 2024.837Z).

[10] *ENAC-AlSi9Cu3(Fe) / ENAC-46000 - SteelNumber - Aluminium equivalent, chemical composition, properties.* [Online]. Available: https://www.steelnumber.com/en/steel_alloy_ composition_eu.php?name_id=1244 (accessed: Jul. 5 2024.533Z).

[11] *ENAC-AlSi9Cu3(Fe) / ENAC-46000 - SteelNumber - Aluminium equivalent, chemical composition, properties.* [Online]. Available: https://www.steelnumber.com/en/steel_alloy_composition_eu.php?name_id=1244 (accessed: Jul. 5 2024.533Z).

[12] P. C. Bollada, P. K. Jimack, and A. M. Mullis, "Faceted and dendritic morphology change in alloy solidification," *Computational Materials Science*, vol. 144, no. 3, pp. 76–84, 2018, doi: 10.1016/j.commatsci.2017.12.007.

[13] ASM TECHNICAL BOOKS, *Symbols, Abbreviations, and Intermetallic Phase Designations | Aluminum-Silicon Casting AlloysAtlas of Microstructures | Technical Books | ASM Digital Library* (accessed: Jul. 17 2024.508Z).

[14] Q. Miao *et al.,* "Comparative study of microstructure evaluation and mechanical properties of 4043 aluminum alloy fabricated by wire-based additive manufacturing," *Materials & Design*, vol. 186, p. 108205, 2020, doi: 10.1016/j.matdes.2019.108205.

[15] NADCA, *NADCA Product Specification Standards for Die Casting: Aluminum, Aluminum-MMC, Copper, Magnesium, Zinc and ZA Alloys,* 9th ed. Illinois, United States of America: NADCA, 2015.

[16] NADCA, *NADCA Gating Manual*. Illinois, United States of America: NADCA.

[17] J. K. Pancholi, B. Padhiyar, and V. Sutariya, "Design and Analysis of Die Casting Die With Conformal Cooling Channel," *International Journal of Engineering and Computer Science*, vol. 9, no. 3. [Online]. Available: https://www.researchgate.net/publication/344235476_Design_and_Analysis_of_Die_Casting_Die_With_Conformal_Cooling_Channel

[18] Z.-C. Lin and M. H. Chou, "Design of the Cooling Channels in Nonrectangular Plastic Flat Injection Mold," vol. 2, 2002.

[19] E. Vojnová, "The Benefits of a Conforming Cooling Systems the Molds in Injection Moulding Process," *Procedia Engineering*, vol. 149, pp. 535–543, 2016, doi: 10.1016/j.proeng.2016.06.702.

[20] S. Feng, A. M. Kamat, and Y. Pei, "Design and fabrication of conformal cooling channels in molds: Review and progress updates," *International Journal of Heat and Mass Transfer*, vol. 171, p. 121082, 2021, doi: 10.1016/j.ijheatmasstransfer.2021.121082.

[21] A. Souza *et al.,* "Thermal Contact Resistance between Mold Steel and Additively Manufactured Insert for Designing Conformal Channels: An Experimental Study," *JMMP*, vol. 6, no. 5, p. 99, 2022, doi: 10.3390/jmmp6050099.

[22] ESI Group, *QuikCast | Casting Simulation Software*. France: ESI Group. [Online]. Available: https://myesi.esi-group.com/

[23] ESI Group, *ProCAST | Casting Simulation Software*: ESI Group. Accessed: Jun. 13 2024.038Z. [Online]. Available: https://www.esi-group.com/products/procast

[24] FLOW-3D, *Free Gridding Saves Time.* [Online]. Available: https://www.flow3d.com/resources/cfd-101/free-gridding/ (accessed: Jun. 13 2024.523Z).

[25] NATIONAL AERONAUTICS AND SPACE ADMINISTRATION, *Navier-Stokes Equations.* [Online]. Available: https://www.grc.nasa.gov/www/k-12/airplane/nseqs.html (accessed: Mar. 23 2024.132Z).

[26] Wikipedia, *Navier–Stokes equations.* [Online]. Available: https://en.wikipedia.org/w/index.php?title=Navier–Stokes_equations&oldid=1217632972 (accessed: May 6 2024).

[27] Glenn Research Center | NASA, *Newton's Laws of Motion | Glenn Research Center | NASA.* [Online]. Available: https://www1.grc.nasa.gov/beginners-guide-to-aeronautics/newtons-laws-of-motion/ (accessed: May 6 2024.359Z).

[28] Department of Mechanical Engineering, Columbia University, *A Numerical Analysis for 2-D Navier-Stokes Equations by FDM and FVM.* [Online]. Available: https://www.columbia.edu/~ll2998/documents/A%20Numerical%20Analysis%20for%202-D%20Navier-Stokes%20Equations%20by%20FDM%20and%20FVM_Lei%20LEI.pdf (accessed: Jun. 11 2024).

[29] Wikipedia, *Poisson's equation.* [Online]. Available: https://en.wikipedia.org/w/index.php?title=Poisson's_equation&oldid=1214748818 (accessed: Jun. 17 2024).

[30] Wikipedia, *Continuity equation.* [Online]. Available: https://en.wikipedia.org/w/index.php?title=Continuity_equation&oldid=1221543206 (accessed: May 6 2024).

[31] J. H. Lienhard, IV and J. H. V. Lienhard, *A Heat Transfer Textbook*, 2001. Accessed: Jun. 13 2024. [Online]. Available: http://web.mit.edu/lienhard/www/ahtt.html

[32] Cadence CFD Solutions, *Energy Equations: The Navier-Stokes Method of Analysis | System Analysis Blog | Cadence.* [Online]. Available: https://resources.system-analysis.cadence.com/blog/msa2022-energy-equations-the-navier-stokes-method-of-analysis (accessed: Mar. 23 2024.285Z).

[33] COMSOL Multiphysics, *Heat Transfer: Conservation of Energy.* [Online]. Available: https://www.comsol.com/multiphysics/heat-transfer-conservation-of-energy (accessed: Jun. 13 2024.559Z).

[34] S. K. Mohammed, M. H. Arbo, and L. Tingelstad, "Leveraging model based definition and STEP AP242 in task specification for robotic assembly," *Procedia CIRP*, vol. 97, no. 4, pp. 92–97, 2021, doi: 10.1016/j.procir.2020.05.209.

[35] Wikipedia, *STL (file format).* [Online]. Available: https://en.wikipedia.org/w/index.php?title=STL_(file_format)&oldid=1210489843 (accessed: Apr. 5 2024).

[36] Adobe Acrobat, *What are IGES files and how do you open them? | Adobe.* [Online]. Available: https://www.esi-group.com/sites/default/files/resource/publication/1284/finegi-ans.pdf (accessed: Apr. 5 2024.094Z).

[37] Scratcha Pixel, *Geometry.* [Online]. Available: https://www.scratchapixel.com/lessons/mathematics-physics-for-computer-graphics/geometry/transforming-normals.html (accessed: Apr. 5 2024.481Z).

[38] *Two-Dimensional Conduction: Finite-Difference Equations and Solutions: Chapter 4 - Sections 4.4 and 4.5.* [Online]. Available: https://www.visualslope.com/Library/FDM-for-heat-transfering.pdf (accessed: Jun. 4 2024).

[39] I. P. Villalobos and I. U. Martinez, *Guía Práctica de QuikCAST- Visual Environment: Para el proceso de HPDC*, 2019.

[40] ESI Group, *Quikcast reference manual*. France: ESI Group, 2014. Accessed: 2014.

[41] Wikipedia, *Finite difference method.* [Online]. Available: https://en.wikipedia.org/wiki/Finite_difference_method (accessed: May 6 2024.526Z).

[42] P. Lobarinhas, *Mecânica Computacional* (accessed: Jun. 4 2024).

[43] J. C. F. Teixeira, *Métodos Numéricos em Transferência de Calor* (accessed: Jun. 5 2024).

[44] Bengt Fornberg, "Finite difference method," *Scholarpedia*, vol. 6, no. 10, p. 9685, 2011, doi: 10.4249/scholarpedia.9685.

[45] M. T. T. Monteiro, *Métodos Numéricos: exercícios resolvidos aplicados à Engenharia e outras Ciências* (accessed: May 6 2024.526Z).

[46] J. E. Marsden, L. Sirovich, S. S. Antman, J. S. Hesthaven, and T. Warburton, *Nodal Discontinuous Galerkin Methods*. New York, NY: Springer New York, 2008.

[47] S. Patankar and D. Spalding, "A calculation procedure for heat, mass and momentum transfer in three-dimensional parabolic flows," *International Journal of Heat and Mass Transfer*, vol. 15, no. 10, pp. 1787–1806, 1972, doi: 10.1016/0017-9310(72)90054-3.

[48] Wikipedia, *Explicit and implicit methods.* [Online]. Available: https://en.wikipedia.org/w/index.php?title=Explicit_and_implicit_methods&oldid=1076468513 (accessed: Jun. 17 2024).

[49] Wikipedia, *Crank–Nicolson method.* [Online]. Available: https://en.wikipedia.org/w/index.php?title=Crank–Nicolson_method&oldid=1188507267 (accessed: Jun. 17 2024).

[50] E. Anglada, A. Meléndez, I. Vicario, E. Arratibel, and G. Cangas, "Simplified Models for High Pressure Die Casting Simulation," *Procedia Engineering*, vol. 132, pp. 974–981, 2015, doi: 10.1016/j.proeng.2015.12.585.

[51] QuickField.com, *Natural convection coefficient calculator.* Accessed: Jun. 20 2024.162Z. [Online]. Available: https://quickfield.com/natural_convection.htm

[52] N. D. Campos Neto, A. L. Korenyi-Both, C. Vian, S. P. Midson, and M. J. Kaufman, "The development of coating selection criteria to minimize die failure by soldering and erosion during aluminum high pressure die casting," *Journal of Materials Processing Technology*, vol. 316, p. 117954, 2023, doi: 10.1016/j.jmatprotec.2023.117954.

[53] V. Nunes, F. Silva, M. F. Andrade, R. Alexandre, and A. Baptista, "Increasing the lifespan of high-pressure die cast molds subjected to severe wear," *Surface and Coatings Technology*, vol. 332, pp. 319–331, 2017, doi: 10.1016/j.surfcoat.2017.05.098.

[54] FOSECO and VESIVIUS, *DYCOTE: Manual.* [Online]. Available: www.vesuvius.com\foundry (accessed: Jun. 21 2024).

[55] Sunrise, "Die Spray & Lubricate," *Sunrise Metal - Aluminium Die Casting Expert*, 28 Apr., 2024. https://www.sunrise-metal.com/die-spray-and-lubricate-technology (accessed: Jun. 21 2024.298Z).

[56] X. Dong, X. Zhu, and S. Ji, "Effect of super vacuum assisted high pressure die casting on the repeatability of mechanical properties of Al-Si-Mg-Mn die-cast alloys," *Journal of Materials Processing Technology*, vol. 266, pp. 105–113, 2019, doi: 10.1016/j.jmatprotec.2018.10.030.

[57] Become a master of CAD Design, *What is injection phase of HPDC Die Casting | Die Casting.* [Online]. Available: https://www.youtube.com/watch?app=desktop&v=SG3xR9d7IPM (accessed: Sep. 5 2024.122Z).

[58] J. G. Fairman, *Experiment on Fluids.* [Online]. Available: https://www.grc.nasa.gov/www/k-12/WindTunnel/Activities/exper_on_fluids.html (accessed: Apr. 15 2024.220Z).

[59] N. Hall, *Bernoulli's Equation.* [Online]. Available: https://www.grc.nasa.gov/www/k-12/airplane/bern.html (accessed: Apr. 15 2024.395Z).

[60] Wikipedia, *Pascal's law.* [Online]. Available: https://en.wikipedia.org/w/index.php?title=Pascal's_law&oldid=1211459295 (accessed: Mar. 23 2024).

[61] P. Szalva and I. N. Orbulov, "The effect of vacuum degree on the porosity and mechanical properties of die cast AlSi 9 Cu 3 (Fe) alloy," *Resolution and Discovery*, vol. 3, no. 2, pp. 33–38, 2018, doi: 10.1556/2051.2018.00061.

# Chapter 5 - GATING DESIGN VALIDATION

The gating design validation consist in evaluating the CAE results which predict the existance of defects within the component's volume and the postprocessing of process variables such as injection pressure for process's validation.

Gating design parameters such as flow angles, filling time, segments' division defined in the gating design will be checked to determine if these were appropriate and provide H.E.L.P. Die Casting with new knowledge for future gating designs. Lately, time spent doing by-hand calculations and modelling were performed to determine the real positive impact of the developed software.

In chapter 4.3 was shown both numeric models to describe the casting simulation. In chapters 4.5.1 and 4.5.2, it was described the process conditions for die cycling simulation and injection simulation. This previous knowledge to describe the casting simulation resulted in various CAE results which shall be evaluated and compared with product specifications and available technology.

Without forgeting the CAE importance, the results given by QuikCast have to be compared with the result of a real casting process.

## 5.1. CYCLING SIMULATION

The cycling simulation described in chapter 4.5.1 originated a thermal field which was shown previously. However, in order to validate such simulation, it was necessary to monitor some point in the die, shown in Fig 5.1. It was choosen symmetrical points in each component, in order to guarantee that a different attack position defined would not result in a completely different shrinkage defect location.

After monitoring these points, it was possible to track its temperature throughout each cycle to find its convergence temperature.

Fig 5.1 - Mould's position of the tracking points.

The opposite points pairs are P01/P14, P02/P13, P03/P12 and P04/P11 and the "Point_Ce_1" which is located at midpoint of both casting components. In Fig 5.2 is shown the temperature variation of the each point during each cycle of the die cycling simulation.

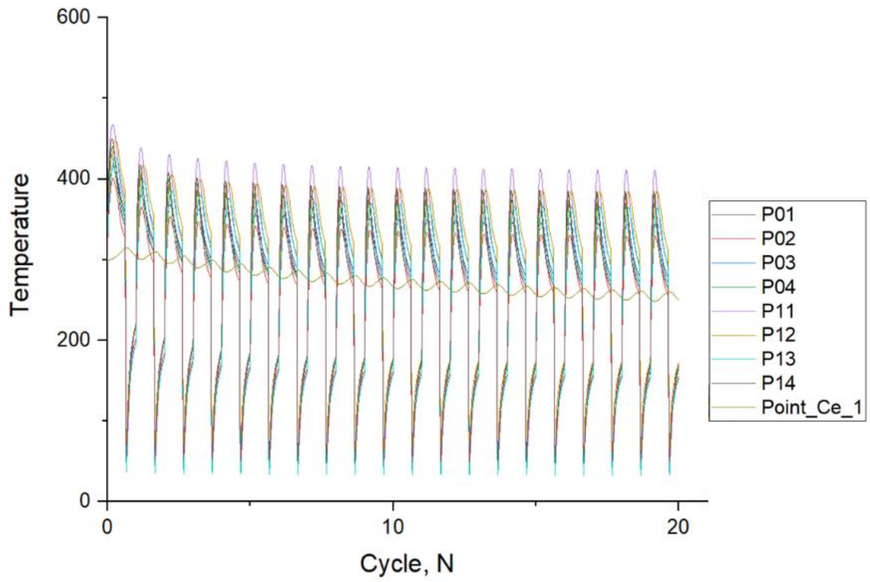


Fig 5.2 - Temperature oscillation within the die cycling simulation.

It was possible to evaluate that the die temperature variation through the die cycling simulation converges. In a more detail analysis it was exclusively evaluated the maximum temperature of each point. In Fig 5.3 (a), (b) are shown the maximum temperature of each cycle to the point P01/P14 and P04/P11, P03/P12 and P02/P13 and Point_Ce_1, respectively.

In Fig 5.3 (a), the temperature difference in pair P01/P14 (13°C) is lower than the pair P04/P11's (31°C), this is caused by the caused by the proximity to the cooling channel in critical region 1 (defined in chapter 4.2). The cooling channel influence on die cavity's temperature is higher in critical region 1 than the one in critical region 2, due to the cooling channel area.

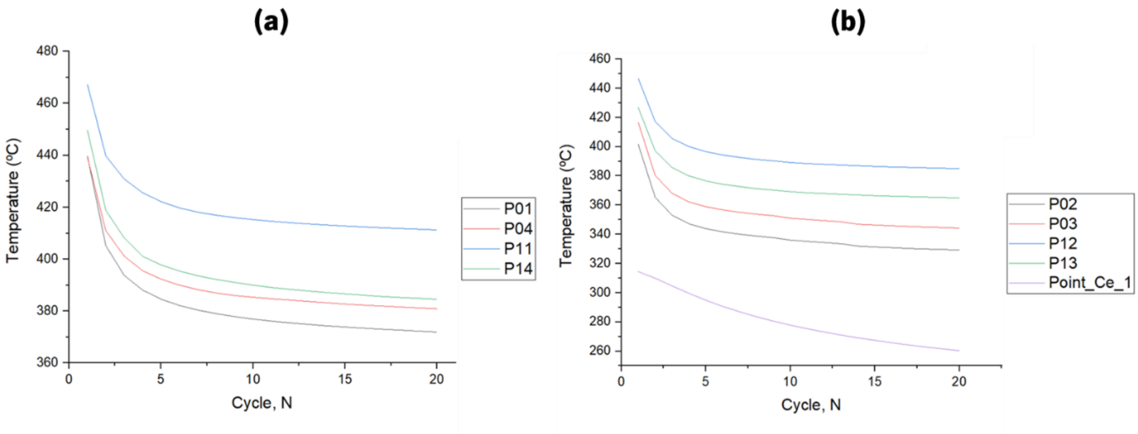


Fig 5.3 - Maximum temperature in each cycle. (a) - maximum temperature in each cycle in points P01, P04, P11 and P14; (b) - maximum temperature reach in each cycle in points P03, P12, P02, P13 and Point_Ce_1.

Even though the temperature variation throughout the die cycling simulations converges, a relative analysis was done (Fig 5.4) to evaluate its relative variation with a convergence threshold of 1%.

It is possible to verify that the points in die cavity (every point exepct Point_Ce_1) converges after the 4th cycle, however the central point (Point_Ce_1) converges after the 9th cycle. This point is exposed to a lower temperature gradient during each cycle, since it is not in contact with the casting alloys. Therefore, this point would reflect the mold's thermal inertia and it's equilibrium point between the process's heat outflux (to the environment and cooling channels) and the heat influx (casting alloy).

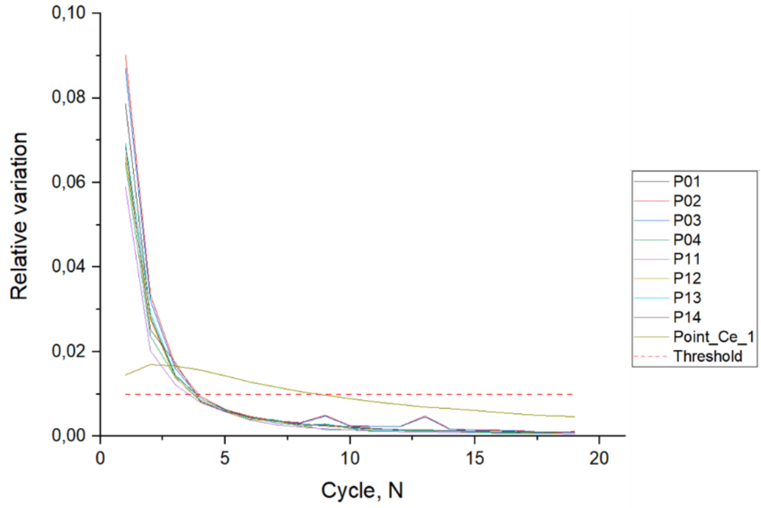


Fig 5.4 - Relative variation of maximum temperature in each cycle and its defined threshold of 1% for acceptance.

In a detailed view of temperature variation of the last cycle, Fig 5.5, it is noticeable the real effect of each process's phase on die's temperature.

The die coating phase causes the highest temperature reduction. This happens due to the high value of heat transfer convection coefficient. However, this process's phase is yet divided into two different step, the spraying of die coating and the air blowing which removes excess of mixture. Consequently, die cavity's surface temperature variation is different in both stages.

Lately, between the last instant of spraying the coating and close mold the die cavity's surface temperature increases due to the its thermal inertia (as it was concluded in chapter 4.5.1).

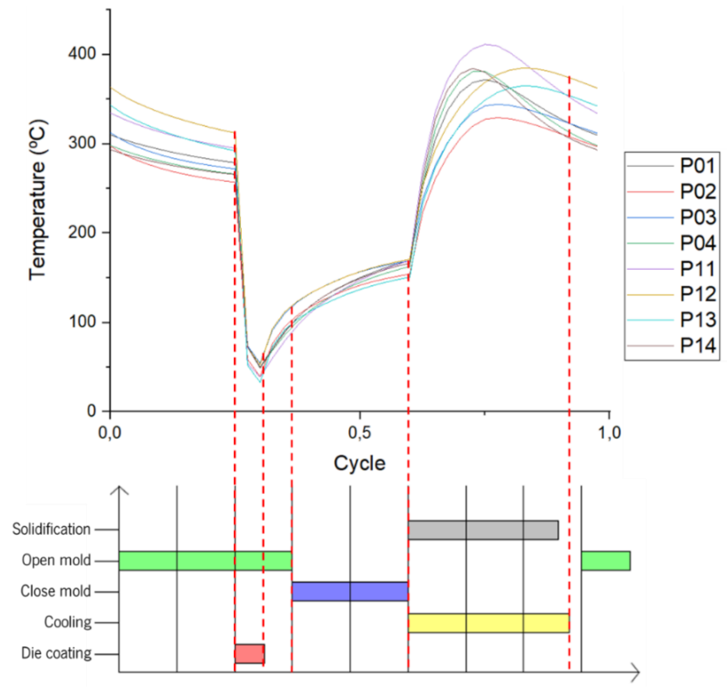


Fig 5.5 - Association between each step of the process and the die cycling defined previously.

## 5.2. CASTING SIMULATION

In the casting simulation, it is possible to predict possible shrinkage defects, air entrainment, a qualitative analysis of the existance of cold shuts, check if the flow pattern and segment division was as predictable during gating design phase. Furthermore, it is possible to determine if the overflow position was correct.

Two extra gating designs were made in order to study the effect of variables such as ingate thickness and flow angle and the ingate continuity. The final gating design of the component is shown in 4.2, which will be used as final solution.

The gating design – final solution will be taken in consideration as the final solution solution.

The results plotted in the postprocessing of the casting simulation in order to validate the gating design are flow pattern, shrinkage porosity, air entrainment and cold shuts location (this result was evaluated based on a user defined result). Fluid's vorticity could be evaluated to determine the location's which are more susceptible to air entrainment, however it would require a finer mesh than the one used. Gating designs A and B analysis will based on shrinkage porosity and air entrainment.

All solutions present a casting yield of 58%. he small changes described in the following chapter amount to less than a 1% variation.

### Gating design – Final solution

The flow pattern evaluation is hard to evaluate due to geometric complexity therefore, its evaluation is done based on the filling sequency of each region in important frames to verify overflows position. In Fig 5.6, it is shown the filling sequency at 0.6004, 0.6029, 0.6116 and 0.6152 seconds.

The validation of overflows position is based in avoiding the encircled air region which will prevent the air from leaving the die cavity.In frames shown in Fig 5.6 (a) and (b), it is verifies the position of the overflows 12, 13 and 14. The position of overflow 1, 2, 3, 5 and 6 are validated in frame (c). Overflows 4, 7, 8 and 9 are validated in frame (d).

Fig 5.6 – Casting's filling sequency. (a) – Filling frame at 0.6004 seconds; (b) – Filling frame at 0.6029 seconds; (c) – Filling frame at 0.6116 seconds; (d) – Filling frame at 0.6152 seconds.

In Fig 5.7, it is shown the shrinkage porosity based on a volume fraction of the cell. The presence of shrinkage porosity within the component domain (excluding overflows) only appears in the critical region 1, due to the region hotspot delaying the solidification.

The formation of shrinkage porosity derives of a poor solidification dynamic. If the liquid phase domains looses its continuity with the runner, it will be impossible to compensate the volume contraction on the discontinued domains during the third advancing phase of the piston. If the continuity is kept, metal in the runner will be pushed to fill the contracted volume of the casting.

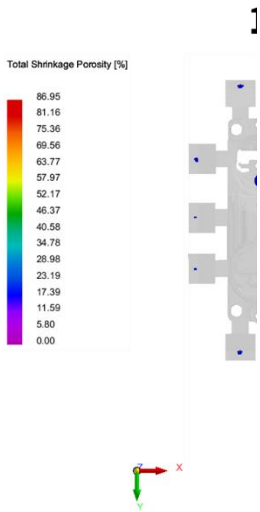


Fig 5.7 - Shrinkage porosity in the end of the solidification process of reference gating design.

The ruling physical law of this stage is the Pascal's principle which states that a change in pressure of incompressible fluid at rest in an enclosed fluid at rest is transmitted equally to all points [1]. Therefore, the entire cavity will be full to guarantee its pressure transmission avoiding the shrinkage porosity. Consequently, it is crucial to guarantee that the runners and especially the ingate keep its liquid state during the entire solidification stage.

In Fig 5.8, it is presented the last instant the liquid domains in both components ($t = 7.2\ s$ and $t = 7.7\ s$ for component 1 and component 2, respectively) during the solidification stage have continuity with the runners. In this plot, it was defined a cut off of the solidification time variable to visualise the regions where solidification time were higher than ingate's.

The remaining liquid phase of instant presented in Fig 5.8 will solidify and cause the appearance of shrinkage defect.

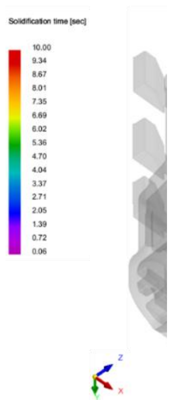


Fig 5.8 - Last frame of continuity of liquid-state domains between the component and the runner.

The air entrainment variable is exclusive to the flow model, therefore it was evaluated in the when the casting was at 90% full. This value was choose cause it is the last frame with domain continuity between the air gap of overflow and the rest of the component (overflow 7 of Fig 5.6).

Even though the overflow position defined previously was verified, air entrainment can only be minimized. In the critical region 1 air entrainment is impossible to reduce due to its geometry. Furthermore, the pin region was found to be a critical region for air entrainment.

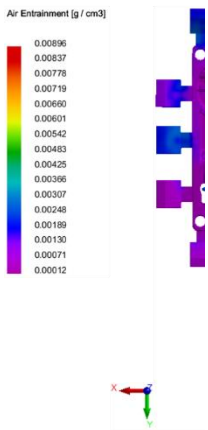


Fig 5.9 - Location of the air entrainment within the casting.

The present assymetry in air entrainment is consequence of an assymetric filling. The critical region 1 of the component 1 posses a filling dynamic different of its counterpart (component 2), which allow the air removal. The circled regions of Fig 5.9 have its remaining empty volume encircled by the casting metal, preventing it from exiting. The avarage quantity of air in the castings (including overflows) are 0.0007 g/cm$^3$ and 0.0008 g/cm$^3$ for the components 1 and 2, respectively.

In order to determine the location of possible cold shuts, it is necessary to monitor the casting's filling fluid origin. The variable shown in Fig 5.10 represents the numerical identification of each cell's volume fraction originating from the corresponding ingate, $C$. The closer a cell is to this index, the higher the volume fraction of fluid that originates from the corresponding ingate.

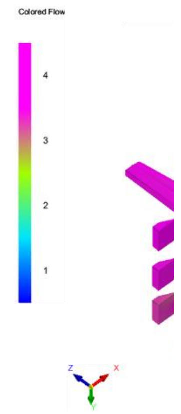


Fig 5.10 - Flow colored path variable.

The post processing of this variable indicates the location of cold shut defect if it exists through equation [5.1]. The gradient of the variable represents the physical transition between the flow of each ingate. In Fig 5.11, it is shown the plot of the same gradient.

$$\|\nabla C\| = \sqrt{\left(\frac{dC}{dx}\right)^2 + \left(\frac{dC}{dy}\right)^2 + \left(\frac{dC}{dz}\right)^2} \qquad [5.1]$$

This variable's gradient unit's is %/mm with represents the variation of volume percentage of fluid in each cell originate from different ingates.

In Fig 5.11, there are some continuous regions where the gradient magnitude is slightly high and well defined which will be location of possible cold shuts.

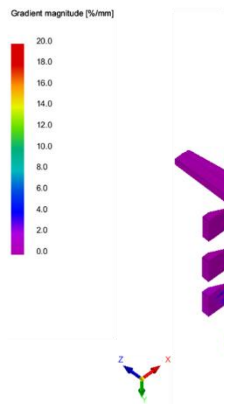


Fig 5.11 - Gradient of the flow colored path variable.

**Gating design – A**

Gating design A ingate modification compared with the reference is presented in Fig 5.12. When compared with reference ingate, the ingate flow angle on each side is 40° outward (reference flow angle is 17° outward). This orientation was choosen to increase the distribution of flow component (when compared to reference gating design), which causes chisel flow and trapped gas. The cross section's dimensions are $1.2 \times 36$ mm$^2$.

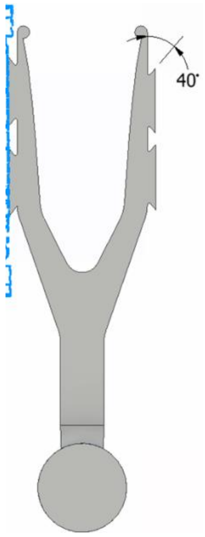


Fig 5.12 - Ingate modification of gating design A.

In Fig 5.13, it is shown the shrinkage porosity, where it is possible to notice the increasing of the appearance of this defected compared to the reference.

In this gating design, a new region with shrinkage porosity emerges. This is resulted of a the discontinuity of a liquid domain with the remaining casting alloy (Fig 5.14), which will prevent the volume change compensation.

The casting's local and ingate's thickness is smaller than the new shrinkage region, therefore the only possible way to reduce the shrinkage porosity is to increase the local cooling rate, which couldn't be done due to technological and geometric restrictions.

The avarage air entrainment quantity in the casting (including overflow) is 0.0002 g/cm$^3$ for both components. This values represent a reduction in air entrainment of 72% and 75% (for component 1 and 2, respectively) compared to the final solution.

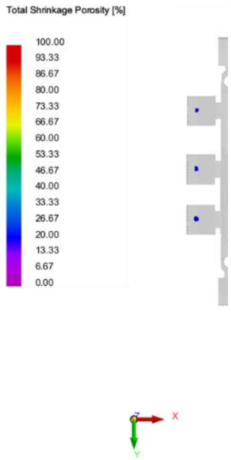


Fig 5.13 - Shrinkage porosity at the end of the solidification process.

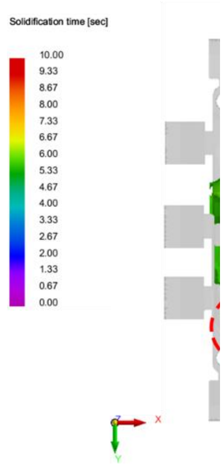


Fig 5.14 - Descontinuity of liquid-state domains between the component and the runner.

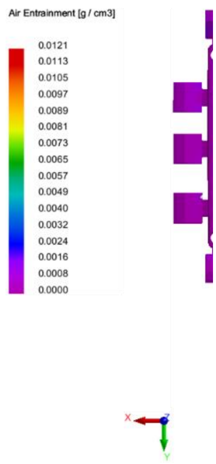


Fig 5.15- Air entrainment within the casting.

When analysing the filling sequency of this gating design, it is possible to notice that the ingate does not possess a uniform filling profile, Fig 5.16. This is resulted of an high flow angle which can not be fulfilled due to fluid's momentum. Even though the ingate design A goal was to improve the flow distribution to reduce the swirl, this design proved to have a flow angle too large. Being therefore an overall result worst than the final solution.

Fig 5.16 – Ingate's last region to fill.

### Gating design – B

Gating design B ingate tunning is presented in Fig 5.17. When compared with reference ingate, the ingate flow angle on the side closest to the biscuit is 30° inward. This orientation was choosen to reduce the difficulty in filling the ingate (when compared to gating design A), which causes backflow and vorticity. Meanwhile, the opposite side of the ingate has a 90° angle. The cross section's dimensions are 1.6×26 mm².

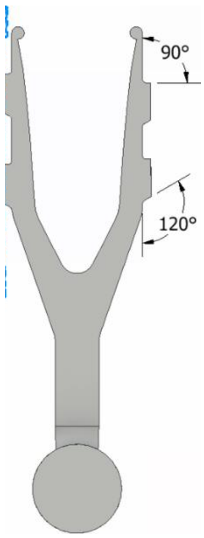


Fig 5.17 - Ingate modification of gating design B.

Shrinkage porosity results are presented in Fig 5.18. It is possible to verify that the shrinkage volume is higher than the reference's. This happens as a consequence of a less thick ingate which will solidify earlier than the reference gating design (cross section is 1.8×23 $mm^2$).

Similarly to the gating design A, in this gating design the appearance of new regions (when compared with reference) with shrinkage porosity is resulted of descontinuity of the liquid state domains within the component (Fig 5.18), which will prevent the compensation of volume change.

Fig 5.18 - Shrinkage porosity at the end of the solidification process.

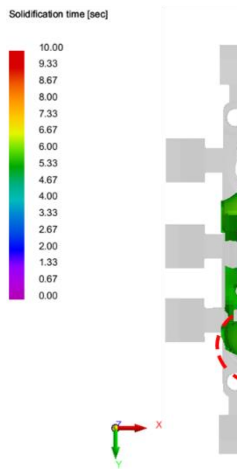


Fig 5.19 - Descontinuity of liquid-state domains between the component and runner.

In Fig 5.20, it is possible to conclude that this gating design reduce the encirclement of air volume present in the die cavity, since the air entrainment in locate almost exclusively in the critical region 1 and in the pin region. The avarage air entrainment quantity of air in the casting (including overflow) is 0.0004 $g/cm^3$ and 0.0005 $g/cm^3$ for component 1 and 2, respectively. This values represent a reduction in air entrainment of 43% and 38% (for component 1 and 2, respectively) compared to the reference.

This solution possesses a lower air entrainment in both components, but had more shrinkage porosity when compared to the final solution.

Fig 5.20 - Air entrainment in the casting.

## 5.3. DYNAMICS OF THE PROCESS

Even though previous calculations were made in order to predict the required dynamic pressure more accurately, lately it would be required to verify experimently. The theoric value of injection of the machine was determined in chapter 4.5.2 without considering the inertial forces and losses of energy. These variables will generally increase the required injection force to grant the casting metal the required ingate velocity (20 m/s).

In Fig 5.21, it is presented the injection pressure required to the process. Local peaks in in the simulated injection pressure are resulted of geometric complexity of the gating design and error cause by difference time-step sizes taken by the solver during processing.

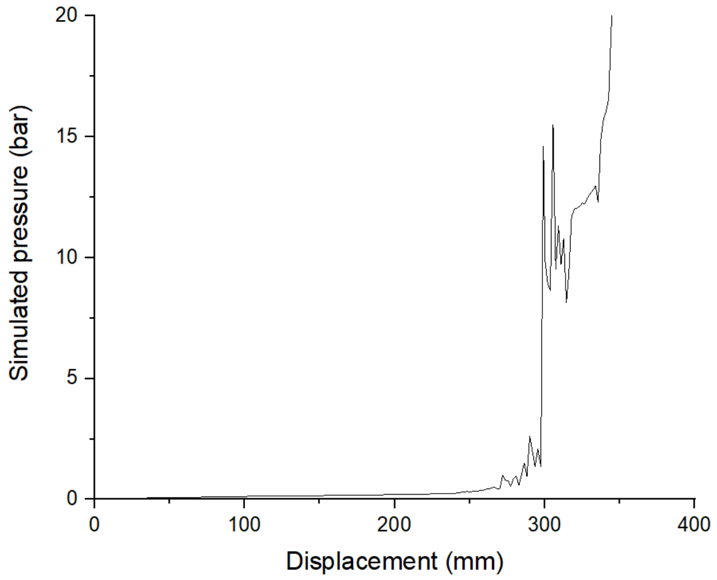


Fig 5.21 - Injection pressure evolution with piston's displacement.

An optical evaluation of the ingate speed would be less accurate when compared to a macroscopic variable (such as injection pressure). This happens cause ingate velocity can only be evaluated when the runner is completely full (and its instant), geometric configuration of the gating design would increase kinetic energy losses, mesh refinement, velocity gradient in the ingate.

It is very clear that the the local peaks in the graphics are resulted of a splash of the casting metal in the piston’s surface. However, these splashes are irrelevant to the overall injection cycle and do not cause air entrainment (problem solver in chapter 4.5.2).

A relation between the filling and pressure is presented in Fig 5.22. It is noticeable three significant relative increases in injection pressure can be identified during the process.. The first occurs within the 1$^{st}$ phase of the piston’s advance when the main runner starts to be filled up, Fig 5.22 (a). This increase happens due to the decreasing of area between the shot sleeve and main runner (minor loss). The second occurs during the 2nd phase , Fig 5.22 (b), where the flow rate increases drastically and the reduction of section area (ratio runner/ingate to guarantee a completely full ingate). The third , Fig 5.22 (c), is related to the transition to the increase of the viscous forces and the transition to the 3rd stage.

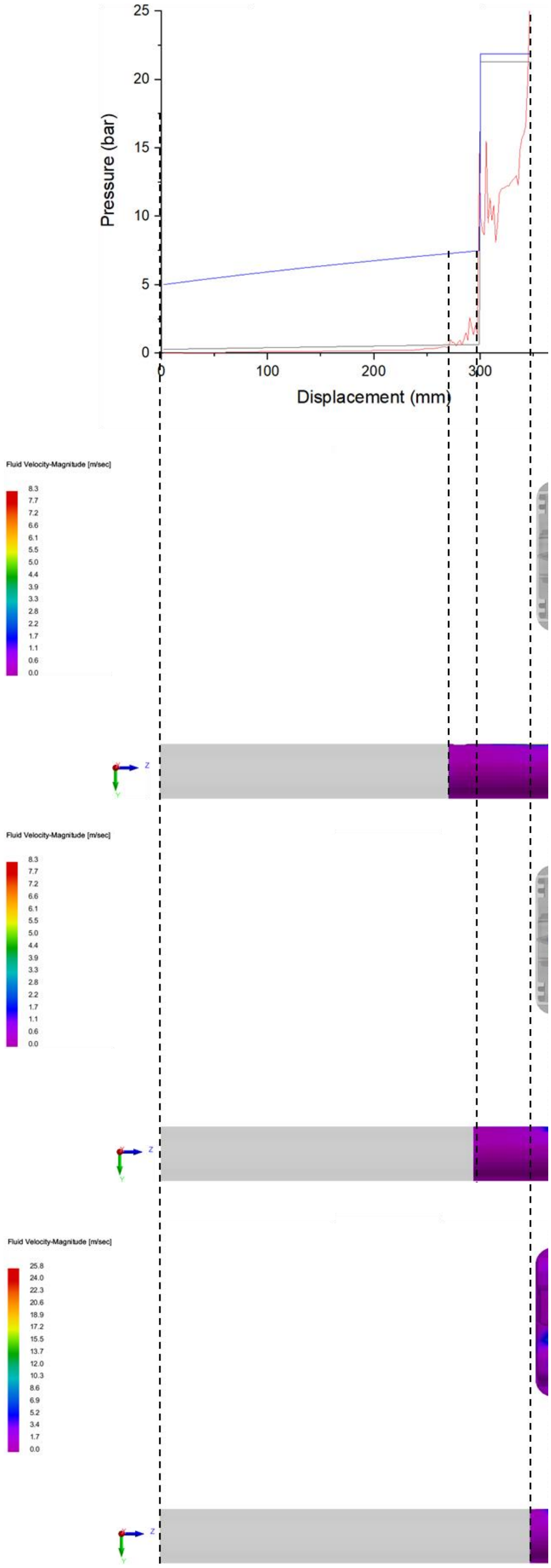


Fig 5.22 - Piston's position relation to the injection pressure. (a) – Shot sleeve at full capacity; (b) – Piston's 2nd advancing stage; (c) – Piston's 3rd advancing stage.

As verified in Fig 5.22, the kinetic energy losses happen in two distinguished locations, at the runners and at ingate. Using the minimum mean square error method [2], it is possible to determine that the energy loss for this gating design using the casting alloys $AlSi_9Cu_3$ during the 1st and 2nd stage is 0.16 and 0.35, respectively. Therefore, it is possible to divide piston's second advancing phase in two stages as it is shown in Fig 5.23 (scenario (b) and (c)), described by two step functions. Lately, this information can be stored in H.E.L.P. Die Casting database.

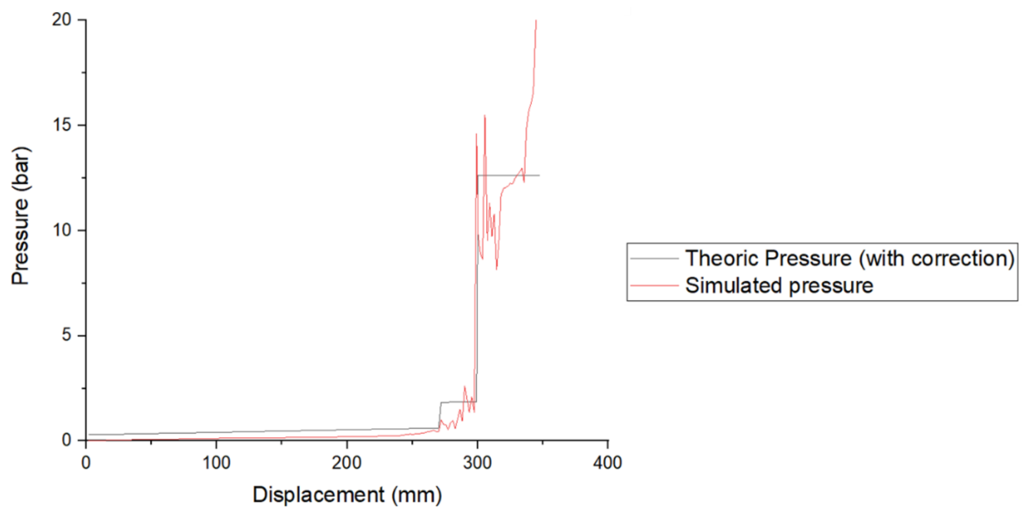


Fig 5.23 - Two step discretization of the machine based on piston's displacement.

The difference between the pressure at distance 295 mm of the piston's displacement in Fig 5.22 and Fig 5.23 (beginning of the second phase) is a consequence of the difference in geometric complexity. This happens due to the runner is geometrically less complex than the component which causes minor losses.

It is noticable that the injection pressure mentioned previously corresponds to the sum of the dynamic pressure and static pressure during the second advancing stage of the piston and not to the static pressure during the third stage.

The pressure vs displacement is a macroscopic variable that allows to evaluate a processes dynamics globally avoiding the velocity gradient at the ingate [3]. This also plays a crucial role when determining the mesh convergence, since it is possible to analise a tendency of the mesh refinement.

## 5.4. Chapter references

[1] Adam Augustyn, *Pascal's principle | Definition, Example, & Facts.* [Online]. Available: https://www.britannica.com/science/Pascals-principle (accessed: Jul. 31 2024.160Z).

[2] Wikipedia, *Minimum mean square error.* [Online]. Available: https://en.wikipedia.org/w/index.php?title=Minimum_mean_square_error&oldid=1212895420 (accessed: Jul. 22 2024).

[3] W. Heywang, K. Lubitz, and W. Wersing, *Piezoelectricity: Evolution and Future of a Technology*. Germany: Springer, 2008. Accessed: Jul. 24 2024.013Z. [Online]. Available: https://books.google.pt/books?id=8KyawZ92eIEC&pg=PA534&lpg=PA534&dq=macroscopic+variable+in+cae+software+engineering&source=bl&ots=JxmAz2tZa1&sig=ACfU3U2U1JXh9N2wbD3swCJFFCm3ewgyNw&hl=pt-PT&sa=X&ved=2ahUKEwj2ksnrsMCHAxVQcKQEHaluBYoQ6AF6BAgnEAM#v=onepage&q=macroscopic%20values%20like%20displacement%20and%20force%20and%20internal%20loading&f=false

# Chapter 6 - CONCLUSION

The conclusion of this dissertation summarizes the project giving it an overview. Therefore, it will be divided into two main topics "Summary" and "Future work".

The dissertation focused on the virtualization of the process of gating design for high pressure following NADCA methodology. The main challenges faced was during the development and study of the interface between Python and CAD software (Autodesk Inventor). The language used by most CAD software's is VBA and almost no information for the Python language increasing the number of attempts to create any sort of feature.

## 6.1. SUMMARY

The main goal of the dissertation was achived. It was to model and simulate the high-pressure die casting process in aluminum alloys which brought the programming interface with the CAD environment.

Progresses were made to make pyhton programming language a useful tool to the gating design in the manufacturing technology high-pressure die casting. The industrialization of this software would reduce the time spent modelling the gating system, however it remains a branch to develop. However, small adjustments had to be made before exporting to CAE environment. Furthermore, H.E.L.P. Die casting was designed in such way the user could to add more data about casting and mold materials which the NADCA manual would not possess.

Lately, the second part of the goal was done in the CAE environment QuikCast software to validate possible solutions.

To an early validation of the process before doing a more intensive postprocessing of the results, it was made a cycling simulation to determine if the die temperature would reach a stable thermal gradient at the beginning of each cycle. This stable thermal gradient was found after the $9^{th}$ cycle.

Three gating designs were made to determine the best solution using the H.E.L.P. Die casting. In all of the three gating designs were evaluated variables such as filling pattern, flow colored path and air entrainment in the using QuikCast's flow module and solidification time and shrinkage porosity using the thermal module.

Regarding the casting process, the final solution presented a process yield of 58% and a cycle time of 42 seconds.

Analysing the shot's dynamic, it was possible to conclude that the injection pressure of the second stage was slightly inferior to the calculated. This happened due to the reference value of kinetic energy loss mentioned in the NADCA manual was higher. Furthermore, it was possible to notice the losses in two distinguished periods. The first was in the first stage of the piston where the losses were equal to 16% of the initial kinetic energy. The second was during the injection phase of the piston where the losses reach 35%.

In conclusion, the H.E.L.P. Gating design contributed by allowing the user to generate as many gating designs as it wished following the structure of the NADCA manual saving time during the modelling and simulating process.

## 6.2. FUTURE WORK

The primary advantage of the HELP Gating Design software is its ability to significantly reduce the time required for casting project execution. It can generate the dimensions of a gating system in just 15 minutes, with the data stored in Excel along with the corresponding geometric modeling. The software is also versatile, reliable, and adaptable to both the user's preferences and the geometry of the component.

However, there is always space for improvement to make it easier and clearer for users. Some future features to add would be:

- Read previous data: This software remains exclusively academic and to a one-user only (its author). Therefore it was possible to increase its user-friendliness, for example, allowing the user to use previous sessions and project parameters instead of filling all the parameters again;

- Expanding to other CAD softwares: implementing the same Python rountine to other CAD softwares with compatible interfaces such as NX Siemens and Autodesk Fusion360. The same possibility can be extended indirectly to Solidworks using two methods. The first method is using third party libraries which guarantee direct interface SolidWorks which still in development. The second method is using VBA language which allows a direct connection with SolidWorks;
- Recognization of the STEP file: importing the CAD file to a Python environment allows the user to not fill some parameters and a future analysis based on the recognization would allow the modelling of ingate adapted to the geometry. If this was possible, a new door would be open to model instantly in the STEP file without needing the Inventor-Python interface. However, the link between STEP and Python is underdeveloped;
- Casting environment: continuing the development of the CAE environment to reduce the time of creating new boundary conditions. Furthermore, it would be possible to costumize the boundaries conditions automatically without user interference;
- Connection between CAD and CAE environments: improving the connection between CAD and CAE environments using "os" and "win32com.client" libraries, so the user only has to edit small details. Power Automate Windows system application also may play a crucial role.